University of Massachusetts Amherst
ScholarWorks@UMass Amherst

Masters Theses | Dissertations and Theses

October 2022

Characterization of the Poly (ADP-Ribose) Polymerase Family in the Fusarium oxysporum Species Complex

Daniel Norment
University of Massachusetts Amherst

Follow this and additional works at: https://scholarworks.umass.edu/masters_theses_2

 Part of the Biochemistry Commons, Bioinformatics Commons, and the Molecular Biology Commons

Recommended Citation

Norment, Daniel, "Characterization of the Poly (ADP-Ribose) Polymerase Family in the Fusarium oxysporum Species Complex" (2022). *Masters Theses*. 1246.
https://doi.org/10.7275/30861899 https://scholarworks.umass.edu/masters_theses_2/1246

This Open Access Thesis is brought to you for free and open access by the Dissertations and Theses at ScholarWorks@UMass Amherst. It has been accepted for inclusion in Masters Theses by an authorized administrator of ScholarWorks@UMass Amherst. For more information, please contact scholarworks@library.umass.edu.

Characterization of the Poly (ADP-Ribose) Polymerase family in the *Fusarium oxysporum* species complex

A Thesis Presented

by

DANIEL H. NORMENT

Submitted to the Graduate School of the University of Massachusetts Amherst in partial fulfillment of the requirements for the degree of

MASTER OF SCIENCE

September 2022

Molecular and Cellular Biology

Characterization of the Poly (ADP-Ribose) Polymerase family in the *Fusarium oxysporum* species complex

A Thesis Presented

by

Daniel H. Norment

Approved as to style and content by:

_____ Li-Jun Ma, Chair

_____ Ludmila Tyler, Member

_____ John Gibbons, Member

_____

Tom Maresca

Graduate Program Director

Molecular and Cellular Biology

DEDICATION

I dedicate this work to my friends and family. I would not be able to be where I am today without their unwavering love and support.

ACKNOWLEDGMENTS

I would first like to thank Professor Li-Jun Ma, who in both my undergraduate and graduate careers has been a fantastic mentor and pushed me to become a better scientist. Dr. Ma has been an incredible and thoughtful PI whose passion for research has helped to teach me perseverance, communication, and how to think like a scientist. It has truly been an honor to be a part of the Ma lab over the past year. I would also like to thank Professors Ludmila Tyler and John Gibbons for agreeing to be members of my thesis committee, and for all of their help and advice over the past year.

I would like to extend a special thank you to Dr. Shira Milo Cochavi, who served as my mentor for this project. Dr. Milo Cochavi provided tireless contributions and served as an inspiring leader of the PARP team. I would also like to thank Cecelia Murphy, whose hard work and dedication to the PARP project was instrumental for the success of this research.

Finally, I would like to thank all of the members of the Ma lab who provided support and friendship over the past year and helped to create an environment where I was excited to go into the lab every day. I would also like to thank Dr. Daniel Hebert and his lab for their invaluable advice about my project, in addition to their generosity of allowing me to use their lab's equipment.

This project was supported by the Natural Science Foundation (IOS-165241) and the National Eye Institute of the National Institutes of Health under award number: R01EY030150.

ABSTRACT

CHARACTERIZATION OF THE

POLY (ADP-RIBOSE) POLYMERASE FAMILY IN THE

***FUSARIUM OXYSPORUM* SPECIES COMPLEX**

SEPTEMBER 2022

Daniel Norment, B.S., UNIVERSITY OF MASSACHUSETTS AMHERST

M.S., UNIVERSITY OF MASSACHUSETTS AMHERST

Directed by: Professor Li-Jun Ma

Fusarium oxysporum is a filamentous fungus that is known to invade over a hundred different hosts and poses a major threat to the economy and food supply world-wide. Poly (Adenosine diphosphate-Ribose) Polymerase (PARP) is a family of regulatory proteins that affect change in the cell through transfer of ADP-Ribose moieties onto target molecules. The most well-studied PARP protein is the human PARP1, a PARylating nuclear protein that serves as our model PARP protein. *F. oxysporum* was found to contain a large expansion of PARP catalytic-domain-containing proteins compared to other filamentous fungi. We utilized *in silico* multiple sequence alignments and domain predictions to identify a human PARP1 homolog termed foPARP1 that was conserved within the core chromosomes in all three strains within our comparative system. Our *in silico* predictions also stated that only one strain, an Arabidopsis pathogen, Fo5176, contained several other predicted catalytically active PARP homologs within the accessory chromosome. To test the effect that foPARP1 knockout would have on DNA damage tolerance, we created a *foParp1* knockout and found that only strains Fol4287 and

Fo5176 had a significant reduction in tolerance upon being plated with methyl methanesulfonate (MMS), a DNA alkylating agent. To test how global PARylation trends would be affected by *foParp1* knockout, we utilized immunodot-blotting with PAR antibodies to assess PARylation in total protein extracts. We found that all strains of the comparative system had the capacity to catalyze the synthesis of long PAR chains, while only Fo47 and Fo5176 had a significant PARylation increase when exposed to MMS, and no samples had a significant increase in PARylation within the *foParp1* knockouts. Finally, we utilized RNA-Sequencing to determine the transcriptional impacts that *foParp1* knockout would have and found aberrant DNA repair pathways and disruptions in stress responses. Taken together, we conclude that *foP*ARP1 is in fact a functional PARP1 homolog and exhibits similar post-transcriptional modification and transcriptional impacts as its human counterpart. However, we were not able to correlate PARP copy number with DNA stress tolerance, and further research would be needed to assess the full function of the PARP expansion.

TABLE OF CONTENTS

Page

LIST OF TABLES

Title Page

LIST OF FIGURES

Title Page

CHAPTER

1. INTRODUCTION

1.1 PARP1 and PARP protein family

1.1.1 What is PARP?

Enzymes in the Poly ADP-ribose Polymerase (PARP) family serve as master regulators of the cell. PARPs are involved in processes such as DNA repair, apoptosis, cell cycle control, and transcriptional regulation (Jubin, T. *et al.* 2016). The PARP family of proteins is conserved in all eukaryotes, except yeasts, and these enzymes share functional and sequence homology with exotoxins that can be found in several pathogenic bacteria (Alemasova, E. E. & Lavrik, 2019, Mikolčević, P., *et al*. 2021). The PARP family is characterized by a well-conserved catalytic domain; however, most PARP proteins contain additional domains such as the zinc finger domains of human PARP1 (hPARP1), WGR domain, BRCA1 C-Terminus (BRCT) domain and several others. PARPs are known for their ability to catalyze the transfer of ADP-ribose moieties from NAD+ via the hydrolysis cleavage of the N-glycosidic bond of the ribose and nicotinamide units followed by the attachment of ADP-ribose to other proteins, nucleic acids, small molecules, or PARPs themselves in a process called Poly(ADP)-ribosylation (or PARylation) (Bellocchi, D. *et al.* 2006). The addition of ADP-ribose can change the structure, function, and stability of the target molecule (Gibson, B. A. & Kraus, W. L. 2012). The PARP family can be largely classified into two major groups based on the substrates that the enzymes utilize: the Mono ADP-ribosylating (MARylating) proteins and the Poly ADP-ribosylating (PARylating) polymerases. The addition or transfer of a single ADP-ribose molecule to a protein is known as Mono ADP-ribosylation (MARylation) and is carried out by a multitude of PARP family members and related bacterial exotoxins, most notably PARP10 in humans and the

cholera exotoxin (Vyas, S. *et al.* 2014, Holbourn, K. P., *et al*. 2006). The synthesis and addition of a chain of ADP-ribose molecules, either in a linear or branched fashion, is referred to as PARylation. The best-characterized PARP is the human PARP1. hPARP1 is a PARylating nuclear protein which converts NAD+ into Poly ADP-ribose (pADPr or PAR) chains, which are then attached to other nuclear proteins, nucleic acids, or the PARP protein itself as a post-translational modification (Thomas, et al., 2019). The PARylation modifications created by PARP activity are quickly degraded in the cell by the protein poly ADP-ribose glycohydrolase (PARG) which serves as a PARP antagonist (Kamaletdinova, et al., 2019). The most well-known function of the pADPr chains is to signal for the attachment of other nuclear proteins, which are involved in a variety of different cellular processes, with DNA repair being the best-understood (Chaudhuri, et al., 2017). In its role as a DNA repair protein, PARP1 is responsible for detecting DNA damage, including mismatched bases and strand breaks, and attaching to these abnormal structures and auto-modifying the PARP BRCT domain, which serves as a scaffold for the recruitment of other DNA repair proteins (Thomas, C. *et al.* 2019, Gibson, B. A. & Kraus, W. L. 2012). The most similar human PARPs to PARP1 in structure and function are hPARP2 and hPARP3. Together with hPARP1, these human PARPs all localize in the nucleus and are the only known PARPs to directly bind to DNA damage sites (Amé, et al., 2004; Sousa, et al., 2012). Generally, the length of the chain influences the signaling effect of the modification; two examples of varying activity based on length are: short chains are catalyzed and automodified onto the PARP1 protein in order to signal for DNA repair protein recruitment, while longer and branched chains can be attached to histone tails to allow for chromatin remodeling (Thomas, et al., 2019). Much of the previous research into PARP1 has focused on the protein's DNA repair activities; however, PARP1 also interacts with several other critical cellular pathways such as

glycolysis, transcription, chromatin remodeling, cell cycle progression, messenger RNA (mRNA) splicing, and apoptosis, making PARP1 a prime target for investigation to gain insight on a multitude of important cellular processes (Thomas, et al., 2019; Chaudhuri, et al., 2017; Fouquerel, et al., 2014; Matveeva, et al, 2016).

1.1.2 PARP1 protein structure

The human PARP1 is a 166 kDa protein that is the most abundant member of the PARP family and localizes within the nucleus (Amé, J.-C., *et al*. 2004). PARP1 consists of several domains, most notably the catalytic domain which is conserved in all members of the PARP family from bacteria to humans (Jubin, T. *et al.* 2016, Aravind, L., *et al*. 2014). While the catalytic domain is not well-conserved on an amino acid level, there is a well-conserved secondary structural motif in the catalytic domain of all PARPs, known as the catalytic ADP-ribose transferase (ART) loop (Cohen, M. S. & Chang, P. 2018). The ART loop is responsible for highly specific NAD+ binding and processing and generally consists of two halves of a beta sheet, one antiparallel in orientation and one mixed, that encompass at least three strands (Barkauskaite, E., *et al*. 2015). The ART loop functions by binding specifically to NAD+ through its amide group, while putting strain on the N-glycosidic bond that connects the nicotinamide molecule to the rest of the NAD+ molecule (Cohen, M. S. & Chang, P. 2018). There are two major conserved catalytic amino acid sequences within the ART loop which divide the PARP family into two groups, the H-Y-E family and R-S-E family (Alemasova, E. E. & Lavrik, 2019, Mikolčević, P., *et al*. 2021). The family that we will focus on contains the eukaryotic PARPs and notable bacterial ADP transferases and is characterized by the Histidine-Tyrosine-Glutamate (H-Y-E) motif, which will be explained in depth in chapter 1.3.2. Many PARPs contain several other domains, which

mainly aid the enzyme in protein-protein interactions or protein-nucleic acid interactions or serve a regulatory role. hPARP1 for example contains three other major domain types: the zinc finger domains, BRCT domain, and the Trp-Gly-Arg (WGR) domain. The zinc finger domains, labeled ZnI, ZnII and ZnIII, are responsible for DNA interaction and intramolecular folding. One proposed mechanism is that the zinc fingers I and II act as "legs" which walk along the chromatin scanning for lesions within the DNA and once found will bind to the damaged region and begin a pADPr response (Thomas, C. *et al.* 2019). The zinc finger III domain has been implicated in intramolecular folding, and along with the WGR domain, aids in reducing the distance between the catalytic domain and automodification domain during DNA damage response (Jubin, T. *et al.* 2016). The automodification domain, consisting of the BRCT domain, is the location where the pADPr chain is attached and elongated when PARP1 automodifies itself; this domain has been shown to facilitate protein-protein interaction (Alemasova, E. E. & Lavrik, O. I. 2019, Amé, J.-C., *et al*. 2004). Other notable domains in PARP1 or other PARP family members include the PARP regulatory domain, the Ubiquitin Conjugating (Ubc) domain of fungal PARPs, and the WWE motif (Amé, J.-C.,*et al*. 2004).

1.2 PARP function and related pathways

1.2.1 Metabolism of NAD+

Nicotinamide adenine dinucleotide (NAD+) is an important metabolite and coenzyme whose best-known role in the cell is as a redox factor during aerobic respiration in eukaryotes. NAD+ is an integral player in oxidative phosphorylation, allowing for the transport of protons which help drive the production of adenosine triphosphate (ATP), the energy currency within the cell. However, NAD+ can also serve as a substrate for other cellular consumers such as sirtuins and,

most importantly for this study, the PARP family of proteins (Rongvaux, A., *et al*. 2003, Croft, T., *et al*. 2020). NAD+ pools in the cell are tightly regulated and can be created by three major pathways, the *de novo* pathway, the Nicotinamide (NAM) salvage pathway (Figure 1), or the Preiss–Handler pathway (Croft, T., *et al*. 2020, Covarrubias, A. J., *et al*. 2021). The *de novo* pathway, the most energetically and materially expensive pathway, is generally used when the cell is low on NAD+ and converts Tryptophan into NAD+. (Croft, T., *et al*. 2020, Covarrubias, A. J., *et al*. 2021). The *de novo* pathway begins with Tryptophan being converted into Quinolinate via several enzymatic reactions; then a phosphoribose unit is added, creating a nicotinic acid mononucleotide (NaMN) molecule, where an AMP group from ATP is added to create nicotinic acid dinucleotide (NaAD), and finally an amide group is added to NaAD to create the NAD+ molecule (Croft, T., *et al*. 2020, Covarrubias, A. J., *et al*. 2021). The Preiss-Handler pathway begins with dietary nicotinic acid, which is converted into NaMN, which is then transformed into NaAD and finally converted to NAD+ (Croft, T., *et al*. 2020, Covarrubias, A. J., *et al*. 2021). Finally, the energetically preferred pathway, the NAD+ salvage pathway, begins with nicotinamide, a byproduct of NAD+-dependent enzymes that is converted into NMN and finally transformed into NAD+ (Croft, T., *et al*. 2020, Covarrubias, A. J., *et al*. 2021) (Figure 1). Importantly in the context of the PARP family, the byproduct of the PARylation reaction, nicotinamide, may serve as a PARP inhibitor at high concentrations, likely to ensure that there are sufficient amounts of NAD+ available for the cell to have adequate ATP supply (Salech, F., *et al*. 2020). Overactivity of PARP, generally caused by excessive DNA damage, leads to the depletion of NAD+, which is thought to starve the cell of ATP. Overactivity of PARP has been linked to the release of apoptosis-inducing factor (AIF) and a cell death pathway unique to PARP termed Parthanatos. Two theories as to the cause of AIF release are either that

the starvation of NAD+, and thus the starvation of ATP and cellular energy, causes the release of AIF from the mitochondria or that PAR polymers help to escort AIF out of the mitochondria and into the nucleus (David, K. K. 2009). Maintaining sufficient pools of NAD+ is important to keep the cellular energy demands met and allow for PARP-mediated regulation to maintain a properly functioning homeostasis.

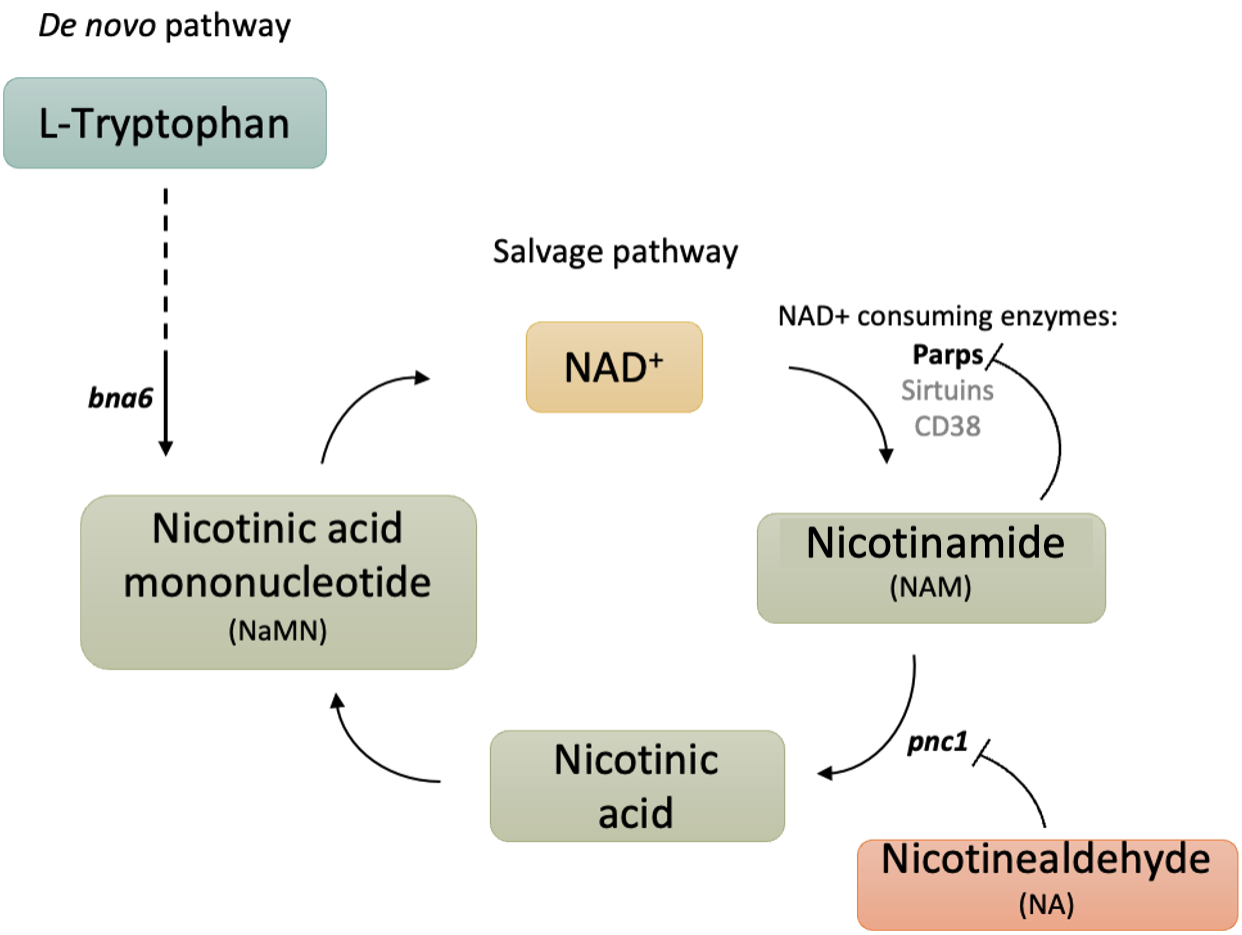

Figure 1: Diagram showing the de novo and salvage pathways of NAD+ metabolism. Figure created by Shira Milo Cochavi.

1.2.2 Metabolism and catabolism of poly(ADP-ribose)

Adenosine diphosphate (ADP) ribose is a nucleic acid, created by PARP proteins by the cleavage of the nicotinamide group belonging to a β-NAD+ molecule (Suskiewicz, M. J., *et al*. 2021). The phosphate backbone of ADP-ribose gives the molecule a bulky size, a large negative charge, and the ability to flex and bend, similar to nucleotides. PAR chains of two or more ADP-ribose molecules are most commonly connected through the 1' ribose to 2' hydroxyl group of the adenosine, creating linear pADPr chains, while ribose-to-ribose bonds will create branched pADPr chains (Ruf, A., *et al*. 1998, Leung, A. K. L. 2014). The addition of pADPr onto proteins can occur on multiple types of amino acids, including aspartate, glutamate, and lysine (Leung, A. K. L. 2014, Burkle, A. 2005). Human PARPs 1-3 have also been shown to be able to add ADP-riboses to DNA containing single- or double-strand breaks, with PARP10, 11, and 15 being able to MARylate single-stranded RNA (Groslambert, J., *et al*. 2021). MARylation and PARylation are reversible modifications, with the removal of pADPr chains primarily being catalyzed by the PARG and the removal of single ADP-ribose molecules being performed by ADP-ribosylhydrolase 3 (ARH3) or macrodomain-containing enzymes such as TARG1 (Leung, A. K. L. 2014, Slade, D. 2020, Groslambert, J., *et al*. 2021). PARG, the primary pADPr regulator of the cell, has the ability to cleave the ribose-adenosine bonds that create the pADPr chains, but is not able to remove terminal ADP-ribose molecules from their attachment to amino acids (Ahel, I. 2021). PARG has a high affinity for pADPr chains, so although there is significantly less PARG present in a nucleus when compared against PARP1, the catabolism of pADPr is a rapid process with most pADPr signals being eliminated minutes after PAR production (Alvarez-Gonzalez, R. & Althaus, F. R. P1989). PAR is cleaved into either single ADP-ribose units, or free chains, which can then be utilized in ATP-producing pathways (Wright, R. H. G. *et al.* 2016, McLennan, A. G. 2006). The misregulation of ADP-ribose can disrupt a well-concerted signaling cascade

and therefore may cause increased sensitivity to DNA damage and alteration to the transcriptional program. Thus, a timely and dynamic relationship between the creation and removal of ADP-ribose is essential for a properly regulated cell.

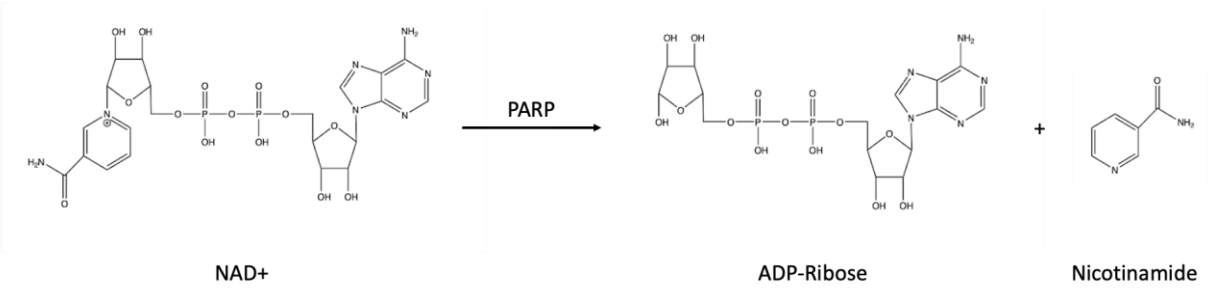

Figure 2: Model of the reaction of NAD+ into ADP-Ribose and Nicotinamide catalyzed by PARP.

1.2.3 The role of PARP1 in DNA repair

The best-defined role of PARP1 in human cells is its function as a DNA repair protein. Major DNA repair pathways in which PARP1 has been implicated are base excision repair (BER), nucleotide excision repair (NER), single-strand break repair (SSBR), and double-strand break repair (DSBR). SSBR begins with detection of a break, followed by end processing where a damaged 3' or 5' end is restored to normal, and finishing with gap filling and ligation (Caldecott, K. W. 2008). DSBRs proceed by two primary repair pathways, the error-free homologous recombination and error-prone nonhomologous end joining (NHEJ) pathways. Homologous recombination is the process whereby the repair machinery uses sister chromatids to find DNA sequences homologous to the site of the break in order to ensure accurate repair of the DNA (Vítor, A. C., *et al*. 2020, Chatterjee, N. & Walker, G. C. 2017). NHEJ is the most common of the DSBR pathways and is performed by ligating the nonhomologous DNA regions around the location where the break occurred (Vítor, A. C., *et al*. 2020, Chatterjee, N. & Walker, G. C.

2017). BER is performed for simple base modifications in DNA and does not cause significant changes in the structure of the double helix; in this process, a single strand break is caused and one base or a small number of bases are excised and replaced (Liu, Y. *et al.* 2007, Chatterjee, N. & Walker, G. C. 2017). NER is performed when bulky adducts are detected in DNA; either GG-NER is activated for global genome repair, or TC-NER is activated if replication machinery is stalled by the bulky adduct (Chatterjee, N. & Walker, G. C. 2017). PARP1 was originally shown to be involved in DNA repair due to its increase in expression and activity following DNA lesion creation, and DNA-damaging agents are often used to this day to stimulate PARP1 response (Semighini, C. P., *et al*. 2006, Hopp, A.-K. *et al.* 2021). Basal PAR amounts in the cell are low; however, upon DNA damage the activity of PARP1 can increase 10- to 500-fold (D'Amours, D., *et al*. 1999). PARP1 serves as a DNA damage detector with the ability to recruit other DNA repair enzymes to begin a variety of single-strand break (SSBR) repair pathways such as base excision repair (BER) and global genome nucleotide excision repair (GG-NER) and was shown to be involved in double-strand break (DSB) mechanisms such as homologous recombination (Ray Chaudhuri, A. & Nussenzweig, 2017, Morales, J. *et al.* 2014). The zinc fingers I and II "scan" the DNA for aberrant structures, such as single-strand breaks or bulky adducts, where the zinc fingers will attach to the lesion (Sousa, F. G. *et al.* 2012). After zinc finger I and II attachment, ZnIII's loop will associate with the DNA-bound ZnI loop to initiate a conformational change that will bring the WGR domain in contact with the ZnI and ZnIII domains (Langelier, M.-F., *et al*. 2012). This conformational change will allow for the catalytic domain to come into contact with ZnIII close to the site of DNA damage, which will allow for the PARP1 automodification reaction, creating a chain of pADPr on the BRCT domain (Thomas, C. *et al.* 2019). Human PARP1 heavily relies on its zinc finger domains in its detection of DNA lesions;

however, not all DNA-binding PARPs have zinc finger domains, and the process by which these PARPs interface with DNA is unclear. Many DNA-interacting PARPs contain a WGR domain, a well-known DNA interacting domain that is believed to be utilized to interact with nucleotides (Huambachano, O., *et al*. 2011). Other studies suggest that some PARPs may form protein complexes with non-PARP proteins to facilitate DNA interaction (Schreiber, V., *et al*. 2006). Once PARP1 has been automodified, the large negative charge intrinsic to pADPr chains will begin to disassociate PARP1 from DNA, given that their negative charges will repel, and the pADPr chain will serve as a scaffold for the recruitment of other DNA repair proteins. As stated earlier, the size and structure of pADPr chains are dictated by the type of DNA lesion or the protein with which PARP1 is associated, serving as a "code" for the recruitment of the correct protein for the job, based on PAR identification motifs on the attracted protein(s) (Kamaletdinova, T., *et al*. 2019, Teloni, F. & Altmeyer, M. 2016, Leung, A. K. L. 2014).

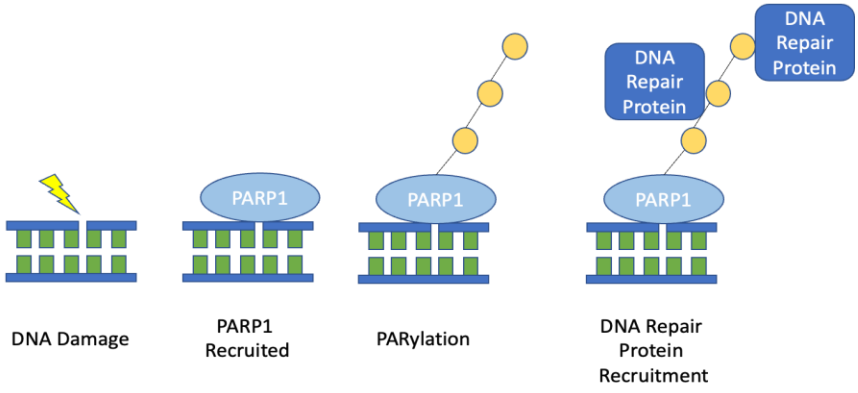

Figure 3: Simplified model of PARP1's role in identifying DNA damage and recruitment of DNA repair proteins through the autocatalytically added PAR chains of PARP1.

1.2.4 PARP1 function in chromatin remodeling and epigenetics

Epigenetics is the study of non-genetic changes that affect a DNA sequence. A notable form of epigenetics is the modification of histones, the proteins that compact and organize DNA. Directly related to the involvement of PARP1 in DNA repair pathways is its role as a chromatin remodeling protein (Morales, J. *et al.* 2014, Ray Chaudhuri, *et al*. 2017). PARP1 can indirectly affect chromatin structure through the recruitment of other chromatin remodeling proteins such as xeroderma pigmentosum group C-complementing protein (XPC), which relaxes chromatin structure during the GG-NER pathway (Ray Chaudhuri, *et al*. 2017). However, PARP1's chromatin remodeling activity is not just limited to the recruitment of other nuclear proteins; PARP1 also has the ability to interact with histone subunits to modulate chromatin structure (Messner, S. *et al.* 2010, Kim, M. Y., *et al*. 2004, Thomas, C. *et al.* 2019). During DNA damage repair, PARP1 has been shown to be able to PARylate lysines in the tail regions of all four core histones, causing histone relaxation and allowing for the recruitment of DNA repair proteins (Messner, S. *et al.* 2010). PARP1 is able to interact with the H4 histone subunit through the PARP1 BRCT domain contained within the automodification region, which triggers PARP1 automodification of pADPr chains, causing histone loosening and allowing transcription factors to access the gene contained within the nucleosome (Thomas, C. *et al.* 2019). PARP1 and histone 1 (H1) have been shown to competitively bind to the chromatin, with H1-bound nucleosomes found to be in a highly condensed state, while PARP1-bound nucleosomes were found in a slightly more relaxed conformation (Kim, M. Y., *et al*. 2004). Interestingly, in NAD+-depleted environments, PARP1 bound to the linker region of the nucleosome was shown to reduce transcription, but upon the addition of NAD+ and subsequent automodification of pADPr chains, PARP1 was released from the linker region and transcriptional activity was restored to the nucleosome (Kim, M. Y., *et al*. 2004). Due to pADPr's strong negative charge, it

has been suggested to outcompete other polynucleotides in associating to positively charged nuclear proteins, such as histones, likely explaining the chromatin loosening properties of PARylated PARP1 (Leung, A. K. L. 2014, Ummarino, S., *et al*. 2021).

PARPs are able to post-transcriptionally apply mono- and poly-ADP-ribose core and linker histones, but this is not the extent of the ability of PARP1 to interact with the epigenome (Ummarino, S., *et al*. 2021). Given that specific amino acids of histones are acceptors of multiple different modifications, from methylation to phosphorylation, it stands to reason that PARP1 does compete with other epigenetic factors to modify chromatin (Hottiger, M. O. 2015). Similarly, PARylation can occur on phosphorylated proteins, but phosphorylation is reduced once a protein is PARylated. PARylation can occur on acetylated histones; however, hyperacetylation seems to block PAR addition, possibly suggesting competitive binding (Hottiger, M. O. 2015). Another NAD+-dependent protein group, Sirtuins (SIRTs), are well-conserved nuclear deacetylases, raising the possibility that PARPs and SIRTs compete in low-NAD+ environments. In mice, it has been shown that ADP-ribosylation of H1 in the hippocampus releases the histone from promoters involved in memory, suggesting ADP-ribosylating epigenetics can modulate expression (Hottiger, M. O. 2015). In a more indirect fashion, PARP1 PARylation of the lysine-specific demethylase 4D (KDM4D) protein allows for the demethylation of histone H3 lysine 9 trimethylation, an epigenetic marker associated with compact chromatin, causing a reduction in chromatin compaction and allowing for DNA damage response to occur in heterochromatin regions (Ummarino, S., *et al*. 2021).

1.2.5 PARP1 effects on transcriptional regulation and alternative splicing

As stated in the previous subchapter, PARP1 has a role in the regulation of chromatin structure, allowing or restricting access to genes; however, this is only part of the role of PARP1 in transcriptional regulation (Kim, M. Y., *et al*. 2004, Thomas, C. *et al.* 2019). PARP1 functions as a recruiter of promoter- and other DNA-binding factors (Kraus, W. L. & Lis, J. T. 2003). In a similar fashion to its DNA repair response, PARP1 can serve as a scaffold, attaching to promoters and enhancers, allowing nuclear proteins to initially bind to PARP or the PAR chain and begin to form the necessary complexes to promote transcription (Kraus, W. L. & Lis, J. T. 2003). A well-known transcriptional interaction of PARP is its role in the regulation of the inflammatory pathway via interactions with the transcription factor Nuclear factor kappa B (NF-κB) (Kamaletdinova, T., *et al*. 2019, Burkle, A. 2005). NF-κB is an inflammatory pathway protein which activates the transcription of several genes involved in cytokine release (Oliver, F. J. 1999). PARP1-knockout mice have been shown to have defective expression of proteins downstream of NF-κB, implying that PARP1 is a key regulator of this pathway; however, the exact mechanism is not well-understood (Oliver, F. J. et al. 1999, Kamaletdinova, T., *et al*. 2019). Another example is that PARP1 has been found to facilitate complex formation of Elongation factor of RNA Polymerase II (ELL2) proteins, which are responsible for the transcription of important HIV-1 genes, revealing that PARP1 has key roles not only in normal transcription but also in the expression of viral proteins within a disease context (Yu, D.,*et al*. 2018). Additionally, PARP1 has been found to be recruited to certain promoter regions by promoter RNA (pRNA), where PARP1 attaches to the promoter region of a gene and subsequent automodification of PARP1 represses transcription, like in the case of ribosomal DNA in *Drosophila* (Hottiger, M. O. 2015). PARP1 has also been observed to directly repress transcription by binding to regions upstream of promoters or directly on specific introns,

blocking transcription (Kraus, W. L. 2008). Interestingly, catalytic activity is not necessary for some transcriptional regulation, as shown in *Drosophila* by the catalytic-domain-lacking PARP-e isoform, which can impact the transcription of fully functional PARPs (Tulin, A., *et al*. 2002).

PARP1 can impact not only the transcription of genes but also the processing and maturation of mRNA. RNA splicing is thought to occur simultaneously during transcription and greatly improves the diversity of proteins that a eukaryotic cell is able to produce (Matveeva, E. *et al.* 2016). Splicing factors are often impacted by DNA sequences, chromatin formation and histone modifications, while splicing itself was suggested to promote stalling of RNA polymerization (Ray Chaudhuri, A. & Nussenzweig, A. 2017). PARP1 has been shown to block RNA polymerase, either through automodification when bound to DNA or with the PARylation of histones in the path of the polymerase (Matveeva, E. A., *et al*. 2019). PARP1 has also been found to bind to pre-mRNA, splicing factors, and histones, suggesting that PARP1 acts as a bridge for the recruitment of splicing factors to active transcription sites (Matveeva, E. *et al.* 2016, Ray Chaudhuri, A. & Nussenzweig, A. 2017). PARP1 has been shown to indirectly affect alternative splicing by modifying splicing proteins through direct protein-protein interaction, direct PARylation of the proteins, and interaction between PAR and splicing proteins containing PAR-reading domains (Ray Chaudhuri, A. & Nussenzweig, A. 2017). In the processing of pre-mRNA into mature mRNA, one of the final steps is the creation of the poly-Adenosine tail, catalyzed by the poly(A) polymerase (PAP) protein. During heat shock, PARP1 has been shown to bind to and PARylate PAP proteins, causing detachment of PAP from the mRNA, leading to decreased poly-Adensoination, which ultimately affects the trafficking of the mRNA (Di Giammartino, D. C., *et al*. 2013). PARP1 is thought to affect mRNA stability, as indicated by an increased RNA decay in PARP1-knockout *Drosophila* cell lines; however, the exact mechanism

of this interaction is not known (Matveeva, E. A., *et al*. 2019). Finally, PARP1 has been implicated in ribosome synthesis, as during non-stress conditions, 40% of PARP1 is localized within the nucleolus, the region where ribosome biosynthesis and tRNA creation occurs (Ray Chaudhuri, A. & Nussenzweig, A. 2017). PARP1 likely serves a guardian role to protect ribosomal DNA (rDNA) from damage, has roles in interacting with several nucleolar proteins, and potentially affects ribosome biosynthesis via its influence on transcription (Meder, V. S., et al. 2005, Ray Chaudhuri, A. & Nussenzweig, A. 2017).

1.3 Other PARP family members and related proteins

1.3.1 Other Human PARPs

Although PARP1 is the best-studied and understood, 17 other known genes of the PARP family exist within the human genome. PARPs 1-5b are currently the most understood, with PARPs 6-17 being the least; however, there have been recent strides to uncover the function and interactome of these PARPs, as well. The human PARPs are generally separated into three groups: the PARylators (PARPs 1, 2, 5a, and 5b), the MARylators (PARPs 3, 4, 6-8, 10-12, 14-16), and the catalytically inactive (9 and 13) (Amé, J.-C., *et al*. 2004, Vyas, S. *et al.* 2014). In humans, the most similar PARP family member to PARP1, both in conservation of the catalytic domain and in function, is PARP2. PARP1 and PARP2 have overlapping, but not redundant, functions, as shown by PARP1-deficient mice utilizing PARP2 to compensate for PARP1 loss, but PARP2 having exclusive protein binding partners that PARP1 does not share (Perina, D. *et al.* 2014,). PARP3 has been shown to MARylate substrates, with PARylation predicted but not conclusively shown. PARP3 localizes at centrosomes and is thought to impact mitotic checkpoints (Amé, J.-C., 2004). PARP4, a MARylator, is involved in the creation of vaults

nanoparticles, a ribonuclear complex thought to aid in stress responses (Prawira, A. *et al.* 2019, van Zon, A., *et al*. 2003,Frascotti, G. *et al.* 2021). The tankyrase PARPs, PARP5a and PARP5b, are both PARylators with overlapping functions and binding partners; these PARPs are involved in telomere maintenance, signaling, and vesicle transport (Kim, M. 2018, Amé, J.-C., 2004). PARP6 is a MARylator that has been shown to regulate dendrite morphogenesis in the mouse hippocampus, likely through interactions with microtubules (Huang, J. Y., *et al*. 2016, Vermehren-Schmaedick, A. *et al.* 2021). PARP7, a MARylator, has been shown to interact with interferons and plays a role in cancer signaling (Gozgit, J. M. *et al.* 2021, Kamata, T., *et al*. 2021). PARP8, a MARylator, has had no known studies on its function, but is believed to be an oncogene based on its overexpression in colorectal cancer (Yu, Z. L. & Zhu, Z. M. 2022). PARPs 9 and 14, the macroDomain-containing PARPs, are involved in macrophage activation and inflammatory regulation, often thought to be acting as antagonists against each other (Iwata, H. *et al.* 2016, Hakmé, A., et al. 2008). PARP10 is a MARylator capable of automodification and has been implicated in several important pathways such as metabolic regulation, ubiquitin transfer, mRNA regulation, and G1 phase progression (Márton, J. *et al.* 2018, García-Saura, A. G. & Schüler, H. 2021, Chou, H.-Y. E., *et al*. 2006). PARP11, a MARylator, is involved with the immune response, primarily through its interactions with interferon receptors (Guo, T. *et al.* 2019, Guo, T. *et al.* 2019). The rest of the human PARP family, PARPs 12, 13, 15, 16, and 17 are all believed to be MARylators, with the exception of PARP 13, which is hypothesized to be catalytically inactive; although great strides have been taken recently to understand the functions of these PARPs and their impacts within the cell, these family members are relatively unexplored as compared to the previously described PARPs (Vyas, S. *et al.* 2014).

1.3.2 Bacterial ADPRTs and their role in virulence

The proteins mentioned thus far have been members of the PARP family; however, any protein that catalyzes the transfer of ADP-ribose moieties belongs to the larger ART superfamily. Although we have focused on human PARPs as a model for ADP-ribose transferases, this reaction occurs in both prokaryotes and eukaryotes (Perina, D. *et al.* 2014). Many notable bacterial pathogens, such as *Vibrio cholerae* and *Corynebacterium diphtheriae*, utilize the hydrolysis and addition of mono-ADP-ribose units to interfere with important host regulatory pathways (Holbourn, K. P., *et al*. 2006). These bacterial weapons, known as ADP-ribosylating toxins (ADPRTs), are generally protein-specific MARylators that irreversibly target proteins vital to major cellular functions, such as G-protein-coupled receptors, that when MARylated cause extensive misregulation that may promote cell death (Holbourn, K. P., *et al*. 2006, Mikolčević, P., *et al*. 2021). ADPRTs are thought to originate as part of conflict systems, as many viruses and bacteria use ADP-ribose-related proteins in pathogen-versus-host combat (Mikolčević, P., *et al*. 2021). Interestingly, no known poly-ADP-ribosylating proteins are present in bacteria, so it is believed that this is a uniquely eukaryotic expansion of ADP-ribose transferases (Perina, D. *et al.* 2014). There are two major families of ADPRT toxins, the diphtheria toxins (DTXs) and the cholera toxins (CTXs). The DTXs contain a conserved H-Y-E catalytic motif that is also found in many eukaryotic PARPs (Mikolčević, P., *et al*. 2021), while the cholera toxins contain a conserved R-S-E catalytic motif (Cohen, M. S. & Chang, P. 2018, Mikolčević, P., *et al*. 2021). In bacterial H-Y-E domains, the histidine forms hydrogen bonds with the adenine ribose and nicotinamide amide, the tyrosine engages in pi-pi stacking with the nicotinamide ring, and the glutamate is thought to stabilize intermediates (Cohen, M. S. & Chang, P. 2018). Within the R-S-E motif, the arginine interacts with the diphosphate backbone,

the serine hydrogen bonds with the nicotinamide ribose, and the glutamate plays the same role as in the H-Y-E motif. The positioning of NAD+ in the catalytic pocket between these two types of ADP-transferases is similar (Cohen, M. S. & Chang, P. 2018). The two major types of ADP-ribose transferases in eukaryotes, the PARPs and ectoARTS (also referred to as ADP-ribosyltransferase cholera-toxin-like or ARTCs), are inherited from these two major bacterial groups, with PARPs hailing from the H-Y-E motif transferases, and ectoARTs containing the R-S-E motif (Cohen, M. S. & Chang, P. 2018).

1.3.3 Fungal PARPs

Although there has been great progress in the understanding of bacterial ART toxins and human PARPs, the role of PARPs in fungal species is poorly understood. Fungi represent an interesting phylogenetic history with PARP proteins, with one intriguing example that several fungi, mainly yeasts, including *Saccharomyces cerevisiae*, have independently lost their PARP proteins (Citarelli, M., *et al*. 2010). The fungal kingdom does contain some unique PARP-related proteins; an example, which will be referred to in this paper as PARP-Ubc, is a protein that contains a long segment of amino acids with no known functional domains near the N-terminus, a relatively short PARP catalytic domain, and a Ubc domain near the C-terminus shared by *F. oxysporum, Aspergillus nidulans*, *Cryphonectria parasitica*, and other fungi (Citarelli, M., *et al*. 2010). It has been shown that there are conserved PARP1 homologs contained within many filamentous fungi, deemed *PrpA* in *Aspergillus nidulans*, which was shown to retain many functions of the human PARP1 such as DNA repair, apoptosis, and mediating cell cycle progression (Semighini, C. P., *et al*. 2006). There are a multitude of fungal-specific proteins that contain the PARP family catalytic domain; however, to the best of our knowledge, no one ever

investigated this unique expansion of PARP proteins. In this study, we will be examining the PARP family expansion within the *Fusarium oxysporum* species complex, in order to foster an understanding for the role that PARPs play within the fungal kingdom and specifically in a fungal plant pathogen.

1.4 Fusarium oxysporum

1.4.1 *Fusarium oxysporum* life and disease cycle

Fusarium oxysporum is a filamentous fungus which acts as a pathogen to a plethora of different hosts ranging from bananas and cotton to humans. *Fusarium oxysporum* is comprised of over a hundred host-specific strains, *formae speciales*, which reproduce asexually, forming three different types of spores known as macroconidia, microconidia, and chlamydospores (Gordon, T. R. 2017). *F. oxysporum* is a soil-borne pathogen which begins its colonization of a plant host by the germination of a spore into the root tissue (Gordon, T. R. 2017). The germinated spores then feed off of nutrients surrounding the plant roots, where the fungus begins the construction of sporangial germ tubes or mycelia that will eventually pierce into the cell wall of the plant root and begin to invade the root cortex (Gordon, T. R. 2017, G. N. Agrios, 1989). From there, *F. oxysporum* will advance and eventually colonize the xylem, where the fungal cells have greater access to nutrients. A mass of hyphae, spores and secreted compounds creates a blockage within the xylem that causes severe wilt symptoms and plant death (Gordon, T. R. 2017). The remaining *F. oxysporum* will invade other sections of the dying plant host and often persist in the soil, first around the dead host and for many years afterwards (Gordon, T. R. 2017).

1.4.2 Expansion of *Parp* genes in *F. oxysporum*

The genome of *F. oxysporum* is compartmentalized, consisting of two different chromosome types: core chromosomes and accessory chromosomes (Ma, et al., 2010). The core chromosomes harbor housekeeping and basic survival genes, while the accessory chromosomes contain a collection of genes that are involved in pathogenicity and host specificity and can be horizontally transferred (Ma, et al., 2010, Yang, H., *et al*. 2020). Accessory chromosomes contain different genomic landscapes, unique "lineage-specific" genes, and utilize different transposable elements as compared to their core chromosomes (Yang, H., *et al*. 2020). The core and accessory chromosomes have been described as a "two-speed genome" given that segments of the accessory chromosome are more prone to mutation and adaptation, likely to keep evolving in the arms race between host and pathogen interactions (Wang, Q. *et al.* 2017).

Comparative genomic analysis of multiple fungal species revealed that different strains of *F. oxysporum* have a variable number of PARP genes located in both the core and accessory chromosomes (Figure 4). For example: the non-pathogenic strain Fo47 contains 3 core PARPs and no accessory PARPs, the tomato pathogen Fol4287 contains 3 core PARPs and 3 accessory PARPs, the human pathogen MRL8996 contains 3 core PARPs and 6 accessory PARPs, and Fo5176, which infects *Arabidopsis thaliana*, contains 2 core PARPs and 18 accessory PARPs. One commonality is that all of these strains contain a copy of a *Parp1* homolog, a copy of a Ubc *Parp* and in most cases an additional one *Parp* gene that encodes a relatively short PARP catalytic-domain-containing protein on their core chromosomes.

1.4.3 *F. oxysporum* as a model to study genomic expansions

The genus Fusarium contains over 300 phylogenetically closely related species that occupy very different ecological niches (Aoki et al., 2014). The Fusarium x graminearum species complex

contains airborne species that infect wheat and barley, resulting in destructive agricultural losses worldwide (Goswami & Kistler, 2004); the Fusarium oxysporum species complex includes common soil-borne pathogens that cause devastating wilt diseases on a wide range of plant crops (Michielse & Rep, 2009); and members of the Fusarium fujikuroi species complex cause a variety of diseases on hosts such as rice, maize and mango. In addition, several opportunistic Fusarium pathogens are common causes of onychomycosis, endophthalmitis, and skin and musculoskeletal infections in immunocompromised patients (Mansoory et al., 2003). The evolutionary processes, in terms of host specialization and lifestyle, that occurred over time in the genus, as well as the highly dynamic nature of the genome in F. oxysporum, are likely to be reflected as genomic signatures. Therefore, from an agroecological standpoint, Fusarium provides a unique comparative system to study specialized expansions of gene families. One example of a protein family expansion within the F. oxysporum species complex is the kinase family expansion (DeIulio, G. A. et al. 2018). Similar to PARPs, histidine kinase groups and the SPRKL family kinases were found to be largely absent from yeasts but present in high numbers in F. oxysporum with some kinases such as the HisKs not found in animals, similar to the fungal-specific PARP Ubc (DeIulio, G. A. et al. 2018). This expansion as a whole is thought to be linked to fungal pathogenicity, given the relatively large expansion and a few identified kinases being integral to pathogenicity (DeIulio, G. A. et al. 2018). Exploring gene expansions such as those observed for the PARP or kinase families will often lead to a better understanding of the functions of these proteins within a specific phylogenetic group and the discovery of potential targets that can be exploited for the development of novel antifungals.

1.5 Guiding questions for this body of work

Both the structure and function of PARP proteins have been well-characterized from bacteria to humans, with a rapidly growing focus on potential PARP-based therapies in recent years (Slade, D. 2020, Holbourn, K. P., *et al*. 2006). However, there has been virtually no comprehensive research on PARP homologues in fungi. The discovery of the unique expansion of PARP proteins in *F. oxysporum* raises many interesting questions about the nature and role of the highly conserved, in addition to the lineage-specific, PARP proteins in this species complex. Since the number of *Parp* gene copies varies greatly between different *F. oxysporum* strains, I have decided to utilize a comparative system consisting of three different strains that contain distinct numbers of *Parp* gene copies.

The very first question that I asked is whether the structure, at the amino acid level, may predict ADP-ribosylation activity by way of comparing these expansion proteins to functional ADP-ribose polymerases. For this purpose, I have used the human PARP1 protein as a reference and model to extract the highly conserved catalytic amino acid motif to conduct a comprehensive series of multiple sequence alignments to reveal the conservation level of those amino acids in our FO PARP proteins. I then asked if any catalytic similarity between those fungal PARPs and ADRT bacterial exotoxins exists and used both multiple sequence alignment and phylogenetic trees to answer this question.

Given that at least some of the copies have shared key catalytic amino acids that are predicted to allow for PAR- or MARylation, I asked whether this genomic expansion is translated into a functional role within the fungus cell. Quantitative reverse-transcriptase polymerase chain reaction (qRT-PCR) was performed to determine gene expression for all *Parp* genes in our comparative system, showing a significant induction of all the highly conserved

Parp genes located on the core chromosomes and a mixed transcriptional response of the lineage-specific copies. I used the DNA-damaging agent methyl methanesulfonate to assess the differences in DNA damage sensitivity during hyphal growth between the strains and quantified these differences using two survival assays.

Next, I used a biochemical approach and developed an immunodot-blot assay to specifically semi-quantify the differences in poly-ADP-ribose chain levels between the strains. I incorporated *Parp1*-deficient strains that were generated in the lab into the comparative system and used the dot-blot assay to determine the effect of the deletion of *Parp1* on ADP-ribose levels within the different strains.

Finally, given the role of hPARP1 in transcription regulation, the last question I posed is "What is the impact of the deletion of *Parp1* on transcriptional response to DNA damage?". For that, I chose a representative strain, Fol4287, and conducted RNA Sequencing (RNA-Seq) analysis of both wild-type and a *Parp1* mutant under DNA-damage conditions.

CHAPTER

2. MATERIALS AND METHODS

2.1 Fungal strains used in this work

All the strains used in this work are listed in Table 1. The *Fusarium oxysporum* strains *F. oxysporum* f. sp. *lycopersici* (Fol4287), Fusox_FO47 (Fo47), and Fox_Fo5176 (Fo5176) were chosen for all experiments due to their differential PARP family gene copy numbers. Fo47 contains 3 core *Parp* genes with no *Parp* genes on its accessory chromosomes, Fol4287 contains 3 core *Parp* genes with an additional 3 accessory *Parp*s, and Fo5176 contains 2 *Parp* genes on its core chromosomes with 18 additional accessory *Parp*s. These three strains were selected for the comparative system as they will provide insight into the role that both the core and accessory genes play in DNA-damage response and tolerance, PARylation activity, and transcriptional regulation. All three strains share a highly conserved *Parp1* homolog and a fungal-specific *Ubc-Parp* on their core chromosomes. Fo47 contains no additional accessory *Parp*s but shares one additional core *Parp* copy with Fol4287; therefore, this Fo47 strain is expected to give us insight into the function of the core *Parp* repertoire. Fo5176 contains the *Parp*1 and *Ubc-Parp* core homologs, while lacking the additional short core *Parp* shared by Fo47 and Fol4287; however, Fo5176 boasts the largest accessory chromosome collection of *Parp* genes at 18. The Fo5176 strain will provide insight into the effect that an expansive collection of accessory PARPs will have on a variety of phenotypes. Fol4287 acts as a bridge between Fo47 and Fo5176, containing the same core *Parp*s as Fo47 and three additional accessory PARPs shared with Fo5176. A total of six different strains has been used in this work (Table 1). *Parp1*-deficient strains were obtained using a CRISPR/Cas9 system in which the *Parp1* gene was replaced with an hygromycin resistance cassette. The mutated strains were validated by PCR and the deletion of

Parp1 and the insertion of the Hygromycin B gene were confirmed by Sanger sequencing. Mutant generation for all three strains was done in the Ma lab by Cecelia Murphy.

Table 1: Strains used in this work

Strain	Genotype
Fo47	**Wild-type Fo47**
Fol4287	**Wild-type Fol4287**
Fo5176	**Wild-type Fo5176**
Fo47 Parp1Δ	**Parp1Δ-deficient Fo47**
Fol4287 Parp1Δ	**Parp1Δ-deficient Fol4287**
Fo5176 Parp1Δ	**Parp1Δ-deficient Fo5176**

2.2. Fungal growth, conditions, and spore collection

2.2.1 Growth practices and conditions for *F. oxysporum*

Asexual spores (microcondia) of all the *Fusarium oxysporum* strains discussed in this work, Fol4287, Fo47, and Fo5176, were grown in liquid KNO3-based medium (1.36 g of yeast nitrogen base without amino acids, 24 g of sucrose, 8.08 g of KNO_3, and 800 mL of water) on an orbital shaker at 200 rpm for 5 days at 28°C. *Parp1*-deficient strains were supplemented with 150 µg/mL hygromycin to ensure only the growth of the mutant.

2.2.2 Spore collection and storage

The spores were filtered with Miracloth (EMD Millipore, Burlington, MA, USA) and centrifuged at 4000 x *g* for 10 minutes at room temperature, after which the supernatant was discarded and the pellet was resuspended in 1mL of sterile water. The resuspended pellet was then diluted 10,000-fold, and 10 uL of this dilution was placed on a hemocytometer, where the spores were counted. The concentration of the resuspended pellet was calculated using the hemocytometer-provided equation with the dilution taken into account. In any case, the resuspended pellets were stored at 4°C for no more than 72 hours.

2.3 *In silico* protein sequence analysis

2.3.1 Multiple sequence analysis

All fungal protein sequences were downloaded from the Joint Genome Institute (JGI) (https://genome.jgi.doe.gov/portal/) (April 7th, 2022), while all bacterial and human protein sequences were downloaded from National Center for Biotechnology Information (NCBI) (https://www.ncbi.nlm.nih.gov/gene/) (April 7th, 2022) gene database. Note that Fol4287 PARP proteins are labeled "FOXG_#"; this is the NCBI locus tag, while PARPs from Fo47 and Fo5176 will go by their JGI protein ID number. The catalytic domains of the PARP and PARP-related proteins were identified using InterPro (https://www.ebi.ac.uk/interpro/). To receive multiple sequence analysis, Multiple Alignment using Fast Fourier Transform (MAFFT) (https://www.ebi.ac.uk/Tools/msa/mafft/) was used with amino acid sequences as the input; the output format was ClustalW with character counts and the results were viewed using MView (https://www.ebi.ac.uk/Tools/msa/mview/).

2.3.2. Identification of conserved domains and amino acids

To predict the conserved domains within the *F. oxysporum* PARP-like proteins, we utilized InterPro to generate domain predictions for the amino acid sequences obtained from JGI. Based on Alemasova, E. E. & Lavrik, 2019, hPARP1 was used as the primary protein for alignment of the *F. oxysporum* PARP homologs, utilizing the known key catalytic residues, histidine 826, tyrosine 907, and glutamic acid 988 of the hPARP1, to gain insight into the catalytic capacity of the PARP homologs.

2.4 *In vitro* survival assays

2.4.1 Experimental design and conditions

To assess the differences in survival rate between the wild-type strains, spores of three independent biological replicates were plated on PDA (DB Difco, Sparks, MD, USA) plates supplemented with 0.001% methyl methanesulfonate (MMS) (EMD Millipore, India) in three different concentrations (10^4, 10^3, and 10^2 spores/mL) and were allowed to grow in the dark for 48 hours at 28°C. PDA plates with no additional supplements served as controls. Following 48 hours of incubation, the plates were scanned and imaged for a visual representation of the growth. For colony rescue, 500 spores of each strain were plated on control PDA plates and PDA plates supplemented with 0.0012% MMS and were allowed to grow in the dark for 48 hours at 28°C. Colony-forming units (CFUs) were counted and percentage of survival was calculated for each strain based on the ratio of MMS/PDA CFU number. Survival rates were plotted using the R statistical software (version 4.1.2) in RStudio (version 2022.02.3 Build 492) using the ggplot2 package (version 3.3.6) and p-values were calculated using the stat_compare_means() function with ‘method’ parameter set on ‘t.test’.

2.5 Immunodot-blot assay

2.5.1 Experimental design and conditions

In order to ensure maximum PARylation for dot-blot detection, $2x10^8$ spores of each strain were incubated in 10 mL of Potato Dextrose Broth (PDB) (BD Difco, Sparks, MD, USA) medium (19.2 g of Potato Dextrose Broth, 800 mL of water) in an orbital shaker at 200 rpm at 28°C for 3 hours. Following this, samples were removed from the orbital shaker and were split into two groups of samples: a control group with no added supplements and a group where 0.1% MMS, 2 µM of ADP-HPD (Sigma-Aldrich, St. Louis, MO, USA), and 1 mM of NAD+ (Sigma-Aldrich, St. Louis, MO, USA) were added. All samples were reinserted into the orbital shaker at the same rpm and temperature; both of the sample groups were collected after 20 minutes of additional incubation. Collected samples were centrifuged at 4000 x *g* at 4°C for 10 minutes, after which the supernatant was discarded.

2.5.2 Protein extraction and quantification

The pellets generated in the previous section were flash-frozen under liquid nitrogen and allowed to thaw in room temperature conditions. Once the pellets were beginning to thaw, they were vortexed with 125 µL of lysis buffer [40 mM potassium phosphate buffer, pH 7.0, 5 mM Ethylenediaminetetraacetic acid **(**EDTA), 0.1% Triton X-100, 20% glycogen, 1 ug of Dichlorodiphenyltrichloroethane (DDT), and 10 uL of plant protease inhibitor (Sigma-Aldrich, St. Louis, MO, USA) per mL]. Following lysis, the samples are sonicated using a Heat Systems W-385 Sonicator Ultrasonic Processor at 50% duty cycle for 1 second 5 times; samples were then shaken at 50 rpm on an orbital shaker for 15 minutes to allow for mixing of the extraction buffer solution with spores, and finally the samples were transferred to 1.5 mL Eppendorf tubes, where they were centrifuged at 13000 x *g* at room temperature for 10 minutes. The supernatant of the centrifuged samples are transferred to another 1.5 mL tube while the pellet was discarded.

Total protein extracts were quantified using the Bradford method with Bio-Rad Protein Assay Dye Reagent Concentrate (Bio-Rad Laboratories, Hercules, CA, USA) and Bovine Serum Album (Pierce Biotechnology, Rockford, IL, USA) serving as the standard for generating a standard curve; absorbance was measured at 595 nm wavelength. The total protein extracts were then stored at -20°C.

2.5.3 Immunodot-blot assay and signal quantification

Samples were thawed on ice and then diluted to a concentration of 10 µg/mL. Amersham Hybond-N Membranes (GE Healthcare Limited, Buckingshire, England) were cut into the shape of Bio-Rad Bio-Dot/Bio-Dot SF Filter Paper (Bio-Rad, USA), and two filter papers were stacked onto the membrane and submerged in TBS (Tris-Buffered Saline, pH 7.4, Thermo Fisher, Ottawa, ON, Canada) for 10 minutes. The Dot-Blot Apparatus was assembled using two soaked filter papers with the nylon membrane on top. Next, 225 µL of each sample was blotted onto the membrane while 225 µL of PBST (Phosphate-Buffered Saline, pH 7.4, Ottawa, ON, Canada with 0.1% Tween20, Fair Lawn, NJ, USA) was added into any slots where samples were not added. A light vacuum was applied until all of the samples had been vacuumed through the membrane, when an additional 225 µL of PBST was added to all wells. After all wells had been vacuumed empty, the Dot-Blot apparatus was opened and the membrane was removed and placed between two new filter papers, where it was then dried using a Model 583 Gel Dryer (Bio-Rad, USA) for 90 minutes at 80°C. Once the membrane was dried, the membrane was rehydrated in TBST (Tris-Buffered Saline, pH 7.5, with 0.1% Tween20) for 5 minutes. The membrane was then incubated in 10% formaldehyde solution for 20 minutes at 37°C. The membrane was then washed on an orbital shaker with TBS twice for two minutes. Next, the

membrane was placed between two filter papers and dried on a gel dryer for an additional hour at 80℃. The membrane was rehydrated with PBST for 5 minutes. From here, all washing and incubation steps were performed on an orbital shaker at 60 rpm. The membrane was then incubated with a blocking solution (5% Difco Skim Milk, Sparks, MD, USA, in PBST) for one hour. Following the incubation, the membrane was washed three times for 20 minutes each with PBST. Next, the membrane was incubated with the primary antibody solution [1:1000 Poly(ADP-ribose) monoclonal antibody (10H) (Enzo Biochem Inc., New York, NY, USA) in Blocking Solution] overnight at 4℃. The following morning, the membrane was washed three times for 20 minutes each with PBST. The membrane was then incubated with the secondary antibody solution [1:1000 Goat Anti-Mouse IgG Antibody, (H+L) HRP conjugate (EMD Millipore, St. Louis, Missouri, USA) in blocking solution] for one hour. The membrane was washed four times for 30 minutes in PBST. Next, 2.5 mL of Enhanced chemiluminescence (ECL) (Life Technology Corporation, Ottawa, ON, Canada) reagent 1 and 2 were mixed in a 1:1 ratio and pipetted evenly onto the membrane and allowed to incubate while covered for 2 minutes. The membrane was gently dried with filter paper and taken, covered, to a BioRad ChemiDoc Imaging System (Bio-Rad, USA) and imaged for chemiluminescence.

2.5.4 ImageJ Quantification and Statistical Significance

Once the membrane was imaged by the ChemiDoc, the image display was inverted and opened with ImageJ (version 1.53k). In ImageJ, the circle shape tool was used to draw a circle around the dots within the membrane and measure the signal intensity. A circle of the same size was used for all the analyzed dots. Signal intensity was also measured in at least four locations on the membrane image to allow for an average of the background signal. These data points were

entered into an Excel spreadsheet, where the mean background signal was calculated and subtracted from each of the sample measurements. The mean signal value of technical replicates was calculated and used for data points in further analysis. To test the statistical significance of these data points, a two way t-test was used to compare the differences between strains.

2.6 RNA-Seq analysis

2.6.1 Experimental design and conditions

To gain insight into the transcriptional impact that knockout of the core PARP1 homolog would have on *Fusarium oxysporum*, both wild-type and knockout mutant samples were created from the Fol4287 strain. Fol4287 was chosen as the candidate strain to undergo RNA sequencing because it contains the most well-characterized and annotated genome of the three strains and in preliminary dot-blot results exhibited a substantial increase in PARylation upon the addition of MMS. Fol4287 also serves as the "bridge" between the number of PARP accessory genes between Fo47 and Fo5176, containing all three core PARPs of Fo47 and sharing three of the accessory PARPs with Fo5176.

2.6.2 RNA extraction, quality control and quantification

For the creation of samples to be used in RNA sequencing, $2x10^8$ spores of both the wild-type and the PARP1 homolog knockout mutant, containing three biological replicates of each, were incubated in 10 mL of PDB media (19.2 g of Potato Dextrose Broth, 800 mL of water) in an orbital shaker at 200 rpm at 28℃ for 3 hours. Following this, samples were removed from the orbital shaker, and three groups of samples were created: a control group with no additional added reagents, and two groups with 0.1% MMS added. All samples were reinserted into the orbital shaker at the same rpm and temperature; one group of MMS-containing samples was

collected after 20 minutes of additional incubation, and the final MMS group and the control group were collected after 1 hour of additional incubation. Collected samples were centrifuged at 4000 x *g* at 4°C for 10 minutes, after which the supernatant was discarded. At this point the samples were flash-frozen with liquid nitrogen and stored at -80°C overnight. The following morning, the samples were allowed to thaw on ice; once thawed, the spores were ground using Red RINO lysis kit tubes (Next Advance, Troy, NY, USA) for 1 minute x 5 times. The QIAGEN RNeasy Plant Mini Kit was used for total RNA extraction, after which the RNA samples were stored at -80°C. Quality control was performed on the RNA samples by using a Qubit 3.0 Fluorometer (Life Technologies Holdings Pte Ltd, Singapore) with an Invitrogen™ Qubit™ RNA High Sensitivity (HS) Assay Kit to insure sufficiently concentrated RNA; the Agilent 2100 Bioanalyzer RNA 6000 Nano assay was performed to ensure sufficient quality of RNA. 18S and 28S were identified at the desired peaks and a RIN score for each sample was calculated based on the quality of the sample.

2.6.3 Library construction and sequencing

RNA samples were shipped to the Microbial Genome Sequencing Center (MiGS) (now referred to as SeqCenter, https://www.seqcenter.com/) to perform 25 million PolyA enrichment RNA reads on each sample. Services rendered on samples were DNAse treatment, mRNA (PolyA) enrichment, stranded library prep and sequencing. 2 x 51-bp double-stranded reads were received from MiGS in the form of fastq.gz files.

2.6.4 Quality control of raw data and read alignments

Fastq.gz condensed files were unzipped and passed through FASTQC to confirm that the files received were of high quality and uniform length and contained no adaptor sequence. A genome index of an annotated Fol4287 genome (GenBank ID GCA_003315725, 2018) was taken from the Joint Genome Institute (JGI). Mapping of raw data against the Fol4287 genome reference was performed using HISAT2 (version 2.0.5), with the original forward and reverse read fastq.gz files as input and SAM files as the output. Following alignment, unmapped reads were filtered out using the samtools (version 1.9) program view -F 4 commands with a BAM file as the output. Samtools was used again to sort the BAM files, followed by a flagging of duplicate reads using Picard (version 2.23.3) using the MarkDuplicates and "-REMOVE_SEQUENCING_DUPLICATES true" commands. Finally, the duplicate reads once flagged were removed with the samtools -rmdup command, and the final BAM files were indexed using the samtools command -index.

2.6.5 Read count

Raw reads were counted using the Python-based htseq-count program with the following parameters: --idattr parameter set to 'Parent', --mode parameter set to 'intersection-nonempty', and --stranded set to 'reverse'.

2.6.6 Read count normalization and differential expression analysis

Normalization of raw read count and differential expression (DE) analysis were done using the R statistical software (version 4.1.2) in RStudio (version 2022.02.3 Build 492) using the DESeq2 package (version 1.34.0). MA plots of differentially expressed genes (DEGs) were generated using the plotMA function. Volcano plots of DEGs were generated using the

EnhancedVolcano package (version 1.12.0). Principal Component Analysis (PCA) plots were generated using the function plotPCA of the ggplot2 package (version 3.3.6).

2.6.7 Gene ontology term analysis

DEGs were used as input for gene ontology (GO) term analysis using the R statistical software (version 4.1.2) in RStudio (version 2022.02.3 Build 492) using the gprofiler2 package (version 0.2.1) with the correction_method parameter set to ‘g_SCS’. Results were plotted using the ggplot2 package (version 3.3.6).

CHAPTER

3. RESULTS

3.1 *In silico* prediction of conserved PARP motifs and domains

3.1.1 PARP family expansion in *Fusarium oxysporum*

Within the *F. oxysporum* species complex, there is a vast difference in the number of genes encoding PARP-like proteins on the accessory chromosomes, as well as slight differences in the number of *Parp* genes located on the core chromosomes (Figure 4). Our comparative system consists of three strains that were chosen for the variable number of PARP-like genes found within their genomes and their different phytopathological contexts (Figure 4). The Fo47 strain, a nonpathogenic endophyte, contains only 3 core PARP-like proteins with no accessory PARPs. Fol4287, a tomato pathogen, contains 3 core PARP-like genes and 3 accessory PARPs. Fo5176, an Arabidopsis pathogen, contains 2 core PARPs and 18 accessory PARPs (Figure 4).

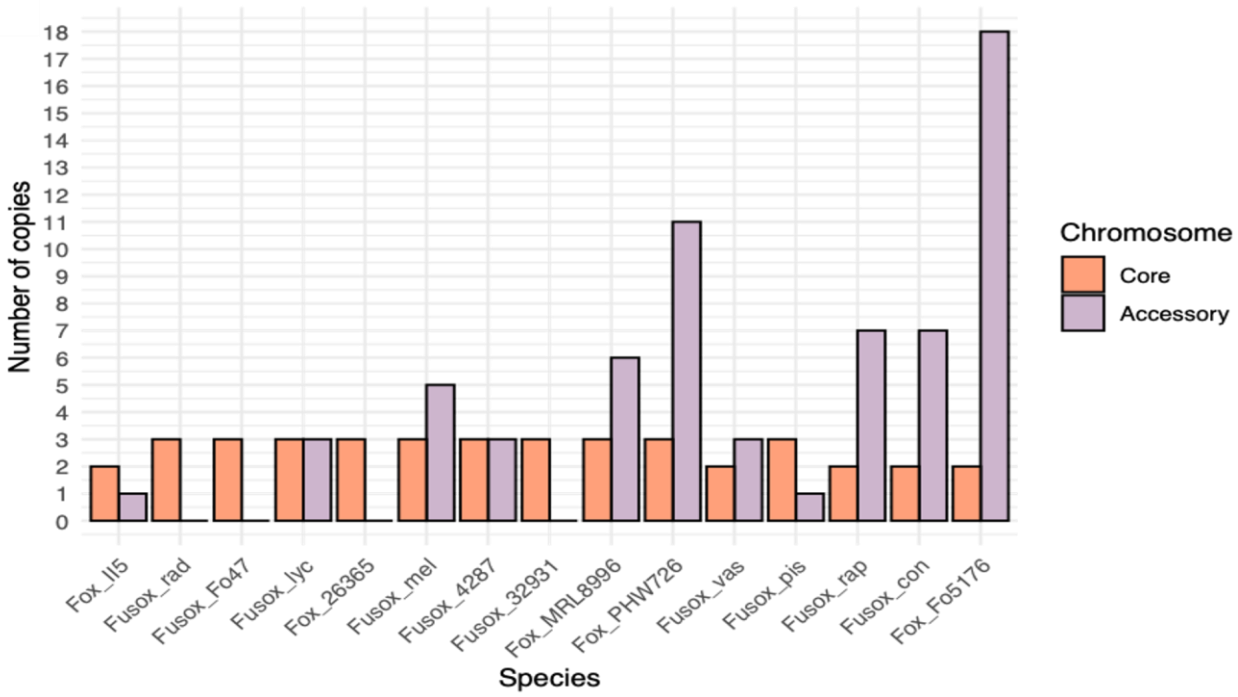

Figure 4: PARP expansion in the F. oxysporum species complex. Along the x-axis are several strains which belong to the F. oxysporum species complex, with the number of Parp gene copies represented in the y-axis. The distribution of Parp genes found within the core and accessory chromosomes are shown in the orange and purple bars respectively. Figure and analysis performed by Shira Milo Cochavi.

3.1.2 Structures of PARP homologs within the comparative system

After the identification of the unique PARP expansion in the *F. oxysporum* complex, efforts were undertaken to identify the protein motifs found within each of the PARP catalytic-domain-containing proteins, to gain insight into their structure and function. Amino acid sequences were downloaded from JGI and used as a query in NCBI (https://www.ncbi.nlm.nih.gov/Structure/cdd/wrpsb.cgi) and InterPro (https://www.ebi.ac.uk/interpro/) conserved domain analysis to begin *in silico* predictions for the

PARP proteins. The first protein characterized in this way was the *F. oxysporum* PARP1 homolog (denoted foPARP1 when referring to the protein and *foParp1* when referring to the gene), which was found to contain the BRCT protein-protein interacting domain, the WGR protein-DNA interacting domain, a PARP family regulatory domain, and finally a PARP catalytic domain located on the C-terminus (Figure 5). Full-protein and catalytic-domain multiple sequence alignments of foPARP1 against hPARP1 revealed that foPARP1 shares a 44.1% percent identity (PID) with hPARP1 (Figure 7). Given foPARP1's similarity to hPARP1 and the low PID of the other core PARPs to foPARP1 (Figure 6), it was predicted that foPARP1 was the only core chromosome PARP homolog predicted to share function with hPARP1. Of note is the protein titled PARP Ubc, which through BLAST and literature review was found to be a fungal-specific PARP (Citarelli, M., *et al*. 2010). This PARP has a long region near the N-terminus containing no known domains, plus a small PARP catalytic domain (54 amino acids as compared to the 234-amino-acid-long foPARP1 catalytic domain) and a Ubc domain near the C-terminus that is highly conserved within the *F. oxysporum* species complex and other filamentous fungi included in our dataset. The 274843 (JGI protein ID) of Fo47 and FOXG_20370 of Fol4287 are relatively small PARP homologs located on a core chromosome harboring only a PARP catalytic domain on the C-terminus of the protein. Although the gene encoding this protein is found on the core chromosomes of Fo47 and Fol4287 with a 97.9 PID, Fo5176 does not contain a homolog of this gene on either its core or accessory chromosomes (Figure 6). Within the accessory chromosomes of Fol4287 are two genes encoding nearly identical proteins containing the PARP family regulatory domain along with a C-terminal catalytic domain and an additional gene for a relatively smaller protein that consists entirely of the PARP catalytic domain. Within the Fo5176 accessory chromosomes were 18 genes encoding

proteins predicted to contain the PARP family catalytic domain, most notably 525699, which appears to be a duplication of foPARP1 and genes for two seemingly identical proteins containing the WGR protein-DNA interacting domain and a C-terminal catalytic domain (Figure 5). From this analysis, it was hypothesized that Fo47 and Fol4287 contained one copy of a protein similar to the DNA-interacting PARPs from humans, foPARP1, while Fo5176 contained two copies of foPARP, along with two PARP catalytic-domain proteins that included protein-DNA interacting domains. To gain further insight into these PARP catalytic-domain-containing proteins, we obtained the sequence of each PARP catalytic domain and generated multiple sequence alignments against the well-defined hPARP1, in order to predict the catalytic capacities of these proteins. Analysis and figure creation for the *F. oxysporum* PARP domain expansion was performed by Shira Milo Cochavi and Cecelia Murphy.

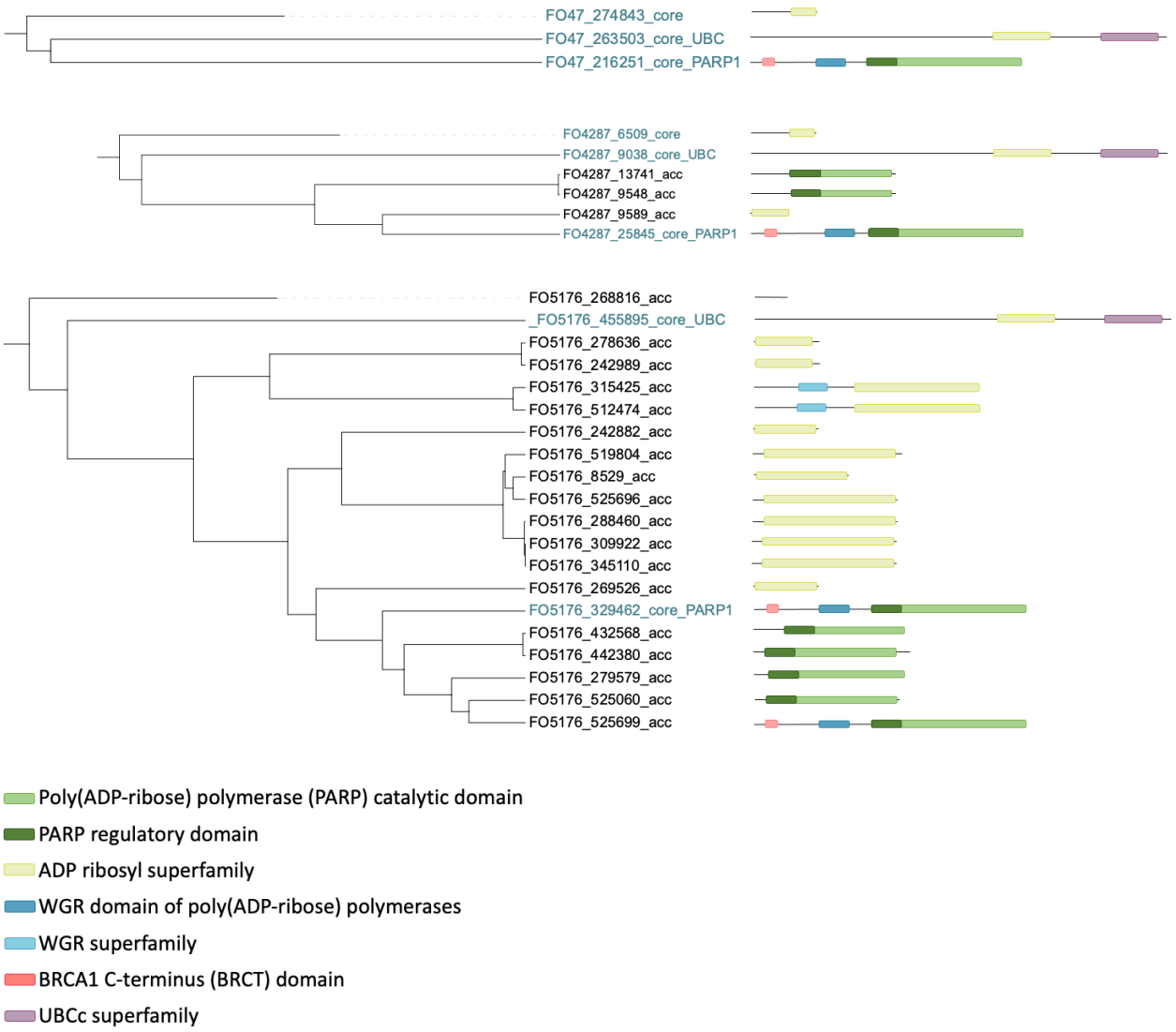

Figure 5: Structural motifs found within the Fusarium oxysporum PARP expansion. All core and accessory proteins that contain either the PARP catalytic domain were subjected to NCB, and InterPro conserved domain analysis. The predicted domains were used to create the images in which the domains correspond with their length and position on the hypothetical proteins. Multiple sequence alignments were created using EMBL-EBI MAFFT and were used to generate phylogenetic trees using the Qtree program to show relationships between the hypothetical proteins. Figure and analysis created by Shira Milo Cochavi and Cecelia Murphy.

3.2 Identification of conserved motifs

3.2.1 MSA + sequence homology of *F. oxysporum* PARPs

In order to begin to characterize the PARP-like proteins, we aligned all of the shared core chromosome PARP catalytic domains to observe any differences in catalytic capacity that the core chromosome PARPs could have (Figure 6A). We began by comparing the catalytic domains of the conserved foPARP1 protein and found that Fo47 and Fol4287 share an identical catalytic domain sequence, while Fo5176's foPARP1 only contained one amino acid variation, resulting in 99.6% identity with the two other foPARP1s (Figure 6A). Next we aligned the catalytic domains of the shared PARP Ubc proteins between the comparative system strains and found no amino acid variation in any strains, showing a perfectly conserved catalytic domain amino acid sequence between all three strains (Figure 6A). Finally, we aligned the third core PARP shared between Fo47 and Fol4287 and found 97.9% identity between the two proteins (Figure 6A). Given these alignments, we can conclude that, for the purposes of our catalytic domain analysis, the foPARP1 and PARP Ubc shared between the strains are effectively identical to each other and can be used interchangeably throughout further analysis (Figure 6A). This also applies to the third core PARP shared between Fo47 and Fol4287; given their high PID, they will be considered essentially identical throughout the analysis (Figure 6A). Next, we aligned the PARPs encoded by genes belonging to the accessory chromosomes of Fol4287 and Fo5176 against their respective foPARP1, in order to gauge their similarity to the best-characterized foPARP1 and to confirm the InterPro prediction that these proteins contain PARP catalytic domains. In our alignments, we used the general rule of thumb in sequence alignment analysis that a percent identity >30% points to the two proteins sharing homology, thus strengthening our prediction of their catalytic capacity (Pearson, W. R. 2013). foPARP1 was chosen as the protein with which to

align the other PARP-like proteins as it contained the highest percent identity to the hPARP1 protein, at a PID of 44.1% (Figure 7A), which we could in turn use as our connection between the well-characterized hPARP1 and the *F. oxysporum* PARP catalytic-domain-containing proteins. In our alignments shown in Figure 6B, nearly every accessory PARP is shown to have a percent identity greater than 30%, which serves to strengthen our hypothesis that these proteins likely contain a PARP catalytic domain; the exception is Fo5176 268816, which only shared a 11.4% identity with foPARP1's catalytic domain (Figure 6B). Fo5176 268816 did initially appear to share the conserved PARP catalytic domain in JGI domain-based analysis; however, further analysis at the amino acid level using both InterPro and NCBI Conserved Domain Search showed no predicted conserved domains, probably due to the short length of this sequence (Figure 5). Due to Fo5176 268816's low percent identity and lack of predicted domains in conserved domain searches, this protein was excluded from further analysis. Finally, the core chromosome PARP catalytic domains were aligned against each other, utilizing Fol4287 as the representative for the comparative system; this alignment surprisingly indicated a 10.4% similarity between foPARP1 and PARP Ubc, and a 16.8% similarity between foPARP1 and the third core PARP 20370 (Figure 6C). Given that PARP Ubc is a fungal-specific protein found within multiple other fungal species, it remained within the analysis despite lower sequence similarity (Citarelli, M., *et al*. 2010). The third core PARP (20370) was shown to have a relatively low PID of 16.8% with foPARP1, but given that both InterPro and NCBI Conserved Domain Search predict that 20370 contains a PARP catalytic domain, we also kept this protein in our analysis. Taken together, foPARP1 is our best candidate to bridge the gap between human and *F. oxysporum* PARPs, given its high percent identity to hPARP1 (Figure 7A) and conservation across all strains of the comparative system. The results of aligning the accessory

PARPs to foPARP1 strengthened the predictions of a catalytic domain residing in our identified accessory PARPs, and further analysis was performed to evaluate potential catalytic function based on conserved catalytic residues experimentally observed in hPARP1 (Marsischky, G. T., *et al*. 1995, Alemasova, E. E. & Lavrik. 2019).

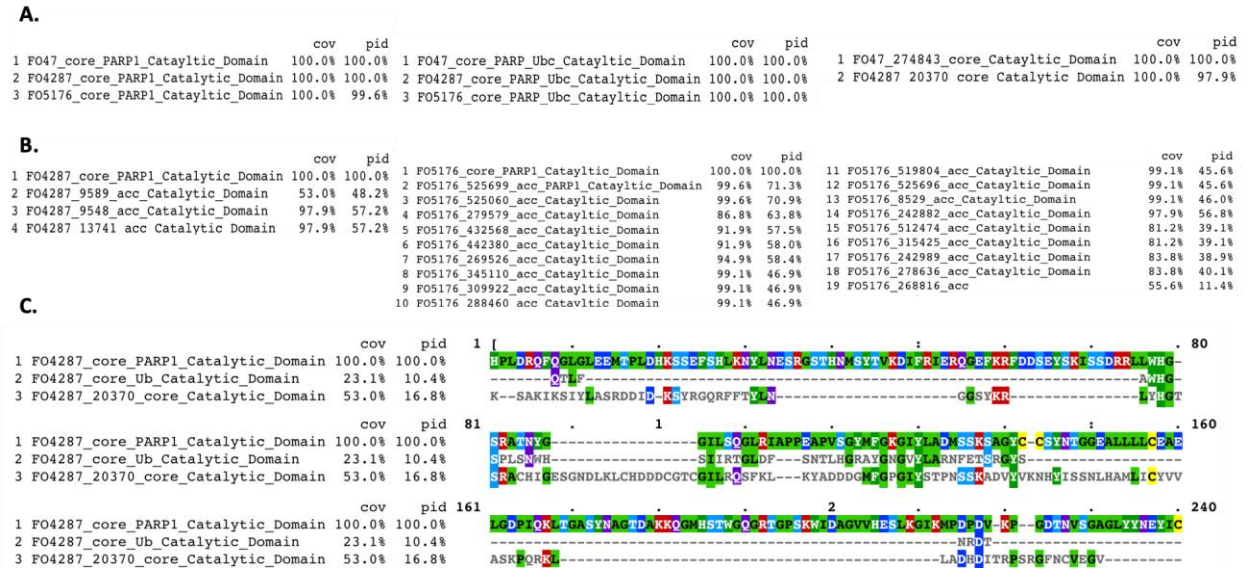

Figure 6: Multiple sequence alignment of Fo47, Fol4287, Fo5176 core and accessory PARP catalytic domains against the foPARP1 catalytic domain. Cov represents the percent of coverage that a protein was able to align with the top-most protein, and PID refers to percent identity. A) Alignments of the foPARP1 in all three strains, UBC in all strains, and Fo47 274843 and Fol4287 20370 B) Alignments of foPARP1 to the respective accessory PARP proteins C) Catalytic domain alignment of Fol4287 foPARP1 to Ubc and 20370 core PARP 3.

3.2.2 Identification of conserved amino acids that indicate catalytic activity

For human poly ADP-ribose polymerase catalytic activity, a three-amino-acid motif has been discovered to be essential in the transformation of NAD+ to ADP-ribose and elongation of

PAR chains. The H-Y-E triad in the human PARP1 protein, Histidine 826, Tyrosine 907, and glutamine acid 988 (Alemasova, E. E. & Lavrik, 2019), is conserved in all of the "*bona fide*" poly ADP ribosylation proteins (human PARP1-5b) (Alemasova, E. E. & Lavrik, 2019). Other human PARP catalytic motifs, such as the H-Y-I, H-Y-L, and H-Y-Y motifs of PARP 6-12, PARP 14-15, and PARP16 respectively were searched for, but no *F. oxysporum* PARP homologs were found to contain these motifs (Figure 7) (Vyas, S. *et al.* 2014). Based on our analysis, within the Fo47 and Fol4287 strains, there is only one PARP-like protein encoded by a gene located on the core chromosome that contains the key H-Y-E motif, foPARP1, as shown by a multiple sequence alignment between Human PARP1, Fo47, and Fol4287 (Figure 7B). Interestingly, within Fo5176, there appear to be two additional PARP-like proteins encoded by genes located on the accessory chromosomes that contain the H-Y-E motif, while there are two other PARP-like accessory genes that encode proteins that contain a H-Y-V motif (Figure 7). From these results we can predict that Fo47 and Fol4287 have only one PARP-like protein that could conceivably catalyze the formation of PAR polymers, while Fo5176 contains up to three proteins that can possibly catalyze the synthesis of PAR polymers. However, this leaves the vast majority of PARP catalytic-domain-containing proteins lacking the conserved H-Y-E sequence derived from the ancient DTX family of exotoxins (from which modern PARPs were derived), so in an effort to identify catalytically important sequences within these PARP-like proteins, we investigated whether any of these proteins contained the CTX family catalytic R-S-E triad (Mikolčević, P., *et al*. 2021).

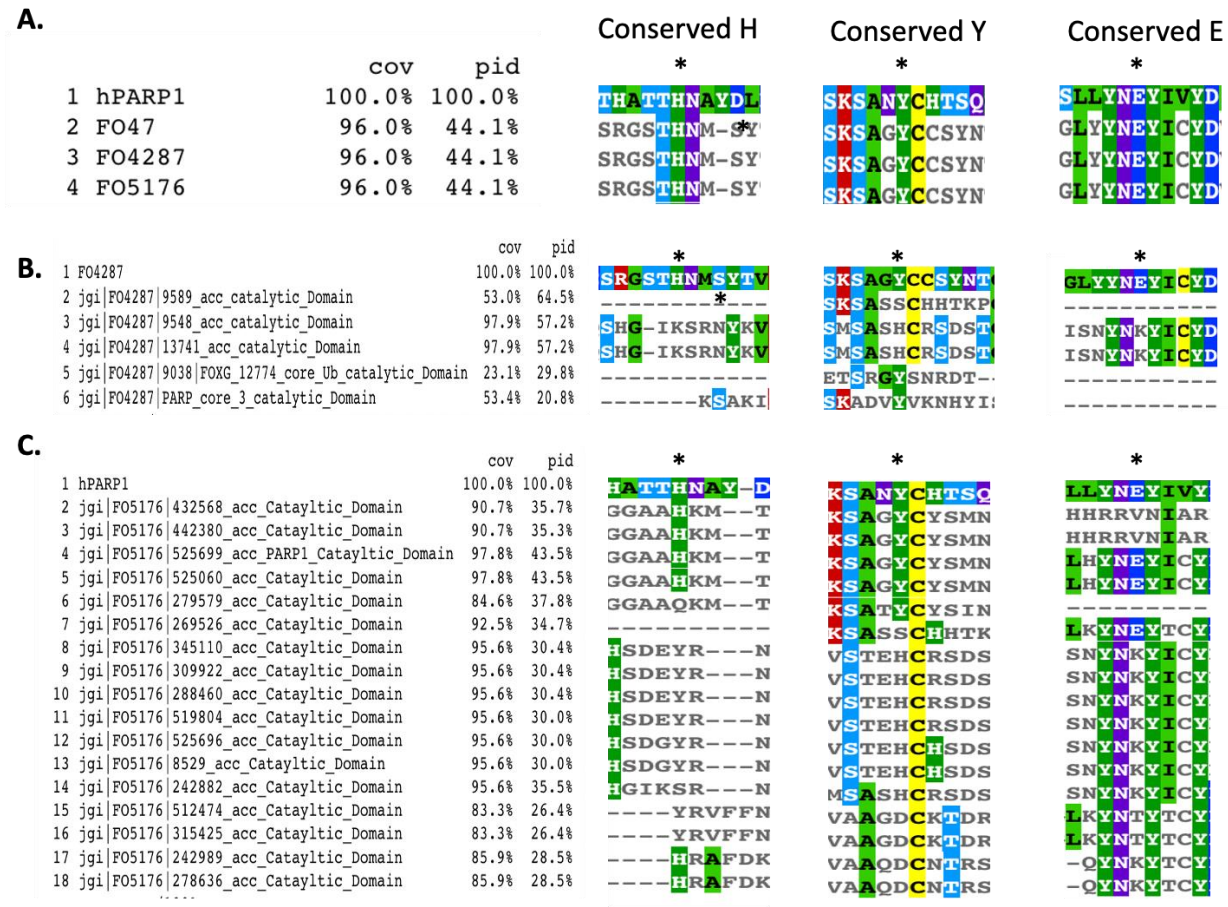

Figure 7: Multiple sequence alignments of the catalytic domains of hPARP1 against all focPARP1 and of hPARP1 against all accessory PARP homologs. All alignments are centered around the conserved amino acid marked with an asterisk above; cov represents the percent of coverage that a protein was able to align with the top-most protein, and pid refers to percent identity. A) hPARP1 was aligned against the focPARP1 protein sequences of Fo47, Fol4287, and Fo5176. B) hPARP1 was aligned against all PARP catalytic-domain-containing proteins encoded within the Fol4287 accessory chromosomes. C) hPARP1 was aligned against all accessory PARP-like proteins within the Fo5176 genome.

3.2.3 Sequence similarity to bacterial ADRTs

After finding that only a few of the *F. oxysporum* PARP proteins contain the conserved H-Y-E catalytic motif found within the human PARPs, and given that *F. oxysporum* acts as a pathogen to a variety of different host species, we decided to investigate whether any of the PARP proteins in *F. oxysporum* shares catalytic similarities with the bacterial ART exotoxins. The cholera toxin was chosen as a model for bacterial exotoxins as it remains one of the best-characterized ART toxins and has the R-S-E amino acid motif identified (Mikolčević, P., *et al*. 2021). Fol4287's core PARP proteins serve as a stand-in for the three Fo47 core PARPs and the Fo5176 two core PARPs due to the nearly identical sequence identity that the strains' core PARPs share (Figure 6A). Sequences were aligned against the cholera toxin to assess whether the MARylating R-S-E motif would be found within the PARP expansion. None of the Fol4287 PARP-like proteins encoded on the core or accessory chromosomes shared the R-S-E motif in its entirety, although proteins 9548 and 13741 did align with R5 and E110 of the cholera toxin catalytic domain; the S61 was aligned with an alanine, but given that these amino acids have differing polarity, it is unlikely that the catalytic activity of this amino acid is conserved (Figure 8A). The accessory PARP-like proteins of Fo5176 were also aligned against the cholera toxin and, as was the case for Fol4287, no individual PARP proteins were shown to share all three of the CTX catalytic motif residues (Figure 8B). Given these findings, it can be concluded that none of the PARP catalytic-domain-containing proteins within any of the comparative complexes shares a catalytic motif with the CTX. Taken together from the domain predictions and multiple sequence alignment results, it was predicted that Fo47 and Fol4287 shared only one PARP-like protein that could perform PARylation, foPARP1, while Fo5176 contained three (Figure 6 and 7). No PARP-like proteins within the comparative system were found to share the catalytic domain motif of the CTX family of exotoxins (Figure 8).

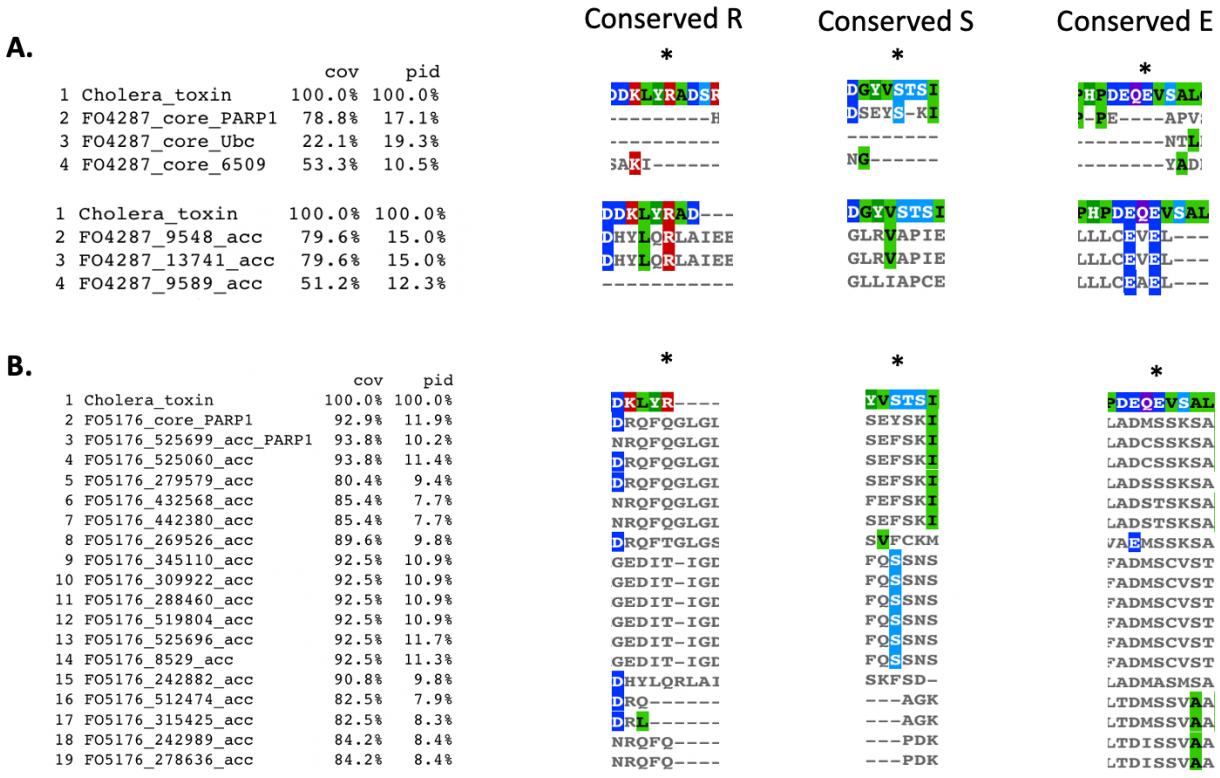

Figure 8: Multiple sequence alignment of cholera toxin against all Fol4287 and Fo5176 PARP homologs, focusing on catalytic domains. All alignments are centered around the conserved amino acid marked with an asterisk above; cov represents the percent of coverage that a protein was able to align with the top-most protein, and pid refers to percent identity. A) The catalytic domains of all Fol4287 core and accessory PARP proteins were aligned against the catalytic domain of the cholera toxin; the alignments were performed in groups of three to maximize coverage. B) The catalytic domains of all Fo5176 accessory proteins and focPARP1 were aligned with the cholera toxin.

3.2 *In vitro* Phenotyping

To begin to observe the phenotypic effects that foPARP1 would have in response to DNA-damage stress, we employed MMS to induce alkylating DNA damage. MMS has been previously used, as reported in the literature, to assess PARylation in mammals and to observe changes in DNA repair responses in *F. oxysporum* (Semighini, C. P., *et al.* 2006, Hopp, A.-K. *et al.* 2021, Milo-Cochavi, S. *et al.* 2019). The next step was to create fo*Parp1* knockout mutants in all of the comparative system strains to assess the changes in phenotype that would occur upon MMS-mediated DNA damage. *foParp1* mutants were generated using a CRISPR/Cas9 system that utilized a hygromycin cassette inserted into the *foParp1* gene to knockout its function. Insertions were confirmed by both PCR and Sanger sequencing. Mutant creation and confirmation were performed by Cecelia Murphy within the Ma lab. First, the WT strains were grown in both control PDA plates and in PDA plates containing 0.01% MMS to induce chronic DNA damage for 48 hours. The plates were then imaged using a plate scanner, and the colony sizes were measured using ImageJ. The ImageJ measurements were used to determine the ratio of colony size between the MMS-treated and control colonies. This ratio was used to observe differences in each strain's ability to tolerate the MMS-induced stress. Finally, R Studio was used to create figures and calculate p-values of the differences in tolerance between the strains. Fo47 showed the highest growth inhibition in the presence of MMS, followed by Fol4287, and Fo5176 showed the best tolerance to MMS-mediated DNA damage (Figure 9). Using this method, the differences in colony size ratios between Fo47 and Fol4287, as well as the differences between Fol4287 and Fo5176 were not statistically significant, with p-values of 0.08 and 0.064 respectively (Figure 9). The differences between Fo47 and Fo5176 were significant with a p-value of 0.022 (Figure 9).

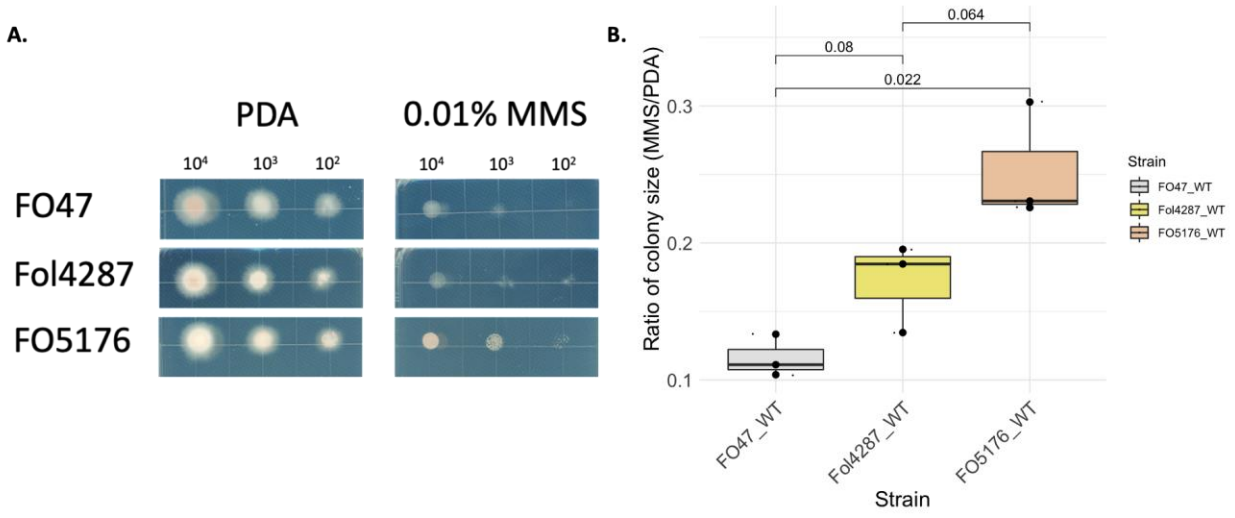

Figure 9: WT phenotyping in control and MMS-stress conditions. A) Images of colony growth on PDA control and 0.01% MMS plates after incubation for 48 hours. Dilutions of F. oxysporum strains were plated in 10^4, 10^3, and 10^2 spores/mL concentrations with three biological replicates. B) The ratios of MMS colony growth size to PDA control colony growth size for all strains were calculated for all three biological replicates and graphed along with p-values indicating the statistical significance of the observed differences between growth ratios of the tested strains. The statistical significance between samples was calculated using two way t-tests.

After the WT phenotypes had been established, the *foParp1* mutants were subjected to the same experiment and analysis (Figure 10A). The Fol4287 *foParp1* mutant showed the highest growth inhibition with the lowest MMS/PDA size ratio, followed by Fo47Δ, while Fo5176Δ exhibited the best tolerance to MMS-mediated DNA damage (Figure 10B). The differences in colony size ratio between Fo47 and Fol4287, as well as the ratios between Fo47 and Fo5176 mutants, were not statistically significant, with p-values of 0.14 and 0.42, respectively (Figure 10B). The ratios of MMS/PDA colony sizes were significantly different when comparing the Fol4287 and Fo5176 strains, with a p-value of 0.034 (Figure 10B).

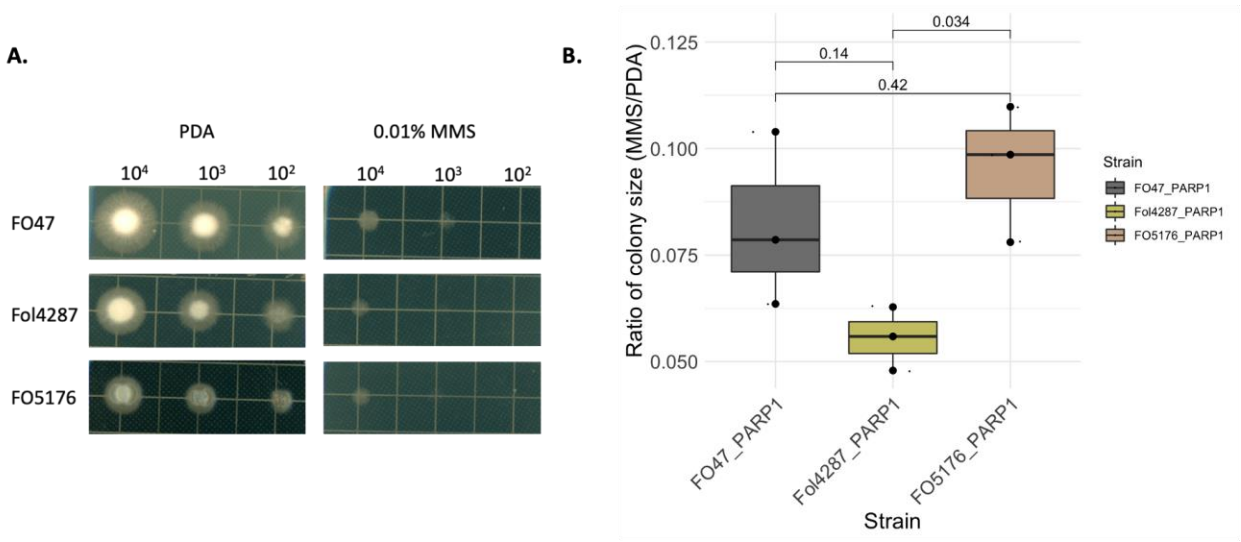

Figure 10: foParp1 mutant phenotyping in control and MMS-stress conditions. A) Images of colony growth on PDA control and 0.01% MMS plates after 48 hours of incubation. Dilutions of mutant F. oxysporum strains were plated in 10^4, 10^3, and 10^2 spores/mL concentrations with three biological replicates. B) The ratios of MMS colony growth size to PDA control colony growth size for all strains were calculated and graphed along with p-values from two way t-tests indicating the statistical significance of observed differences between the growth ratios of the tested strains.

To determine the differences in MMS tolerance between the wild-type and mutant strains, the data gathered from the previous two phenotyping exercises were used to compare the ratios of colony size between the WT and mutant strains. The WT and mutant plates were grown in parallel for the same amount of time and under the same conditions. The analysis showed that the changes in MMS/PDA ratios between the WT and mutant strains of Fol4287 and Fo5176 were statistically significant, with p-values of 0.021 and 0.015 (Figure 11). The differences in colony size ratios between the WT and mutant Fo47 strains were found to be not statistically significant, with a p-value of 0.087 (Figure 11). Fo5176 was shown to have the largest reduction

in MMS tolerance, with an averaged 38% drop in colony size ratio across all data points; Fol4287 was shown to have the second-largest reduction in colony size in the mutant, with a decrease of 32%; and Fo47 did not contain a statistically significant ratio decrease between the WT and *foParp1* mutant (Figure 11).

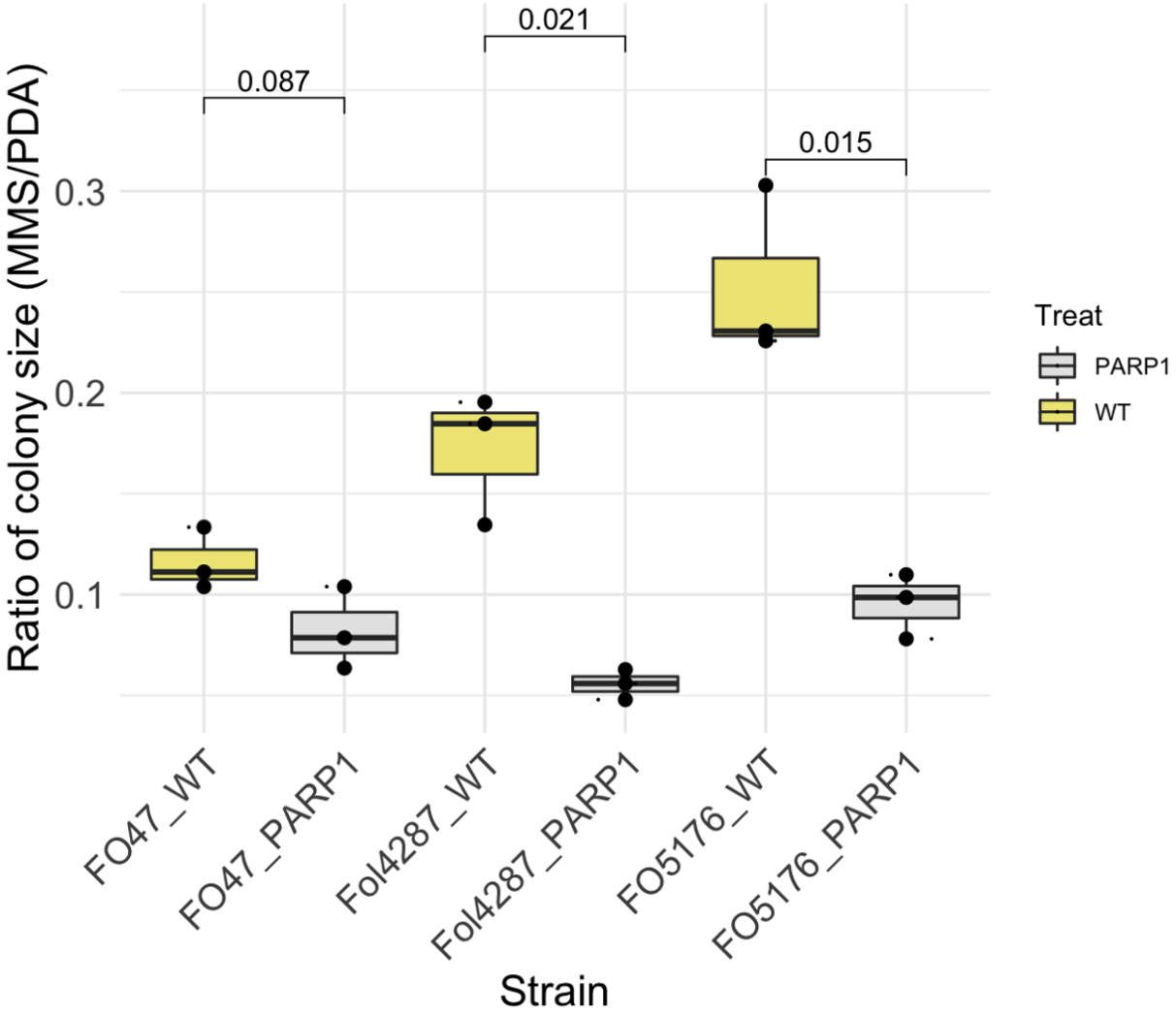

Figure 11: Comparison of ratio of colony size between MMS-induced and PDA control growth for WT and foParp1 knockout in all three strains.

3.3 DNA damage-induced expression of *Parp* genes in *F. oxysporum*

RT-qPCR experiments were performed to reveal which of the *Parp1* gene copies in each strain in our comparative system are active upon MMS exposure (Figure 12). Fo47 had the largest increase in *foParp1* expression upon the exposure to MMS (Figure 12A), while Fo5176 exhibited the least increase in *foParp1* transcriptional activation (Figure 12C). All three copies of the core *Parp* genes showed increased transcriptional activation in Fol4287 under MMS conditions, including the largest increase in the third core *Parp* copy (gene 6509) (Figure 12B). Fo5176 had the least amount of *foParp1* transcriptional activation, with none of the H-Y-E or H-Y-V containing *Parp* homologs showing significant transcriptional upregulation (Figure 12C). However, the uncharacterized 269416 *Parp* homolog, which contains a H-S-E catalytic motif, displayed significant upregulation similar to that of *Parp-Ubc* (Figure 7C). All RT-qPCR experiments were performed at the Ma lab by Shira Milo Cochavi.

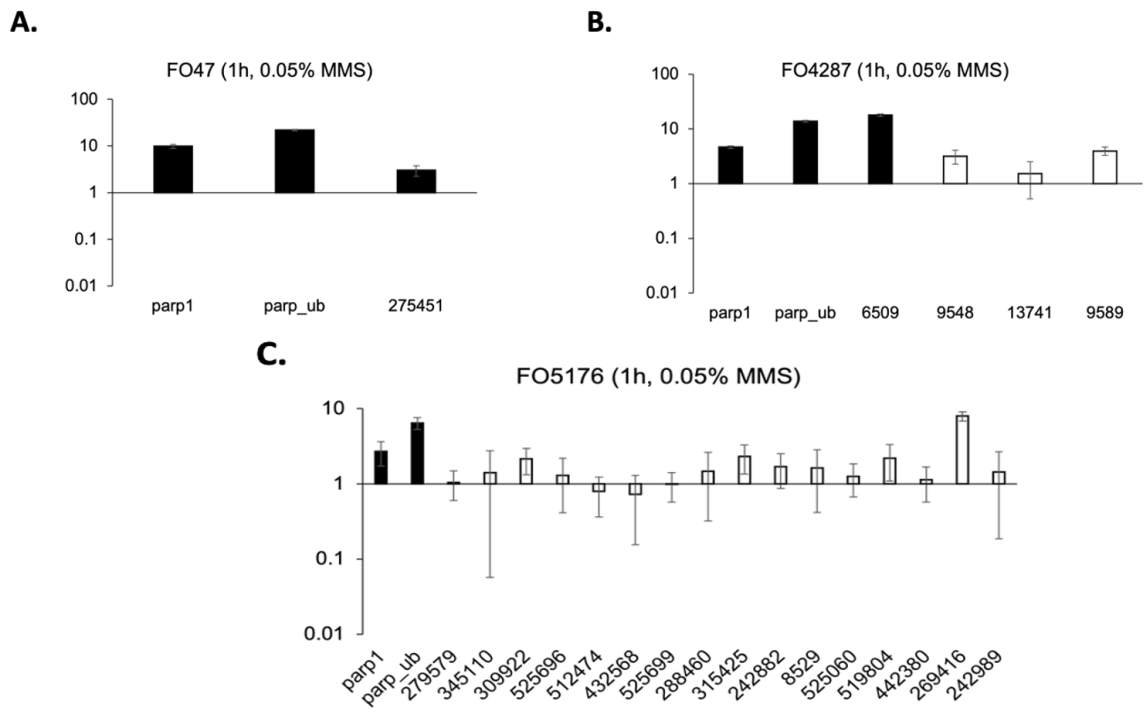

Figure 12: RT-qPCR detection of PARP homolog expression in response to MMS-mediated DNA damage. Parp genes shown with solid black bars are located within the core chromosomes while Parp genes shown with white bars are located within the accessory chromosomes. A) Fo47. B) Fol4287. C) Fo5176. Experiment and figure performed by Shira Milo Cochavi.

3.4 Development of the immunoblot assay

The comprehensive sequence analysis described in Chapter 3 revealed Fo5176 to contain more copies of genes encoding PARP proteins that are predicted to have PARylation activity than in the other two members of our comparative system. The correlation between PARP copy number and DNA damage tolerance was indicated within the phenotyping of Chapter 3.2. Therefore, our next step was to gain *in vitro* insight into the changes in global PARylation upon DNA damage. An immunoblot was chosen to obtain semi-quantitative data on global PARylation, as it allows for a highly specific binding and detection of PAR chains in up to 96

individual samples per membrane. The dot-blot was chosen over other forms of antibody-mediated detection, such as Western blot, as our approach would benefit most from large sample sizes containing multiple biological and technical replicates, to account for high variability in data points. Dot-blot experiments have been performed on PAR in other model organisms, such as mice and human cell lines, but to our knowledge, a protocol to perform an immunoblot for the detection of ADP-ribose has not been performed in any filamentous fungus. Thus, we adapted and optimized the procedure described by Kudo, Y. *et al.* (2018) for the development of a dot-blot protocol for the detection of ADP-ribose in *F. oxysporum*. Notability, antibodies used and concentrations, as well as the addition of the gel-drying and formaldehyde cross-linking steps used within the Kudo, Y. *et al.* 2018 paper were implemented in our protocol to ensure the maximum retention and binding of PAR polymers on the membrane. However, several steps, including protein extraction and purification methods, wash buffers used in each step and incubation/washing times, were adjusted while calibrating the protocol to achieve the optimal PAR detection for our organism. An important insight from the Kudo, Y. *et al.* 2018 paper is that the 10H monoclonal PAR antibody used in their and our experiments is only able to detect "large" PAR polymers of 20 pADPr units or greater and is not able to significantly detect PAR chains less than 20 pADPr units long or single ADP-ribose molecules.

The immunodot-blot assay was used to assess the impact the DNA damage would have on both WT and *foParp1*Δ strains and served as a point of comparison between the three strains, specifically, how much PARylation occurs under normal growth conditions and how PARylation is impacted by DNA damage caused by the DNA alkylating agent MMS. In addition, the dot-blot technique can provide insight into the impact of *Parp1* deletion and the differences in terms of cellular PARylation between the WT and *foParp1*Δ strains.

3.4.1 Assessing PARylation levels in Wild-Type strains using immunodot-blot assay

To quantify global PARylation in the three strains of the comparative system, a novel immunodot-blot assay protocol was developed. To observe the differences in PARylation in basal and DNA-damage conditions, we utilized a control sample group grown only in PDB media and a MMS-treated sample group. Within the MMS-treated groups we added: the PARG inhibitor Adenosine 5′-diphosphate (Hydroxymethyl) pyrrolidinediol NH_4 (ADP-HPD), excess β-NAD+, and MMS. While MMS was used in order to induce DNA damage to increase PARylation, we sought to prevent PAR degradation using the PARG inhibitor and to avoid NAD+ bottlenecking that would prevent PARylation by supplementing with NAD+. The additions to the MMS-treated samples should result in maximum PAR signal detection. There was a visibly clear increase in the detection of PAR within the MMS-treated group as compared to the control (Figure 13A). To assess the significance of the difference between control and MMS-treated samples, the antibody signal intensity values obtained from the ImageJ analysis in each sample were subjected to two way t-tests. Both Fo47 and Fo5176 were shown to have a statistically significant increase of PARylation upon the addition of MMS, with p-values of 0.003 and 0.04 respectively, while Fol4287 did not have significant increase in PARylation, with a p-value of 0.14 (Figure 13B). Fo47 and Fo5176 appeared to be similar to each other in the detected basal and stress-induced PARylation activity, while Fol4287 exhibited the least amount of basal and stress-induced PARylation (Figure 13B).

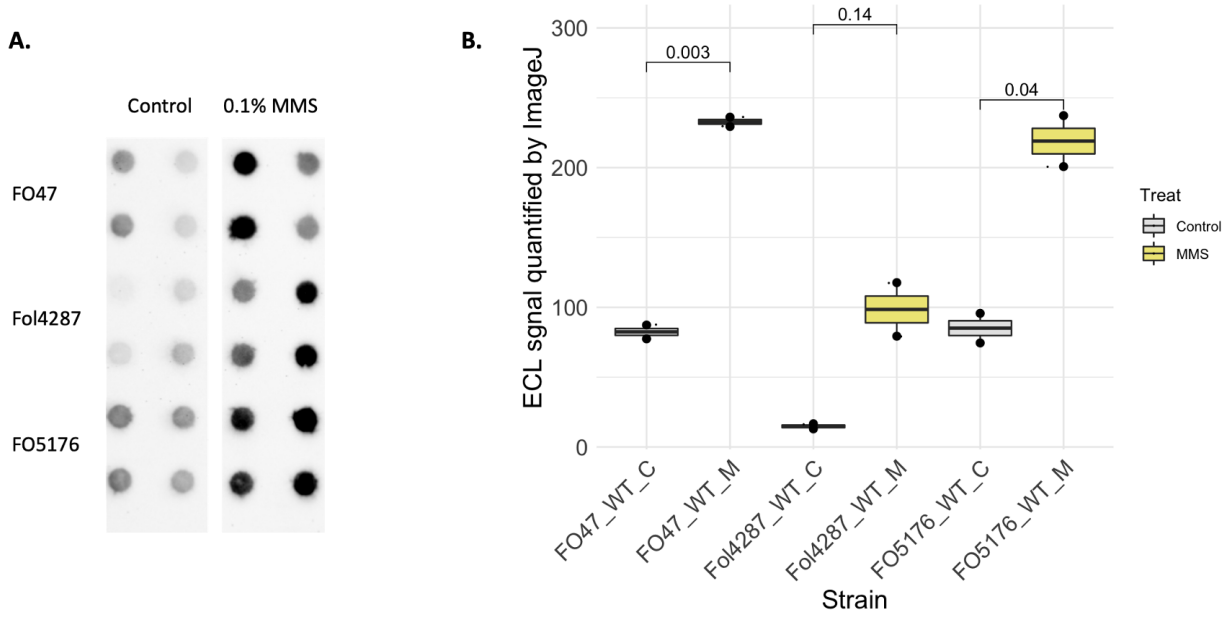

Figure 13: Immunoblot performed on FO Wild-Type strains. A) ECL detection signals from ChemiDoc chemiluminescence imaging of control and MMS-treated Fo47, Fol4287, and Fo5176 wild-type samples. All sample types were blotted using three biological replicates along with two technical replicates. B) The signal intensity of the chemiluminescence imaging was measured using ImageJ, and the background signal was subtracted to allow for comparison between the strains. Note that the maximum signal intensity for this method is 255.

3.4.2 Assessing PARylation levels in *Parp1*-deficient strains using immunodot-blot assay

To assess the impact that *foParp1* knockout has on global PARylation within the comparative system, the same sample groups as in the WT blots were created from the *foParp1*Δ strains: a control group incubated in PDB and a group treated with MMS, excess NAD+, and a PARGi grown in PDB. The most noticeable result gained from the dot-blotting of the mutant strains is the large decrease in PARylation detection in both control and MMS-treated groups within the Fol4287 *Parp1*-deficient strain as compared to the other strains. It was also found that

there was no significant difference in the PARylation between control and MMS-treated samples in Fol4287 mutants (Figure 14A). Both the Fo47 and Fo5176 mutant exhibited no significant changes in PARylation between the control and MMS-treated samples and exhibited roughly similar amounts of PARylation at basal levels (Figure 14B).

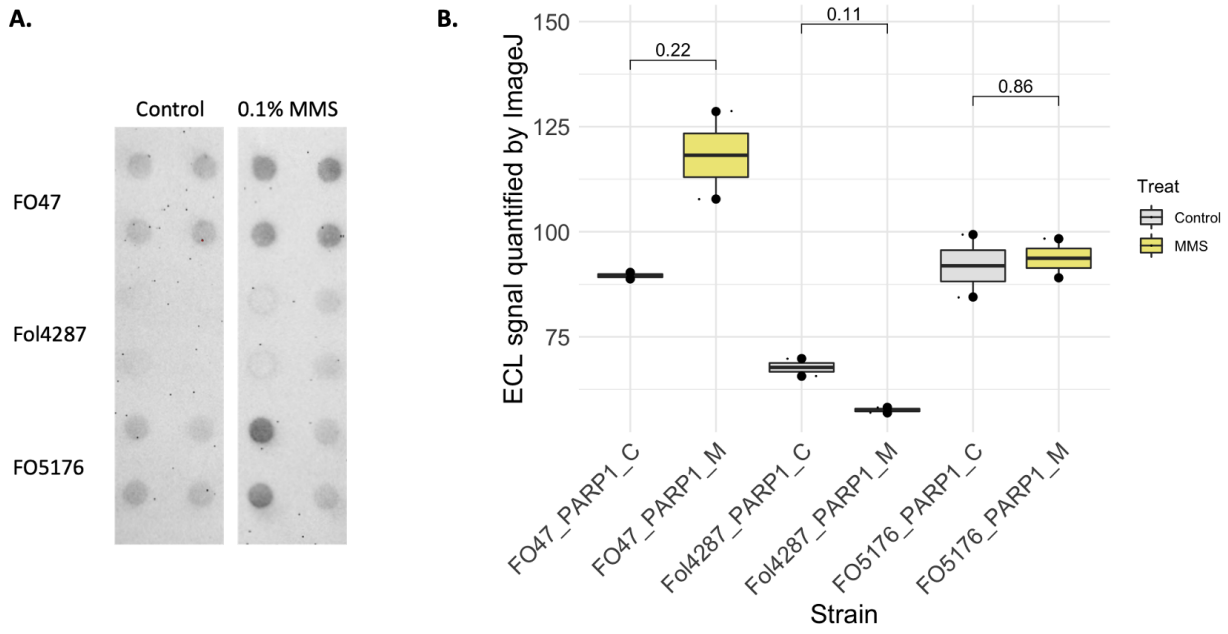

Figure 14: Immunoblot performed on foPARP1 knockout mutants. A) ECL detection signals from ChemiDoc chemiluminescence imaging of control and MMS-treated Fo47Δ, Fol4287Δ, and Fo5176Δ samples. All sample types were blotted using three biological replicates along with two technical replicates. B) The signal intensity of the chemiluminescence imaging was measured using ImageJ, and the background signal was subtracted to allow for comparison between the strains. Note that the maximum signal intensity for this method is 255.

3.4.3 Comparison between WT and mutant

The findings listed above were generated on two separate blots, one containing all of the WT samples and another containing the mutant samples, due to restrictions in the size of the

membrane. This prevents us from directly comparing the data points gained from each blot; however, we utilized the fold change of MMS-treated and control samples as a point of comparison between the two blots. From this comparison, we can assess that Fo47 and Fo5176 have roughly the same amount of PARylation induction when treated with MMS, while Fol4287 has the largest induction of PARylation upon DNA-damage stress and also the greatest variation (Figure 15). Notably, within all strains there is a significant difference in the fold change in PARylation between the WT and mutant strains (Figure 15).

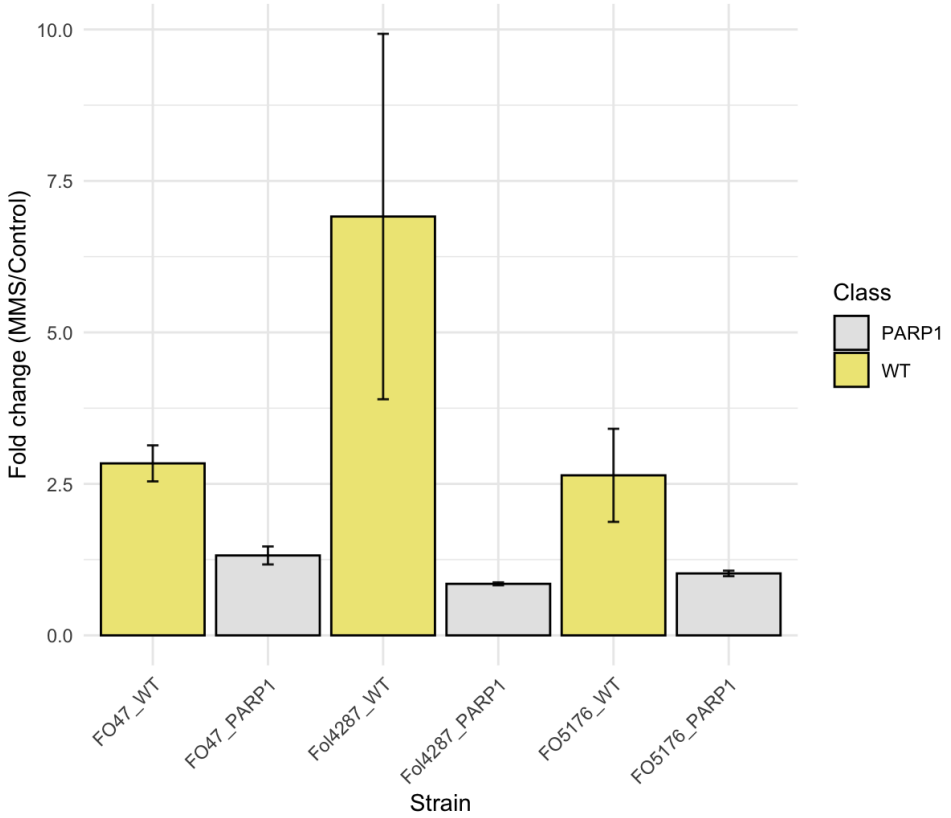

Figure 15: Fold change of the MMS vs control PARylation signal averages for both WT and mutant strains in Fo47, Fol4287, and Fo5176.

3.5 RNA-Seq of WT and *foParp1* mutants under MMS-mediated stress

3.5.1 Using RNA-Seq to reveal the impact of *Parp1* deletion on transcriptional regulation in Fol4287

Thus far we have gained insight into the predicted catalytic domains of the PARP protein family in *F. oxysporum*, assessed tolerance to DNA damage, and utilized immunoblotting to observe PARylation trends under untreated control and DNA-damage conditions for both WT and *foParp1* knockout strains. We ventured to uncover the transcriptional impacts that *foPARP1* has by conducting RNA-Seq on WT and *foParp1* mutants under control and MMS-induced DNA-damage conditions. RNA-Seq is a powerful approach that gives insight into the entire transcriptome, yielding a better understanding of how the cell responds at the transcriptional level. The data produced in such experiments can be used as a starting point for the development and investigation of testable hypotheses. Given the role of hPARP1 in chromatin remodeling and transcriptional regulation, we hypothesized that the knockout of *foParp1* would change the transcriptome of the cell, especially under DNA-damage conditions. For our RNA-Seq experiment, Fol4287 was chosen as the candidate, given that it has the best-annotated genome and no predicted PARylating PARP proteins outside of foPARP1. Two sample groups were prepared, one control group incubated in PDB media, and one group treated with 0.05% MMS to induce DNA alkylation damage. Two time points were used, with 20-minute and 1-hour incubation times, in order to give insight into the “fast” and “longer-term” response that MMS exposure would trigger in the transcriptome. The RNA samples were validated for sufficient quantity and integrity before being shipped for sequencing (Supplementary Table 1 and Supplementary Figure 2).

3.5.2 Transcriptome-wide differential expression

To begin our analysis of the global trends found in our RNA-Seq data, we identified transcriptome-wide differential expression trends directly between control and MMS-treatment groups and compared the number of differentially expressed genes between wild-type and mutant samples at each time point. The comparisons between control groups and 60 minutes of MMS exposure exhibited larger transcriptional impacts than the comparison between control and 20 minutes of MMS exposure, as depicted in Table 2. Overall, the greater the amount of time the samples were exposed to MMS resulted in a larger number of differentially expressed genes (DEGs), likely in response to the ongoing DNA-damage stress the cells underwent, such as the 1027 downregulated genes in the WT control vs MMS20 comparison against the 2539 downregulated genes in the WT control vs MM60 comparison (Table 2). The mutant samples when compared to wild-type showed an overall downregulation of genes, which is especially apparent when directly comparing the WT and mutant DEGs at the same time point (Table 2). This overall downregulation of genes is clearly shown in Figure 16A-C, where the downregulation of genes can be observed as being more frequent than upregulated genes, exhibiting larger $\log_2$ fold changes; in addition, the differences have more statistical significance as shown by the larger $-\log_{10}$ P values (Figure 16A). The RNA-Seq results provide another level of confirmation that the *foParp1* gene (shown as FOXG_07574) was not expressed at all within the mutant samples, confirming that the mutant lacks the ability to express *Parp1* (Figure 16B-C). To assess whether foPARP1 has transcriptional regulation responsibilities over the other core and accessory PARPs, the differential expression patterns of these PARPs were extracted from the comparisons of each sample group and time point (Table 4). The only PARP gene to have significant transcriptional changes in the *foParp1* mutant was the fungal-specific *Parp-Ubc*, which was found to be upregulated sooner in WT samples in the control versus 20-minute

comparison, and more abundantly in WT samples in the control versus 60-minute MMS comparison (Table 4). The third core *Parp*, FOXG_20370, was not significantly impacted in its transcript abundance, and none of the accessory *Parp*s were found to be expressed within any sample group (Table 4). Differential expression data were able to give us the global transcriptional response trends to these conditions; however, to gain more insight into the specific pathways affected by MMS exposure in the WT and mutant, we conducted a functional annotation of the differentially expressed genes using the Gene Ontology database to allow us to observe significant enrichment of biological pathways(Zhao, Y. *et al.* 2020).

Table 2: Number of differentially expressed genes

DE Statistics	Upregulated genes	Downregulated genes	Total differential expression
WT ctrl vs mms20	1818	1027	2845
Mut ctrl vs mms20	1665	912	2577
WT ctrl vs mms60	2839	2539	5378
Mut ctrl vs mms60	2512	2138	4650
WT ctrl vs Mut_ctrl	141	769	910
WT mms20 vs Mut mms20	408	1048	1456

WT mms60 vs Mut mms60	486	1038	1524

Table 3: Differentially expressed genes with intersect labeled

Differentially Expressed Genes	Wild-Type	*foParp1 Δ*	Intersect
ctrl_vs_mms20_down	1027	912	588
ctrl_vs_mms20_up	1818	1665	1350
ctrl_vs_mms60_down	2539	2138	1842
ctrl_vs_mms60_up	2839	2512	2219
mms20_vs_mms60_down	1565	1175	893
mms20_vs_mms60_up	1501	1202	832

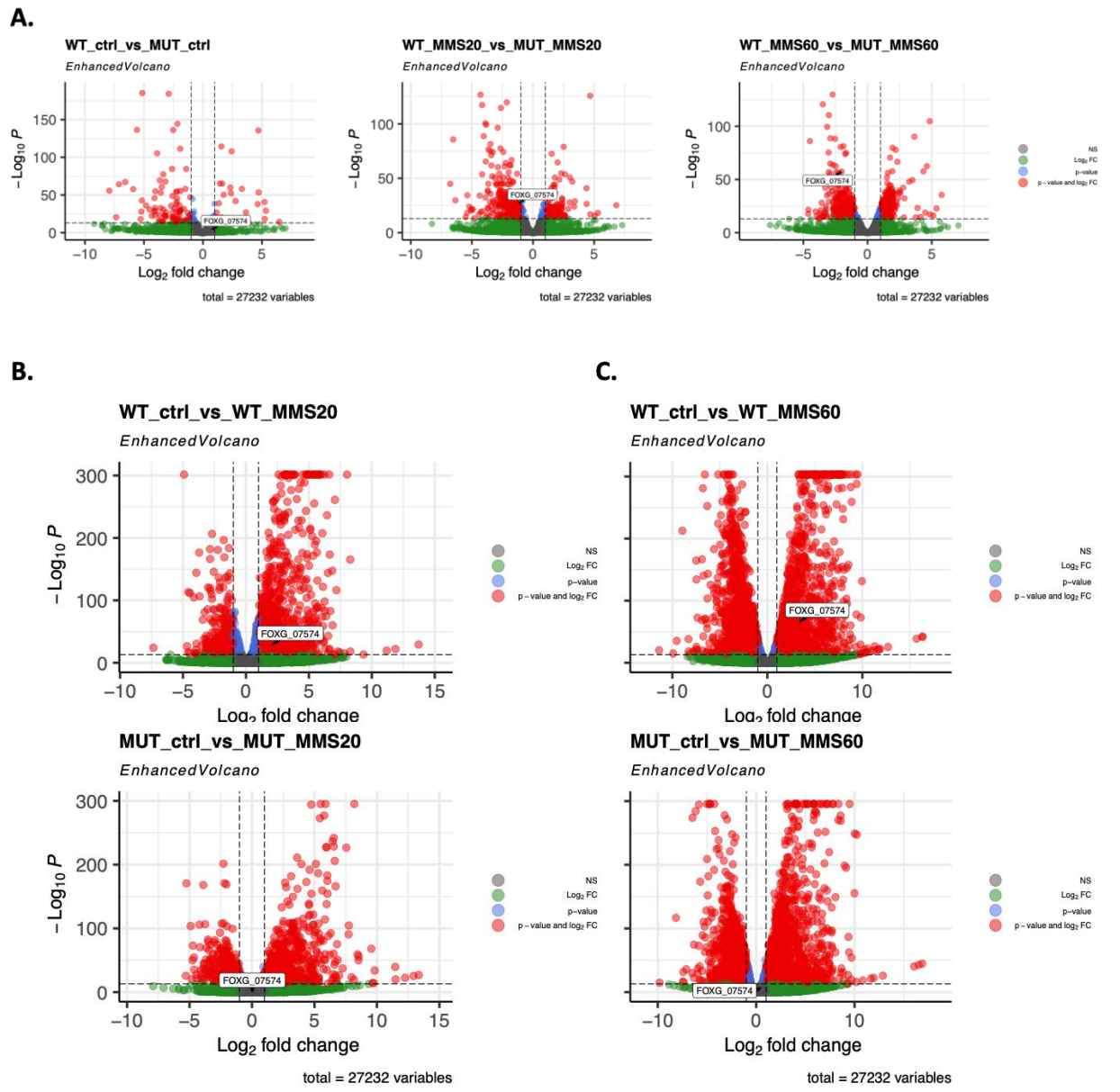

Figure 16: Global differential expression comparison between WT and focPARP1 mutant. A) Volcano plots of differentially expressed genes between the WT vs Mutant samples plotted against the $\log_2$ fold change and $-\log_{10}$ P values within the control, 20-minute MMS exposure, and 60-minute MMS exposure sample types B) DE of WT control vs WT 20-minute MMS and Mutant (Mut) control vs Mut 20-minute MMS samples C) DE of WT control vs WT 60-minute MMS and Mut control vs Mut 60-minute MMS samples.

Table 4: Differential expression of PARP-like transcripts. Note that + represents upregulation, NS stands for non-significant and NA stands for not available.

	PARP-UBC	*FOXG_20370*	*9548*	*13741*	*9589*
WT Control vs 20-minute MMS	*+4.28377612*	*NS*	*NA*	*NA*	*NA*
WT Control vs 60-minute MMS	*+8.38759649*	*NS*	*NA*	*NA*	*NA*
Mutant Control vs 20-minute MMS	*NS*	*NA*	*NA*	*NA*	*NA*
Mutant Control vs 60-minute MMS	*+6.26004907*	*NA*	*NA*	*NA*	*NA*

3.5.3 Gene Ontology Term Analysis

Analysis for the enrichment of GO terms of DEGs in DNA-damage conditions compared to the untreated control was expected to shed light on the pathways affected by loss of *Parp1* in *F. oxysporum*. Focusing on the number of DEGs in the Table 3, where although we do not see a vast difference in differentially expressed genes between the WT and mutant samples, we do see a significant difference in the number of genes that are uniquely expressed in each strain in response to MMS, suggesting that there is a transcriptional change upon the knockout of

foParp1. For example, one of the largest differences is found within the downregulated genes in the control vs MMS20 comparison; WT samples have 1027 DEGs, while the mutants have 913 DEGs, but interestingly only 588 of those DEGs are shared between the WT and mutant (Table 3). Comparing the upregulated genes in controls vs MMS 20, we find largely the same trends between both the WT and mutant samples: an increase in amino acid and protein synthesis pathways and autophagy response (Figure 17A). With the downregulation of genes between these same time points, we find much larger pathway differences; one notable change is that in both WT and mutant there is a decrease in transcripts for cell cycle and nuclear division genes (Figure 17B). However, the mutant GO terms also describe decreases in expression of genes related to DNA replication and metabolism and cellular detection and response to stress stimuli, which are changes unique to the mutant (Figure 18B). The WT and mutant responses to 60-minute exposure to MMS compared to control samples are largely similar, primarily consisting of changes in transcripts associated with vesicle-mediated protein trafficking and protein catabolism (Figure 19A). Direct comparisons between upregulated pathways in MMS60 minutes did provide significant results, showing that the WT samples in this condition had a more robust expression of ribosome biogenesis, gene expression and RNA processing, translation, and methylation-related genes as compared to the mutant (Figure 19B). In regard to the downregulation response in control vs 60-minute MMS, we found that the WT and mutant have similar responses in downregulating ribosome biosynthesis, gene transcription and RNA processing, translation, methylation and nucleotide metabolism (Figure 19A-B). Differences in control vs MMS60 between WT and mutant are the WT's decrease in ATP synthesis and the mutant's decrease in nuclear division pathways (Figure 19). GO term comparisons were also performed between the MMS20 and MMS60 samples to reveal how the DNA-damage response

shifts over time, with similarities between WT and mutants mainly being upregulation of genes associated with proteolysis. The differences in upregulation between WT and mutant between these time points were striking, with WT upregulating nucleotide-excision repair, while mutants continued their upregulation of vesicle-mediated transport and began upregulation of double-strand break repair (Figure 20A). For the downregulated pathways in MMS20 vs MMS60 treatments, similarities included the regulation of ribosome biogenesis, RNA processing, amino acid synthesis, and methylation. Differences in the downregulated genes primarily occurred within the WT samples and included down regulation of translational and transcriptional pathways (Figure 20B). Taken together, we can conclude that *foParp1* knockout did have a significant impact on transcriptional profiles following exposure to a DNA-damaging agent: namely, the mutant's initial decrease in transcripts associated with DNA replication and cellular stress responses upon MMS exposure, the WT's use of the NER pathway from MMS20-MMS60 as opposed to the mutant's use of DSBR pathways, and the WT's increased expression of translation- and transcription-related genes at the 60-minute MMS timepoint.

A.

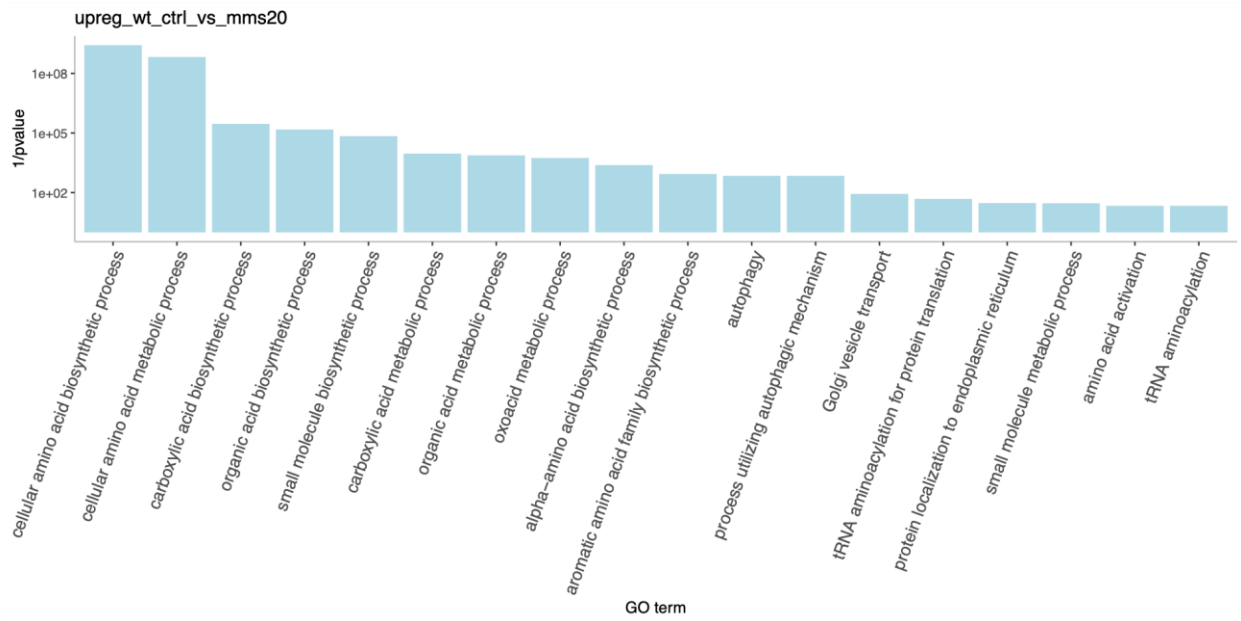
upreg_wt_ctrl_vs_mms20
1/pvalue
1e+08
1e+05
1e+02
cellular amino acid biosynthetic process
cellular amino acid metabolic process
carboxylic acid biosynthetic process
organic acid biosynthetic process
small molecule biosynthetic process
carboxylic acid metabolic process
organic acid metabolic process
oxoacid metabolic process
alpha-amino acid biosynthetic process
aromatic amino acid family biosynthetic process
autophagy
process utilizing autophagic mechanism
Golgi vesicle transport
tRNA aminoacylation for protein translation
protein localization to endoplasmic reticulum
small molecule metabolic process
amino acid activation
tRNA aminoacylation
GO term

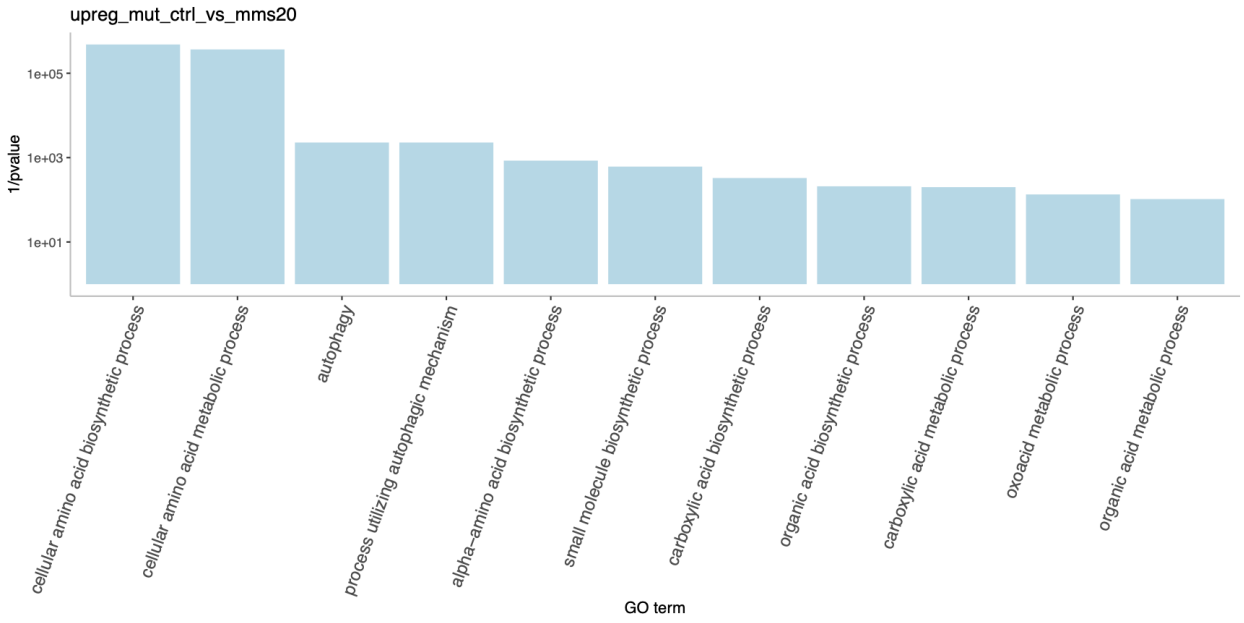
upreg_mut_ctrl_vs_mms20
1/pvalue
1e+05
1e+03
1e+01
cellular amino acid biosynthetic process
cellular amino acid metabolic process
autophagy
process utilizing autophagic mechanism
alpha-amino acid biosynthetic process
small molecule biosynthetic process
carboxylic acid biosynthetic process
organic acid biosynthetic process
carboxylic acid metabolic process
oxoacid metabolic process
organic acid metabolic process
GO term

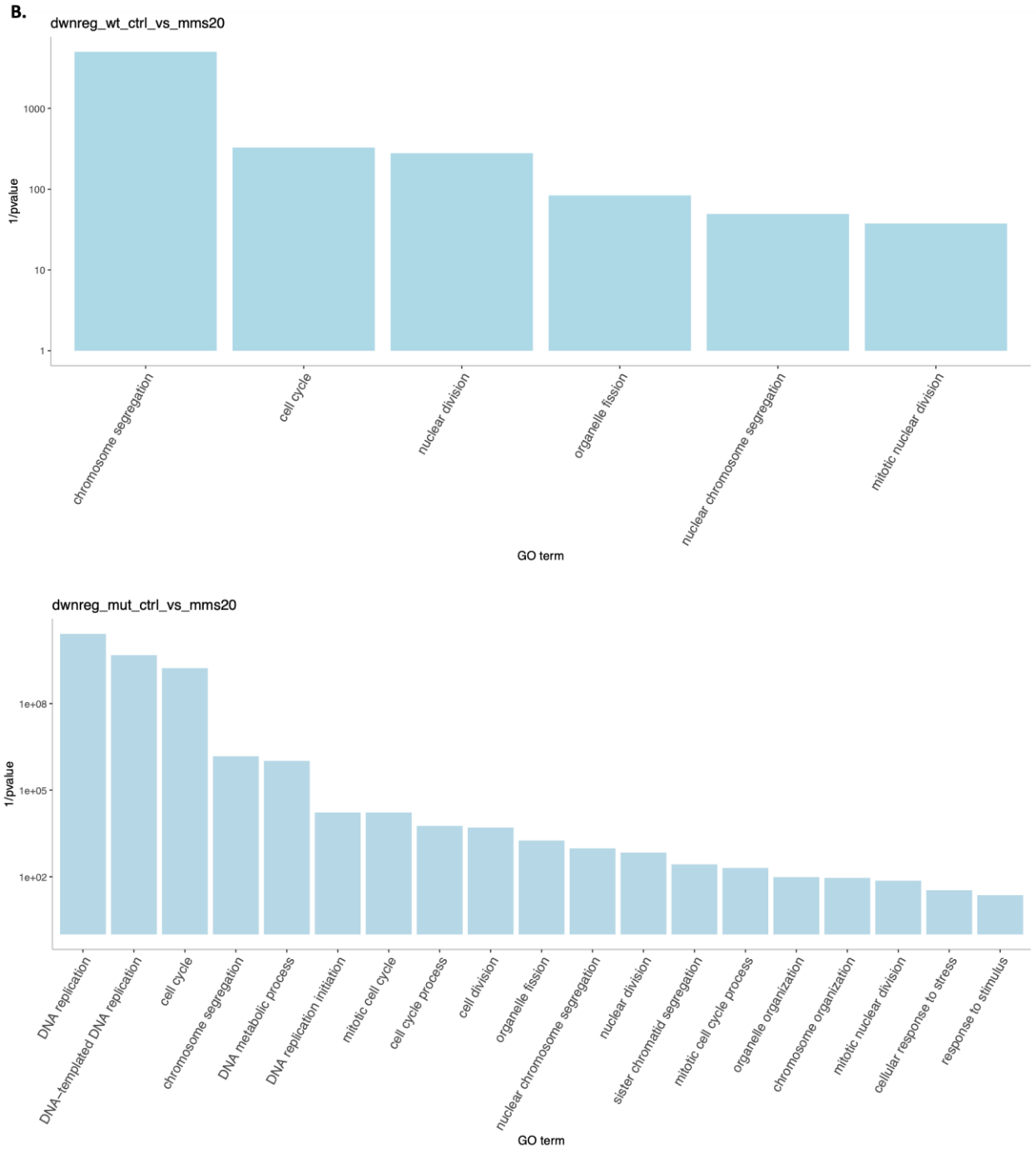

Figure 17: GO term analysis comparison between the WT and mutant Fol4287 strains under control conditions and 20 minutes of MMS exposure. A) The upregulated differentially expressed pathways found between the wild-type and mutant control and 20-minute MMS

exposure samples are shown. B) The downregulated differentially expressed pathways found between the wild-type and mutant control and 20-minute MMS exposure samples are shown.

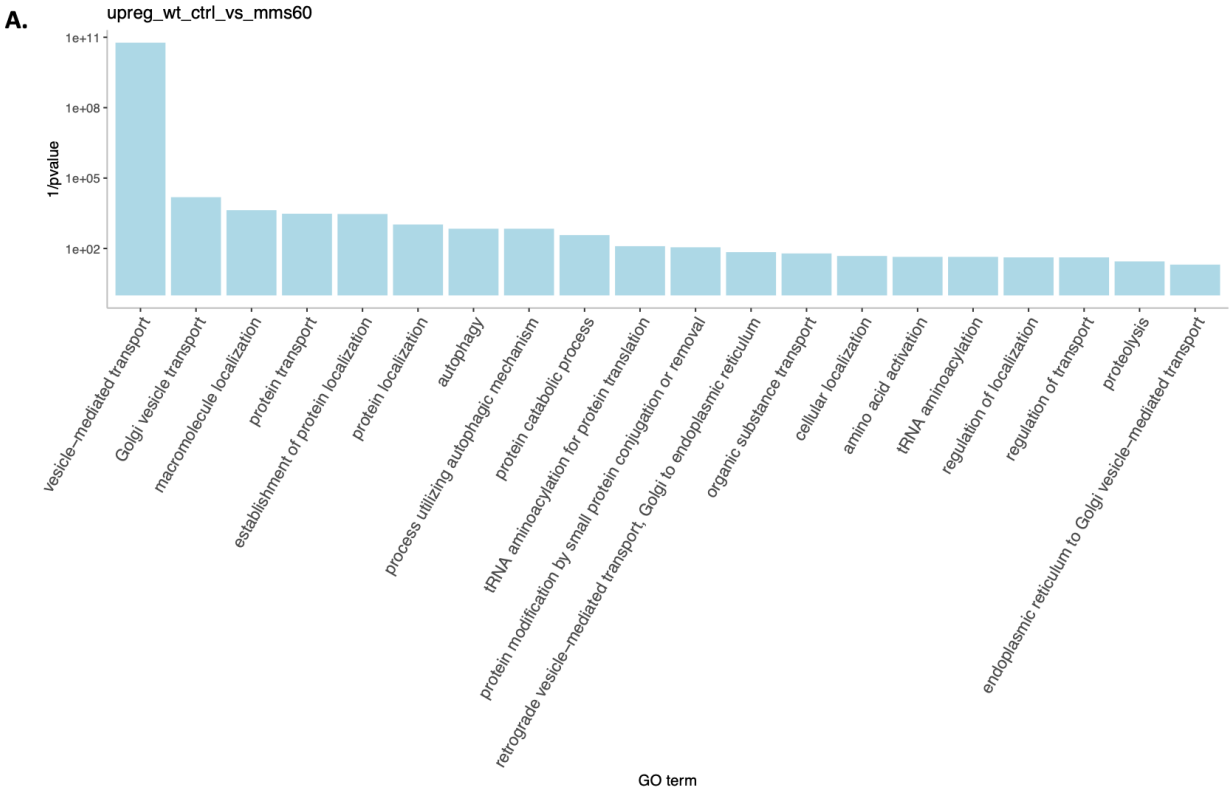

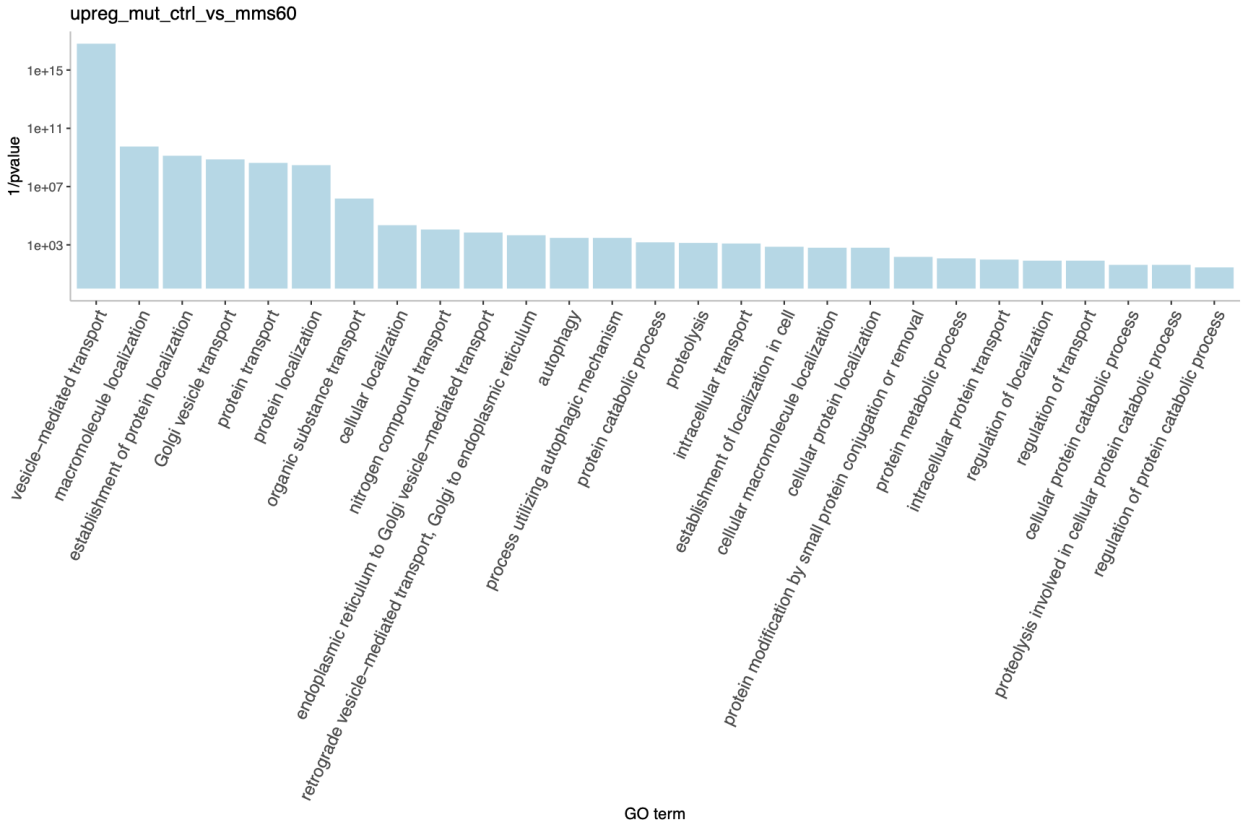
upreg_mut_ctrl_vs_mms60
1/pvalue
1e+15
1e+11
1e+07
1e+03
vesicle−mediated transport
macromolecule localization
establishment of protein localization
Golgi vesicle transport
protein transport
protein localization
organic substance transport
cellular localization
nitrogen compound transport
endoplasmic reticulum to Golgi vesicle−mediated transport
retrograde vesicle−mediated transport, Golgi to endoplasmic reticulum
autophagy
process utilizing autophagic mechanism
protein catabolic process
proteolysis
intracellular transport
establishment of localization in cell
cellular macromolecule localization
cellular protein localization
protein modification by small protein conjugation or removal
protein metabolic process
intracellular protein transport
regulation of localization
regulation of transport
cellular protein catabolic process
proteolysis involved in cellular protein catabolic process
regulation of protein catabolic process
GO term

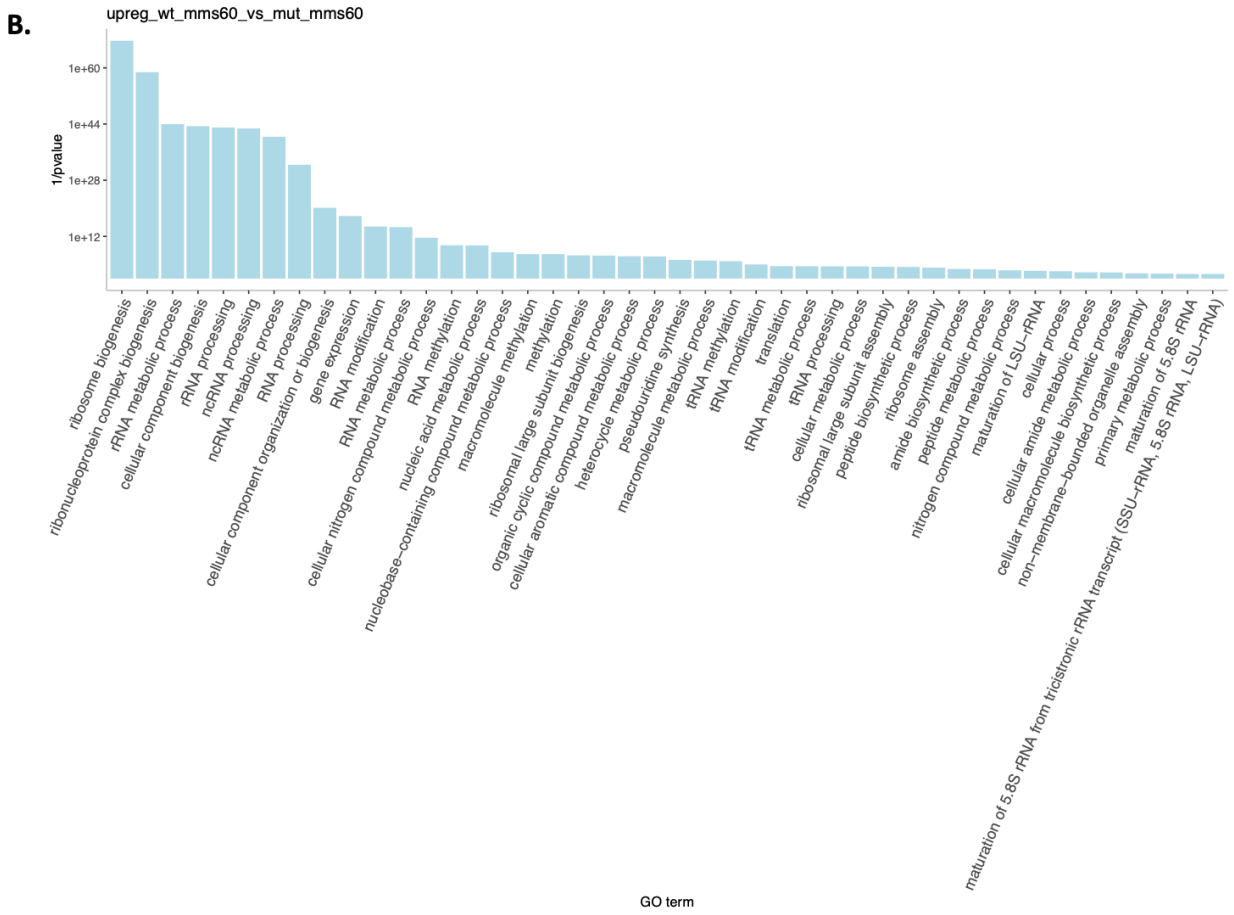

Figure 18: Comparison between the GO terms of genes upregulated between WT and mutant in control groups and 60 minutes of MMS exposure. A) Bar graphs showing the differentially expressed pathways between wild-type and mutant control versus 60-minute MMS exposure samples. The y-axis represents the multiplicative inverse of the p-value.B) Bar graph showing the differentially expressed pathways between wild-type and mutant 60-minute MMS exposure samples. The y-axis represents the multiplicative inverse of the p-value.

A.

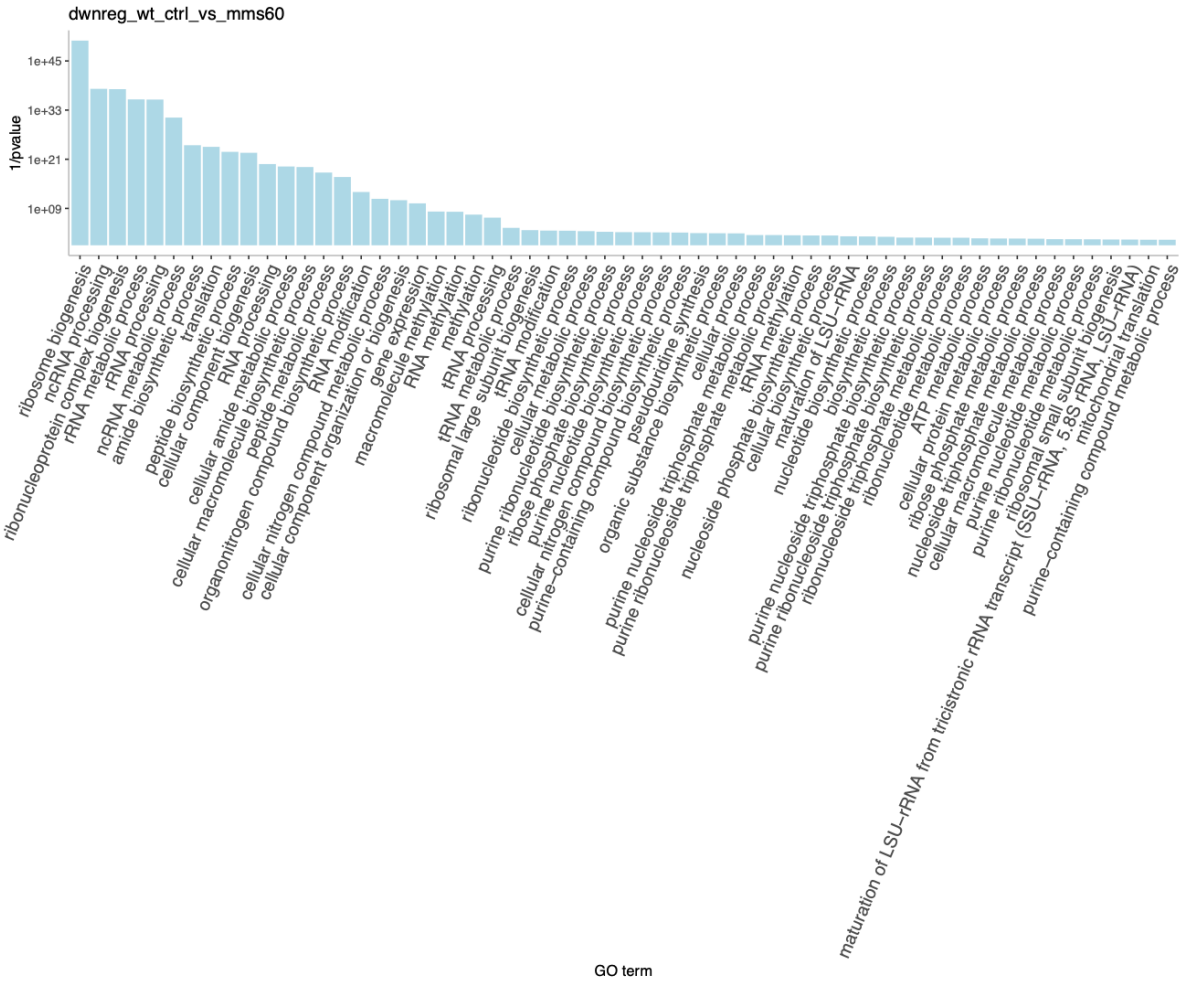
dwnreg_wt_ctrl_vs_mms60
1/pvalue
1e+45
1e+33
1e+21
1e+09
ribosome biogenesis
ncRNA processing
ribonucleoprotein complex biogenesis
rRNA metabolic process
rRNA processing
ncRNA metabolic process
amide biosynthetic process
peptide biosynthetic process
translation
cellular component biogenesis
RNA processing
cellular amide metabolic process
cellular macromolecule biosynthetic process
organonitrogen compound biosynthetic process
peptide metabolic process
cellular nitrogen compound biosynthetic process
RNA modification
cellular component organization or biogenesis
gene expression
macromolecule methylation
RNA methylation
methylation
tRNA processing
tRNA metabolic process
ribosomal large subunit biogenesis
ribonucleotide biosynthetic process
tRNA modification
cellular metabolic process
purine ribonucleotide biosynthetic process
ribose phosphate biosynthetic process
purine nucleotide biosynthetic process
cellular nitrogen compound biosynthetic process
purine–containing compound biosynthetic process
organic substance biosynthetic process
pseudouridine synthesis
purine nucleoside triphosphate biosynthetic process
purine ribonucleoside triphosphate metabolic process
nucleoside triphosphate biosynthetic process
cellular process
cellular biosynthetic process
tRNA methylation
nucleoside phosphate biosynthetic process
maturation of LSU–rRNA
nucleotide biosynthetic process
purine nucleoside triphosphate biosynthetic process
purine ribonucleoside triphosphate biosynthetic process
ribonucleoside triphosphate biosynthetic process
ribonucleotide metabolic process
ATP metabolic process
cellular protein metabolic process
ribose phosphate metabolic process
nucleoside triphosphate metabolic process
cellular macromolecule metabolic process
purine nucleotide metabolic process
purine ribonucleotide metabolic process
ribosomal small subunit biogenesis
mitochondrial translation
maturation of LSU–rRNA from tricistronic rRNA transcript (SSU–rRNA, 5.8S rRNA, LSU–rRNA)
purine–containing compound metabolic process
GO term

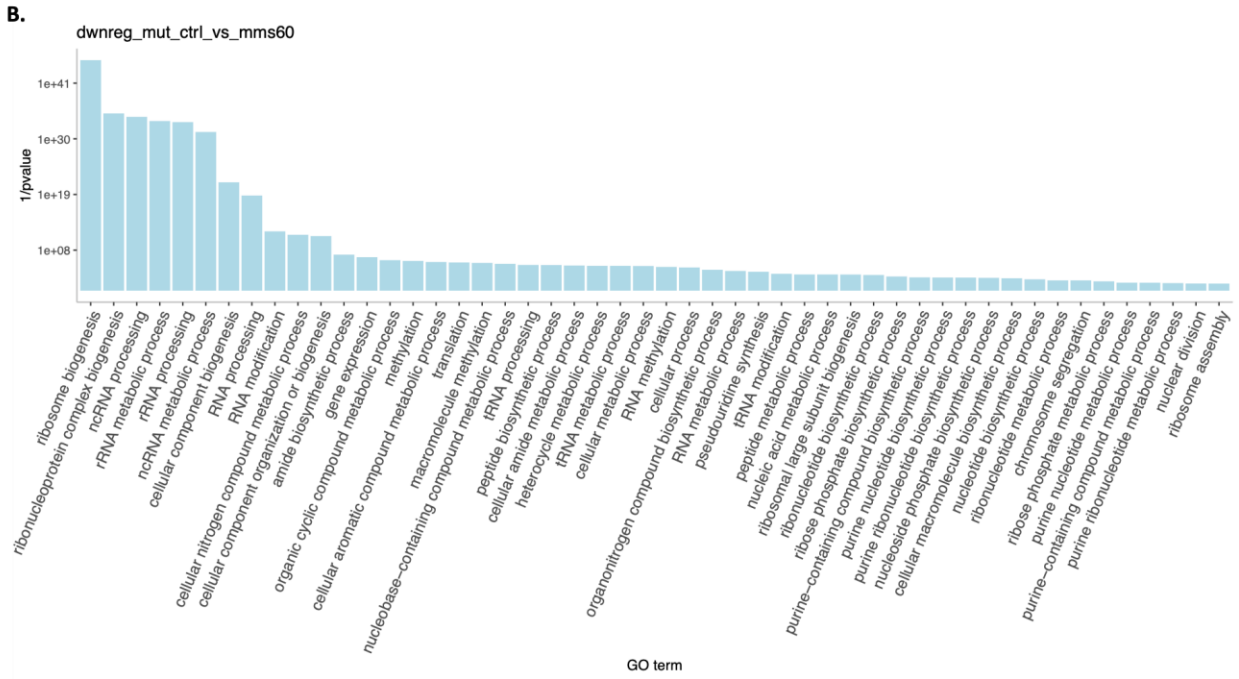

Figure 19: Comparison of the GO terms of genes downregulated? between WT and mutant in control groups and after 60 minutes of MMS exposure. A) Bar chart of the down regulated differentially expressed genes between the wild-type control and 60-minute MMS exposure samples. The y-axis displays the multiplicative inverse of the p-values. B) Bar chart of the down regulated differentially expressed genes between the mutant control and 60-minute MMS exposure samples. The y-axis displays the multiplicative inverse of the p-values.

A.

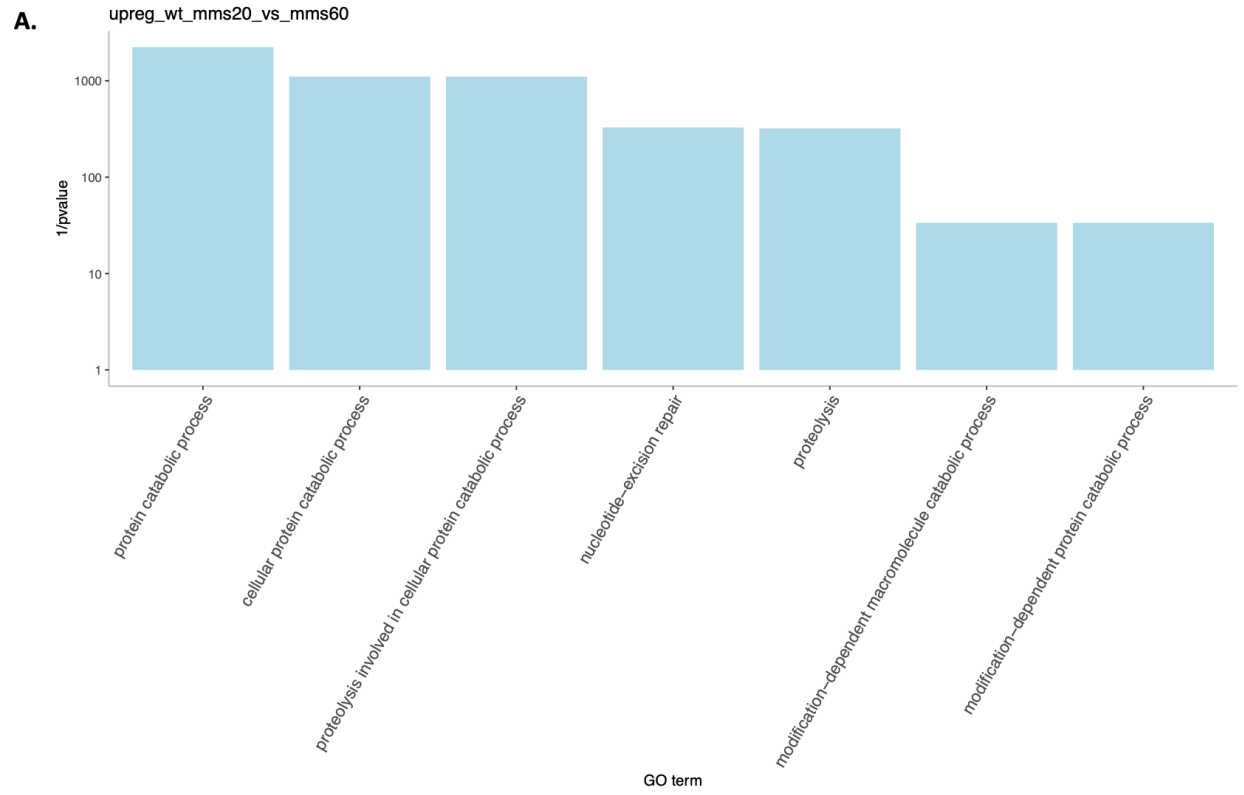
upreg_wt_mms20_vs_mms60
1/pvalue
1000
100
10
1
protein catabolic process
cellular protein catabolic process
proteolysis involved in cellular protein catabolic process
nucleotide−excision repair
proteolysis
modification−dependent macromolecule catabolic process
modification−dependent protein catabolic process
GO term

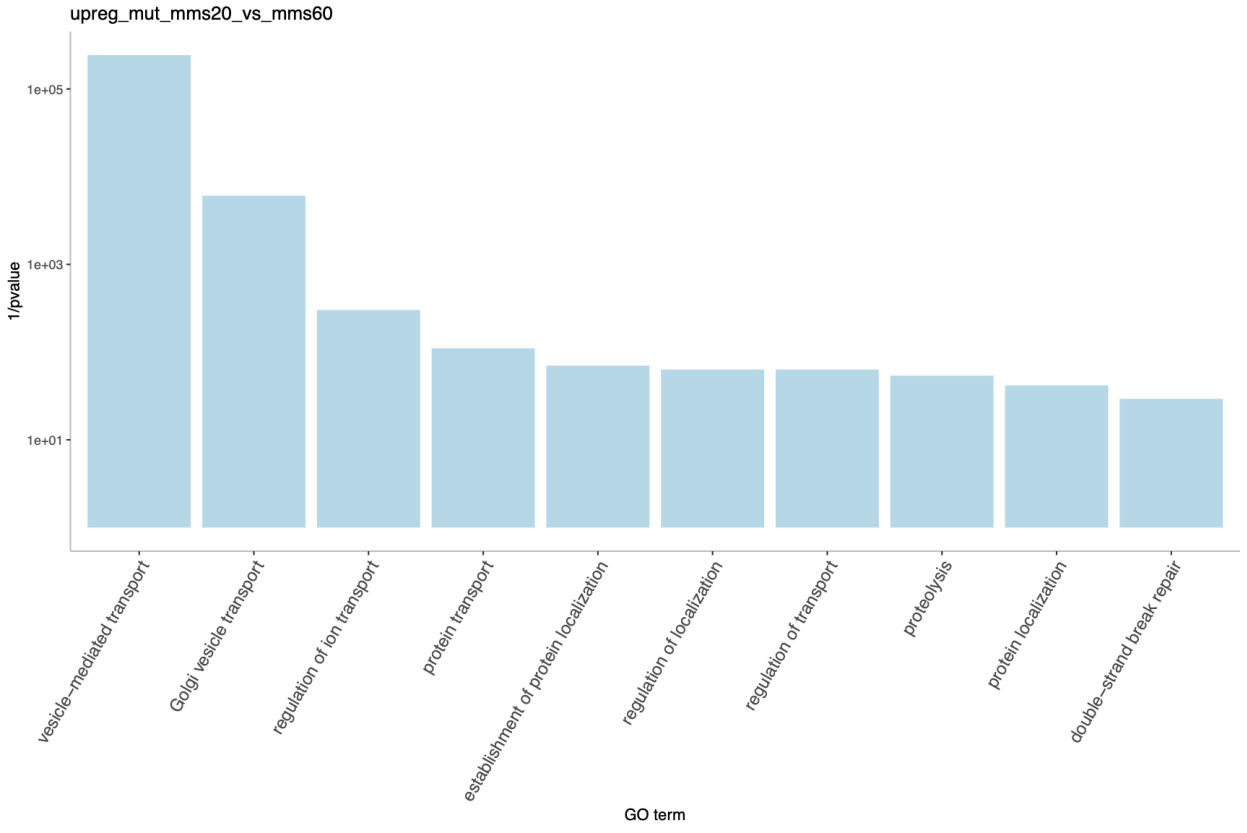
upreg_mut_mms20_vs_mms60
1/pvalue
1e+05
1e+03
1e+01
vesicle−mediated transport
Golgi vesicle transport
regulation of ion transport
protein transport
establishment of protein localization
regulation of localization
regulation of transport
proteolysis
protein localization
double−strand break repair
GO term

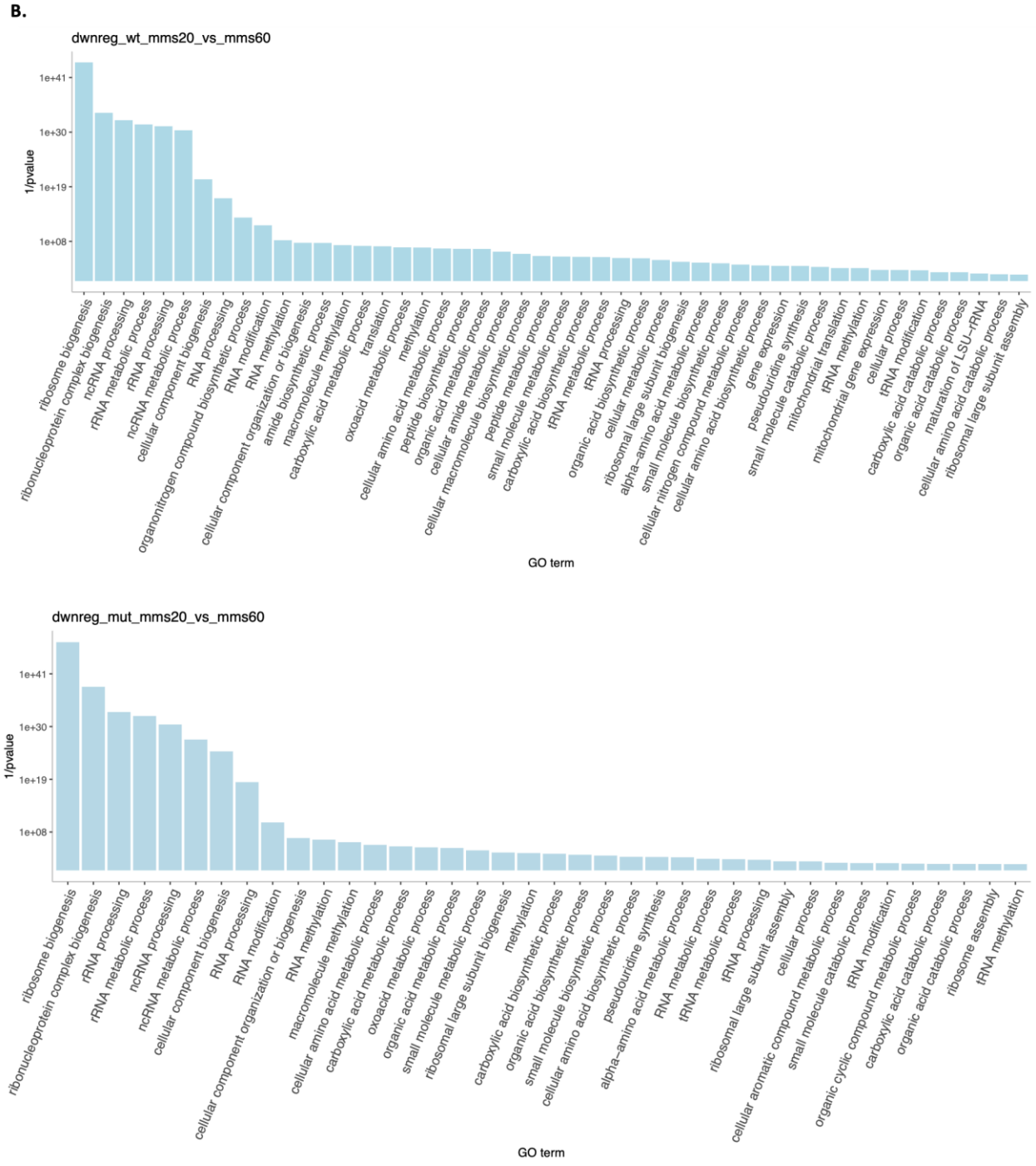

Figure 20: Comparison of GO terms between MMS 20 and MMS 60 in WT and Mutant. A) Upregulated pathways between 20 minutes of MMS exposure and 60 minutes of MMS exposure

in WT and mutant B) Downregulated pathways between 20 minutes of MMS exposure and 60 minutes of MMS exposure and 60 minutes of MMS exposure in WT and mutant.

CHAPTER

4. DISCUSSION

4.1 foPARP1 is predicted to have PARylating catalytic ability

To the best of our knowledge, to date, only one paper has experimentally characterized a PARylating enzyme within a filamentous fungus, *i.e.* in *Aspergillus nidulans* (Semighini, C. P., et al. 2006). Our identified PARylating candidate, foPARP1, contains a highly conserved catalytic domain and shares an H-Y-E catalytic triad with the well-characterized hPARP1 (Figure 7A). Given the high sequence similarity and the presence of the H-Y-E motif in all human PARylating proteins, it can be hypothesized that foPARP1 will have PARylating capacity (Vyas, S. *et al.* 2014). foPARP1 was found to be encoded by one gene copy located on the core chromosomes of all three strains comprising our comparative system (Figure 6). Fo47 does not contain any PARP catalytic-domain-containing proteins on its accessory chromosome (Figure 4), and multiple sequence alignments of Fol4287's accessory chromosome PARP proteins revealed no other *F. oxysporum* PARPs that contain either the H-Y-E or R-S-E conserved ART motifs (Figure 7 and 8). Interestingly, Fo5176 contains a *foParp1* homolog, 525699, within its accessory chromosome; this gene is predicted to encode a protein which has all of the protein domains characteristic of a PARP, aligns with the H-Y-E motif of hPARP1, and shares a similar percent identity as foPARP1 with hPARP1's catalytic domain, 44.1% and 43.5% for foPARP1 and 525699, respectively (Figure 5, 6, and 7). Fo5176 also contains another hypothetical PARP protein, 525060, which contains the H-Y-E motif and shares the same percent identity to hPARP1 as 525699 does (Figure 6). Fo5176 also contains two PARP proteins with a H-Y-V conserved amino acid triad; to our knowledge, no characterized ART transferase is known to contain this motif. However, hPARP 6-12 and hPARP 14-15 contain H-Y-I or H-Y-L motifs,

and given valine's similar nonpolar properties to both isoleucine and leucine, it is possible that these hypothetical PARP proteins could share MARyaltion activity similar to these known hPARPs (Vyas, S. *et al.* 2014, Figure 6). In our alignments, no other predicted PARP proteins contain conserved catalytic motifs of H-Y-E, H-Y-I, H-Y-L, Q-Y-T, or Y-Y-V found in the PARylating, MARylating, and catalytically inactive hPARPs, nor the R-S-E motif found in the CTX family of exotoxins (Figure 6 and G, Vyas, S. *et al.* 2014). Taken together, we predicted that Fo47 and Fol4287 each contains only one functional PARylating protein, foPARP1, while Fo5176 contains three predicted PARylating proteins, foPARP1, 525699, and 525060 and several predicted MARylating/ADP-transferase proteins.

Although multiple sequence alignments can be a powerful predictive tool, this is only part of the story in the characterization of the function of a given protein. The alignment against well-characterized catalytic residues can give insight into the possible catalytic function of an enzyme; this approach is, however, limited by the fact that we are comparing fungal and human proteins, which are from phylogenetically distant species. Also, the fungal PARPs are not well-studied, meaning that there are possible unique fungal catalytic motifs that have not yet been elucidated and therefore cannot be taken into account upon the writing of this document. Finally, percent identity is not a perfect measure of homology; although the 30% identity for homology is a good rule of thumb, it is not confirmation; proteins can have a small percent identity and still be functional homologs or show a higher than 30% identity but have distinct structures and functions. In these cases, generally three-dimensional structures are needed to confirm whether the two compared proteins share conserved secondary and tertiary structures to determine homology. Additional *in silico* analysis that could shed insight into the function of the non-H-Y-E-containing PARP-like proteins could be done with predictive three-dimensional structures,

such as those provided by Robertta, AlphaFold or SwissProt. Analysis on whether the uncharacterized PARP-like proteins share conserved structures of the ART family such as the ART fold, Acceptor and/or Donor Loops could also provide insight into the function of these proteins.

4.2 The number of PARP genes is positively correlated with MMS-induced DNA-damage tolerance.

From the phenotyping data generated for MMS-induced stress, we can conclude that MMS does impact the growth of all strains within the comparative system. We can also conclude that for the pathogenic strains, Fol4287 and Fo5176, the knockout of fo*Parp1* does in fact have a significant effect on the strain's ability to tolerate MMS damage. Notably, the nonpathogenic endophyte Fo47 did not display significant changes in MMS tolerance after the knockout of fo*Parp1*. Fo5176 was shown to have the highest tolerance to MMS-mediated stress in both the WT and fo*Parp1* mutants. Fo47 was shown to have the least tolerance in WT tests to MMS stress, while Fol4287 showed the least tolerance to MMS stress within the fo*Parp1* mutant experiments. Within the WT conditions, although the differences in MMS versus control ratios were not statistically significant between Fo47 and Fol4287 and between Fol4287 and Fo5176, the difference between Fo47 and Fo5176 ratios was statistically significant. This may support a connection between *Parp* copy number and alkylating DNA-damage tolerance in the WT strains; however, further testing encompassing additional replicates and possibly other strains should be conducted to make a strong conclusion on whether the *Parp* copy number or other factors are responsible for this difference in MMS tolerance. Within the mutant phenotyping, the only significant difference in MMS tolerance was between the Fol4287 and Fo5176 mutants, while

the deletion-strain differences between Fo47 and Fol4287 and between Fo47 and Fo5176 were nonsignificant. The mutant strains overall had a smaller difference in MMS tolerance and an overall lowered tolerance as compared to the WT strains. Given that the *foParp1* knockout has been shown to reduce two out of the three strain's ability to tolerate DNA alkylating damage, this finding adds experimental evidence that foPARP1 is in fact a hPARP1 homolog, as one of hPARP1's best-characterized functions is that of a DNA repair protein.

4.3 Basal cellular and MMS-induced PARylation levels in *F. oxysporum* can be detected using PAR-specific antibodies.

From the WT dot-blot, we can confirm that each of the strains within the comparative system has the capacity to catalyze the production of pADPr chains equal to or greater than 20 ADP-ribose units in length (Figure 12, Kudo, Y. *et al.* 2018). The significance of this novel finding serves to confirm that strains within the *F. oxysporum* complex do contain PARP-like proteins, as we predicted in our *in silico* analysis. Using the assay we optimized for *F. oxysporum*, it was shown that with the addition of MMS, PARG inhibitor, and excess NAD+, Fo47 and Fo5176 had significant increases in PARylation (Figure 12).

The results of the mutant dot-blot reviewed in this section are in agreement with the *in silico* analysis and *in vitro* phenotyping, in that knockout of the predicted PARylating PARP1-like gene resulted in a disruption of the capacity to synthesize long pADPr chains, as shown by the decrease in PAR detected in both Fo47 and Fo5176 mutants (Figure 13). It should be noted that the protocols for each of the immunoblots were identical, and that overall the ECL signal detection was lower for the mutant blots as compared to the WT, even with both membranes having been loaded with an identical protein concentration of 10 µg/mL per sample and treated

with the same amount of antibody and ECL solution. This suggests an overall lower concentration of PAR chains detected and thus lower PARylation; however, to confirm this finding, an additional immunoblot would need to be performed containing samples from both the WT and mutant strains. Nevertheless, the mutants exhibit a lower induction of PARylation in response to MMS, confirming that foPARP1 does impact the creation of MMS-induced PAR chains (Figure 14). Longer pADPr chains (such as those greater than 20 units) have been associated with chromatin remodeling (Thomas, C. *et al.*2019), suggesting that the mutants will have an impacted transcriptional activity when compared to wild-type during MMS-mediated DNA stress, which will be discussed further in the next section. Contrary to our hypotheses from the *in silico* and phenotyping section, the Fo47 *foParp1* mutant does retain the capacity to produce long pADPr chains, despite Fo47 being predicted to have only one protein capable of catalyzing the synthesis of PAR chains, foPARP1 (Figure 7 and 13). Our catalytic-domain-prediction software pointed to only three core chromosome proteins that contain the conserved PARP catalytic domain, foPARP1, PARP-Ubc, and the third core PARP 275451, while our multiple sequence alignment programs indicated that only one core chromosome protein, foPARP1, contained a conserved catalytic motif that would be capable of catalyzing the PARylation reaction (Figure 7). We predicted that Fo47 and Fol4287 would completely lose the capacity to produce long PAR chains due to neither strain containing a PARP-like protein that has the H-Y-E catalytic domain; however, this was shown to not be the case, as both strains retain some capacity to produce PAR chains (Figure 14). This suggests that another core chromosome PARP or an undetected protein has the capacity to catalyze the formation of PAR chains of a length of 20 or more ADP-ribose moieties. PAR retention should not be affected by additional PARG proteins, as all three strains contain one conserved PARG gene, and DNA-

damage samples were all treated with equal amounts of PARG inhibitors. It is also unlikely that Fo47Δ and Fol4287Δ's maintained ability to catalyze the synthesis of long pADPr chains was due to a failure of our CRISPR knockout system, given that the deletion of *Parp1*, as well as the insertion of the Hygromycin B gene into the *foParp1* open reading frame, was confirmed by both PCR and Sanger sequencing (Supplementary Figure 1). This leaves an open question: how are Fo47Δ and Fol4287Δ able to retain their ability to synthesize long pADPr chains? Possibilities could range from undiscovered PARP-like genes that reside within the core or accessory chromosomes, an ability of the other two core PARP-like proteins to form complexes by oligermizing with other proteins to gain PARylation activity, the binding of the primary antibody to a molecule similar to PAR, or a previously undiscovered pathway capable of synthesizing poly-ADP-ribose chains without PARP proteins. The retained ability for Fo5176Δ to form long pADPr chains was observed in the mutant dot-blot as hypothesized in earlier sections, likely due to the additional PARP gene copies located within the accessory chromosomes that shared a high percent identity of their catalytic domains with hPARP1 and the presence of the conserved H-Y-E motif also found within human PARylating PARPs (Figure 7, Vyas, S. *et al.* 2014). However, given the ability of FO47Δ to synthesize or preserve pADPr chains by some unknown mechanism, it cannot be concluded that the reason for FO5176Δ's retained PARylating ability is solely caused by the additional H-Y-E-containing proteins. Overall, we can conclude that all strains do have the capacity to produce PAR chains and that foPARP1 does have an influence on the production of these PAR chains.

The results of the dot-blot open exciting avenues of continued research into the PARP expansion within *F. oxysporum*. One avenue of investigation would be to expand the immunoblotting approach from a dot-blot to a Western blot; the data generated thus would be

able to separate pADPr-bound proteins by size; this coupled with insights from further RNA-Seq analysis could serve to identity proteins involved in the foPARP1 interactome. Additionally, utilizing the protocol generated for the dot-blot, the MARylating capacities of the PARP expansion could be explored, as well as investigations into shorter pADPr chains (<20 ADP-ribose units in length). The mechanism behind Fo47Δ and Fol4287Δ retaining their ability to make long pADPr chains would provide great insight into the PARP expansion and the roles of related proteins.

4.4 Transcriptome analysis of *Parp1*-deficient strains reveals attenuated transcriptional response to MMS-induced DNA damage in *F. oxysporum.*

From the results shown above, it can be concluded that *foParp1* is involved in transcriptional regulation under DNA-damage conditions as shown by the changes in gene expression impacting a variety of biological pathways in Fol4287Δ (Figures 16-19). The first analysis performed after receiving the DE data was to ensure that the knockout of *foParp1* within the mutant samples was successful, which was confirmed by no expression of *Parp1* in the mutant (Figure 16). Global differential expression trends were recorded and observed, with the most noticeable trend being an overall decrease in the differential expression of genes within Fol4287Δ when compared to WT (Table 2). Within the global DE data, there were also significant transcriptional differences between the mutant and WT with regard to the number of differentially expressed genes, generally varying by the thousands in each sample type (Table 2). hPARP1 is known to competitively bind with H1 and to associate with RNA polymerase II, which could serve as a possible explanation for the global decreases we saw in transcriptional activity within our comparative system (Yu, D., *et al*. 2018, Kim, M. Y., *et al*. 2004, Schiewer,

M. J. & Knudsen, 2014). We also noted that – except for *foParp1* itself – only the expression of *Parp-Ubc*, the fungal-specific PARP, had its expression changed significantly within the *foParp1* mutant, with all other *Parp* genes showing either no significant change or no transcript detected by our sequencing (Table 4). This finding lays the foundation that foPARP1 has a possible transcriptional impact on *Parp-Ubc* and may be involved in the regulation of this gene during the response to alkylating DNA damage. Taken together, it can be concluded that *Parp-Ubc* is involved in the alkylating DNA repair response, as seen by its significant upregulation in both the RNA-Seq and RT-qPCR data (Figure 12 and Table 4). However, the picture is less clear in regards to the accessory and FOXG_20370 core PARPs, which were shown by qRT-PCR to be differentially expressed in response to MMS-mediated stress (Figure 12). These apparent contradictions could be explained by the accessory PARPs having low transcript levels which might not be detected during RNA-Seq, but could be detected upon amplification with PARP-specific primers in qRT-PCR. More experimentation would be needed to confirm if foPARP1 does or does not have a direct or indirect impact on the other PARPs' expression, such as a repeated qRT-PCR experiment using the WT and mutant strains.

With these transcriptional differences between the WT and mutant samples, we proceeded to tag differentially expressed genes to Gene Ontology terms, allowing for pathway-level analysis of the transcriptional changes. Comparing the GO term results of the different sample conditions between the same sample types gave us evidence of the effects that *foParp1* knockout had on the mutant. Where the GO analysis yielded the most striking results was in the comparisons between control and 20-minute exposure to MMS, 20-minute exposure to MMS and 60-minute exposure to MMS, and WT and mutant expression during the 60-minute MMS treatment samples. The mutant and wild-type samples shared a similar response to the 20

minutes of MMS exposure, upregulating genes associated with amino acid and protein synthesis and shutting down cellular division; however, *foParp1Δ* mutants did show a unique reduction in transcripts linked to DNA replication and cellular stress response pathways, including several DNA-damage pathways during this period of stress (Figure 19B.). This finding suggests an increased cell cycle arrest, possibly caused by the loss of function of the classically defined DNA repair activities of PARP1 and its ability to regulate chromatin structures when encountering DNA damage (Ray Chaudhuri, A. & Nussenzweig, 2017). In comparing 20 minutes of MMS exposure to 60 minutes of exposure, one of the most striking differences in expression was the upregulation of the expression of NER-related genes in the WT samples, while in the mutants, genes involved in double-strand-break response were induced (Figure 20A). This finding suggests that foPARP1 has a role in the regulation of NER pathway genes. The observation that mutant samples expressed genes contained within the double-strand-break-repair pathway, as opposed to the NER pathway of the WT samples, may suggest that more SSB damage is accumulating in the mutants that, when not efficiently repaired, transforms into DSBs and therefore induces DSB-repair mechanisms. MMS has been shown in previous work to induce the expression of NER-related genes; the decrease in NER gene expression within our mutant RNA-Seq data suggests that *foParp1* is involved in regulating the expression of these genes (Milo-Cochavi, S. *et al.* 2019). Within the direct comparison of WT and mutant samples after 60 minute of MMS exposure, the WT samples in this condition had a more robust expression of ribosome synthesis, gene expression and RNA processing, translation, and methylation-related genes as compared to the mutant, even though many of these genes were being downregulated when comparing the wild-type response in 20 minutes of MMS exposure to 60 minutes of exposure (Figures 18B and 19). These findings, along with the downregulation of stress-response

genes in the control vs 20-minute mutants, suggest a larger role of *foParp1* (Figures 17, 18). The loss of *foParp1* appears to contribute to creating a transcriptome less responsive to the stress stimuli affecting the cell, slowing down the transcriptional response to the changing conditions caused by a prolonged exposure to DNA stress agents (Figures 17, 19, and 20).

Although the Differential Expression and Gene Ontology analysis give insight into the global changes in the transcriptome that are caused by DNA damage and *foParp1* knockout, these forms of analysis are broad and require further analysis to determine direct causes for the changes viewed in the transcriptome. Our approach thus far does not focus on any one gene, outside of the *Parp* genes themselves, and further investigations into the dataset that we generated could provide insight into the global changes we have outlined and may elucidate interaction partners of *foPARP1*, which could serve to expand our knowledge of the *foPARP1* interactome.

4.5 Conclusion

Taken together, we can be confident in concluding that all strains of our comparative system have a hPARP1 homolog in a core chromosome, encoding a PARP-like protein, foPARP1. The presence of a conserved H-Y-E catalytic motif, the reduction in tolerance to DNA damage seen in the growth assays, the decrease in PARylation induction seen in the immunodot-blot, and the transcriptional impact caused by *foParp1* knockout, all serve to show that foPARP1 shares many similar functions to hPARP1 and can be thought of as a hPARP1 homolog. From the immunoblot results received from the *foParp1* knockouts in Fo47 and Fol4287, it appears that some level of PARylation is present in the cell even in the absence of foPARP1, an observation that was not predicted within our *in silico* analysis. From the *in vitro* phenotyping and immunoblotting results, we were able to show the contribution of PARP1 to DNA damage

tolerance and cellular PARylation. However, at this point, we were not able to definitively determine if the PARP copy number had a significant impact on the tolerance to DNA damage across our three-strain comparative system. The impact that any of the PARP-like proteins have on infection or invasion of a host was also outside the purview of the study, so the exact adaptive pressures that spurred the expansion of PARP genes within the *F. oxysporum* species complex remain unknown. Still, our initial characterization of this gene family in *F. oxysporum* provides a foundation for further studies into the effect that this unique expansion has within the species complex.

SUPPLEMENTARY FIGURES

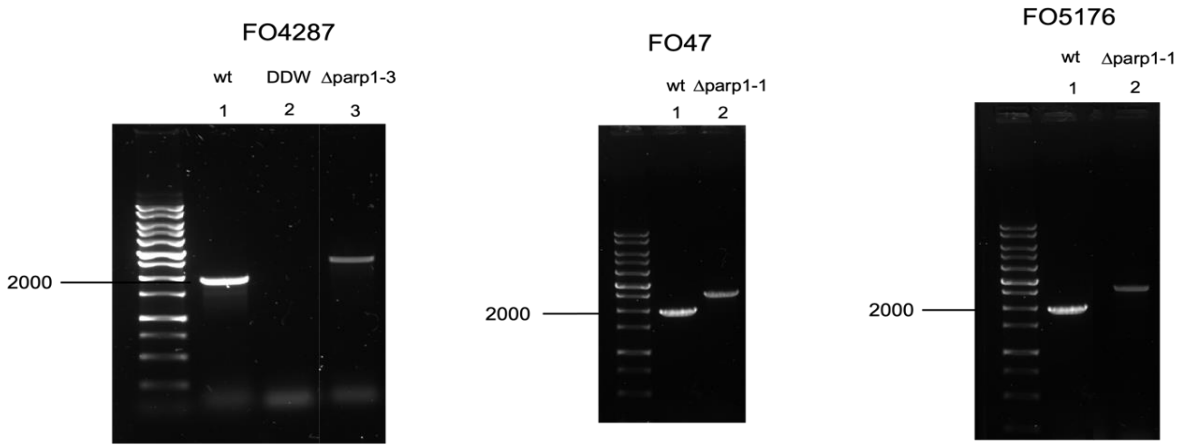

Supplementary Figure 1: PCR results from all three strains showing size difference between WT foParp1 genes and the foParp1 genes with a hygromycin-resistance cassette inserted. A 1 kb ladder was used with the 2000 base pair band marked. The foParp1 gene was detected using a primer whose product would result in a fragment 1.9-kb in size. A 1.1-kb fragment was deleted from the Parp1 gene, and a 2.1-kb hygromycin-resistance gene was inserted in its place for a total length of ~3 kb as seen in lane #2 (Fo47, Fo5176) and 3 (Fol4287) in the gel images. Lane #1 shows a WT Parp1 PCR product, with the length of 2.1 kb, for each strain. Mutants and figures created by Cecelia Murphy.

Supplementary Table 1: Qubit RNA concentrations of WT and mutant samples sent for RNA-Sequencing.

Sample Name	Sample Number	Concentration (ng/μL)
WT 4287 Control 1	1	148

WT 4287 Control 2	2	244
WT 4287 Control 3	3	186
WT 4287 20 minutes MMS 1	4	63
WT 4287 20 minutes MMS 2	5	83.8
WT 4287 20 minutes MMS 3	6	69
WT 4287 1 hour MMS 1	7	71.6
WT 4287 1 hour MMS 2	8	141
WT 4287 1 hour MMS 3	9	120
Mutant 4287 Control 1	10	242
Mutant 4287 Control 2	11	197
Mutant 4287 Control 3	12	224
Mutant 4287 20 minutes MMS 1	13	150
Mutant 4287 20 minutes MMS 2	14	95.8
Mutant 4287 20 minutes MMS 3	15	108
Mutant 4287 1 hour MMS 1	16	185
Mutant 4287 1 hour MMS 2	17	137
Mutant 4287 1 hour MMS 3	18	194

Supplementary Figure 2: Bioanalyzer results from the 18 samples sent for RNA-Sequencing. A) The first 12 samples from Supplemental Table 1 were tested for lack of RNA degradation, as seen as peaks around 18 and 28 nt which signify the presence of intact 18S and 28S ribosomal RNAs. B) Sample 9 from the first batch of Bioanalyzer results was retested as sample 1, while samples 2-7 correlate to samples 13-18 in Supplemental Table 1.

Supplementary Table 2: Total read numbers from all RNA-Seq samples

Sample Name	Total Read Pairs	Total Reads (R1 + R2)
WT Control 1	30915251	61830502
WT Control 2	26483457	52966914
WT Control 3	23763760	47527520
WT 20 min MMS 1	24138981	48277962
WT 20 min MMS 2	24236150	48472300
WT 20 min MMS 3	21727171	43454342
WT 60 min MMS 1	26410685	52821370
WT 60 min MMS 2	30366278	60732556
WT 60 min MMS 3	27283204	54566408
Mut Control 1	30342154	60684308
Mut Control 2	31076963	62153926
Mut Control 3	33493748	66987496
Mut 20 min MMS 1	30370227	60740454
Mut 20 min MMS 2	28963917	57927834
Mut 20 min MMS 3	23236428	46472856
Mut 60 min MMS 1	25734765	51469530
Mut 60 min MMS 2	25501195	51002390
Mut 60 min MMS 3	24933538	49867076

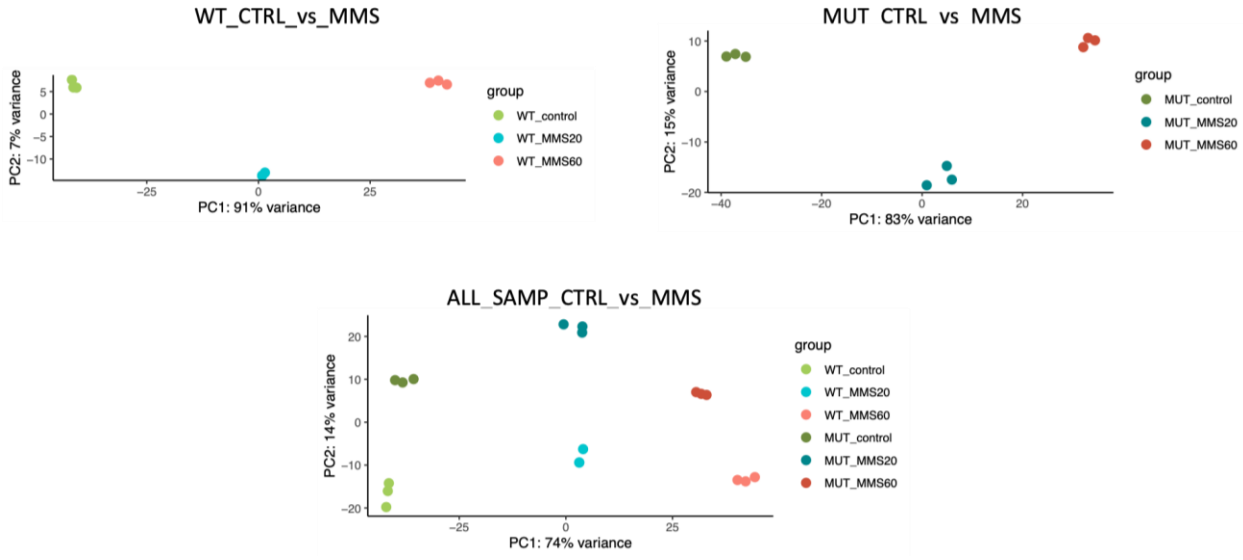

Supplementary Figure 3: PCA plots of WT and mutant RNA-Seq groups. PCA plots were created using the raw read data of each sample type.

BIBLIOGRAPHY

1.

Alemasova, E. E. & Lavrik, O. I. Poly(ADP-ribosyl)ation by PARP1: reaction mechanism and regulatory proteins. *Nucleic Acids Res* **47**, 3811–3827 (2019).

2.

Alvarez-Gonzalez, R. & Althaus, F. R. Poly(ADP-ribose) catabolism in mammalian cells exposed to DNA-damaging agents. *Mutation Research/DNA Repair* **218**, 67–74 (1989).

3.

Amé, J.-C., Spenlehauer, C. & de Murcia, G. The PARP superfamily: Review articles. *Bioessays* **26**, 882–893 (2004).

4.

Anderson, K. A., Madsen, A. S., Olsen, C. A. & Hirschey, M. D. Metabolic control by sirtuins and other enzymes that sense NAD+, NADH, or their ratio. *Biochimica et Biophysica Acta (BBA) - Bioenergetics* **1858**, 991–998 (2017).

5.

Aoki, T., O'Donnell, K. & Geiser, D. M. Systematics of key phytopathogenic Fusarium species: current status and future challenges. *J Gen Plant Pathol* **80**, 189–201 (2014).

6.

Aravind, L., Zhang, D., de Souza, R. F., Anand, S. & Iyer, L. M. The Natural History of ADP-Ribosyltransferases and the ADP-Ribosylation System. in *Endogenous ADP-Ribosylation* (ed. Koch-Nolte, F.) vol. 384 3–32 (Springer International Publishing, 2014).

7.

Barkauskaite, E., Jankevicius, G. & Ahel, I. Structures and Mechanisms of Enzymes Employed in the Synthesis and Degradation of PARP-Dependent Protein ADP-Ribosylation. *Molecular Cell* **58**, 935–946 (2015).

8.

Bellocchi, D. *et al.* Poly(ADP-Ribose)-Polymerase-Catalyzed Hydrolysis of NAD+: QM/MM Simulation of the Enzyme Reaction. *ChemMedChem* **1**, 533–539 (2006).

9.

Burkle, A. Poly(ADP-ribose). The most elaborate metabolite of NAD+. *FEBS Journal* **272**, 4576–4589 (2005).

10.

Caldecott, K. W. Single-strand break repair and genetic disease. *Nat Rev Genet* **9**, 619–631 (2008).

11.

Chatterjee, N. & Walker, G. C. Mechanisms of DNA damage, repair, and mutagenesis: DNA Damage and Repair. *Environ. Mol. Mutagen.* **58**, 235–263 (2017).

12.

Chou, H.-Y. E., Chou, H. T. & Lee, S.-C. CDK-dependent Activation of Poly(ADP-ribose) Polymerase Member 10 (PARP10). *Journal of Biological Chemistry* **281**, 15201–15207 (2006).

13.

Citarelli, M., Teotia, S. & Lamb, R. S. Evolutionary history of the poly(ADP-ribose) polymerase gene family in eukaryotes. *BMC Evol Biol* **10**, 308 (2010).

14.

Cohen, M. S. & Chang, P. Insights into the biogenesis, function, and regulation of ADP-ribosylation. *Nat Chem Biol* **14**, 236–243 (2018).

15.

Covarrubias, A. J., Perrone, R., Grozio, A. & Verdin, E. NAD+ metabolism and its roles in cellular processes during ageing. *Nat Rev Mol Cell Biol* **22**, 119–141 (2021).

16.

Croft, T., Venkatakrishnan, P. & Lin, S.-J. NAD+ Metabolism and Regulation: Lessons From Yeast. *Biomolecules* **10**, 330 (2020).

17.

D'Amours, D., Desnoyers, S., D'Silva, I. & Poirier, G. G. Poly(ADP-ribosyl)ation reactions in the regulation of nuclear functions. *Biochem J* **342 (Pt 2)**, 249–268 (1999).

18.

David, K. K. Parthanatos, a messenger of death. *Front Biosci* **Volume**, 1116 (2009).

19.

DeIulio, G. A. *et al.* Kinome Expansion in the *Fusarium oxysporum* Species Complex Driven by Accessory Chromosomes. *mSphere* **3**, e00231-18 (2018).

20.

Di Giammartino, D. C., Shi, Y. & Manley, J. L. PARP1 Represses PAP and Inhibits Polyadenylation during Heat Shock. *Molecular Cell* **49**, 7–17 (2013).

21.

Feng, B., Liu, C., Shan, L. & He, P. Protein ADP-Ribosylation Takes Control in Plant–Bacterium Interactions. *PLoS Pathog* **12**, e1005941 (2016).

22.

Fouquerel, E. *et al.* ARTD1/PARP1 Negatively Regulates Glycolysis by Inhibiting Hexokinase 1 Independent of NAD + Depletion. *Cell Reports* **8**, 1819–1831 (2014).

23.

Frascotti, G. *et al.* The Vault Nanoparticle: A Gigantic Ribonucleoprotein Assembly Involved in Diverse Physiological and Pathological Phenomena and an Ideal Nanovector for Drug Delivery and Therapy. *Cancers* **13**, 707 (2021).

24.

García-Saura, A. G. & Schüler, H. PARP10 Multi-Site Auto- and Histone MARylation Visualized by Acid-Urea Gel Electrophoresis. *Cells* **10**, 654 (2021).

25.

Gibson, B. A. & Kraus, W. L. New insights into the molecular and cellular functions of poly(ADP-ribose) and PARPs. *Nat Rev Mol Cell Biol* **13**, 411–424 (2012).

26.

Gordon, T. R. *Fusarium oxysporum* and the *Fusarium* Wilt Syndrome. *Annu. Rev. Phytopathol.* **55**, 23–39 (2017).

27.

Goswami, R. S. & Kistler, H. C. Heading for disaster: *Fusarium graminearum* on cereal crops: Fusarium graminearum on cereal crops. *Molecular Plant Pathology* **5**, 515–525 (2004).

28.

Gozgit, J. M. *et al.* PARP7 negatively regulates the type I interferon response in cancer cells and its inhibition triggers antitumor immunity. *Cancer Cell* **39**, 1214-1226.e10 (2021).

29.

Groslambert, J., Prokhorova, E. & Ahel, I. ADP-ribosylation of DNA and RNA. *DNA Repair* **105**, 103144 (2021).

30.

Guo, T. *et al.* PARP11 regulates total levels of type-I interferon receptor IFNAR1. *Nat Microbiol* **4**, 1771–1773 (2019).

31.

Guo, T. *et al.* ADP-ribosyltransferase PARP11 modulates the interferon antiviral response by mono-ADP-ribosylating the ubiquitin E3 ligase β-TrCP. *Nat Microbiol* **4**, 1872–1884 (2019).

32.

Hakmé, A., Huber, A., Dollé, P. & Schreiber, V. The macroPARP genesparp-9 andparp-14 are developmentally and differentially regulated in mouse tissues. *Dev. Dyn.* **237**, 209–215 (2008).

33.

Holbourn, K. P., Shone, C. C. & Acharya, K. R. A family of killer toxins: Exploring the mechanism of ADP-ribosylating toxins. *FEBS Journal* **273**, 4579–4593 (2006).

34.

Hopp, Grüter, & Hottiger. Regulation of Glucose Metabolism by NAD+ and ADP-Ribosylation. *Cells* **8**, 890 (2019).

35.

Hopp, A.-K. *et al.* Mitochondrial NAD+ Controls Nuclear ARTD1-Induced ADP-Ribosylation. *Molecular Cell* **81**, 340-354.e5 (2021).

36.

Hottiger, M. O. Nuclear ADP-Ribosylation and Its Role in Chromatin Plasticity, Cell Differentiation, and Epigenetics. *Annu. Rev. Biochem.* **84**, 227–263 (2015).

37.

Hottiger, M. O., Hassa, P. O., Lüscher, B., Schüler, H. & Koch-Nolte, F. Toward a unified nomenclature for mammalian ADP-ribosyltransferases. *Trends in Biochemical Sciences* **35**, 208–219 (2010).

38.

Huambachano, O., Herrera, F., Rancourt, A. & Satoh, M. S. Double-stranded DNA Binding Domain of Poly(ADP-ribose) Polymerase-1 and Molecular Insight into the Regulation of Its Activity. *Journal of Biological Chemistry* **286**, 7149–7160 (2011).

39.

Huang, J. Y., Wang, K., Vermehren-Schmaedick, A., Adelman, J. P. & Cohen, M. S. PARP6 is a Regulator of Hippocampal Dendritic Morphogenesis. *Sci Rep* **6**, 18512 (2016).

40.

Iwata, H. *et al.* PARP9 and PARP14 cross-regulate macrophage activation via STAT1 ADP-ribosylation. *Nat Commun* **7**, 12849 (2016).

41.

Jubin, T. *et al.* The PARP family: insights into functional aspects of poly (ADP-ribose) polymerase-1 in cell growth and survival. *Cell Prolif.* **49**, 421–437 (2016).

42.

Kamaletdinova, T., Fanaei-Kahrani, Z. & Wang, Z.-Q. The Enigmatic Function of PARP1: From PARylation Activity to PAR Readers. *Cells* **8**, 1625 (2019).

43.

Kamata, T., Yang, C.-S. & Paschal, B. M. PARP7 mono-ADP-ribosylates the agonist conformation of the androgen receptor in the nucleus. *Biochemical Journal* **478**, 2999–3014 (2021).

44.

Kim, M. Novel insight into the function of tankyrase (Review). *Oncol Lett* (2018) doi:10.3892/ol.2018.9551.

45.

Kim, M. Y., Mauro, S., Gévry, N., Lis, J. T. & Kraus, W. L. NAD+-Dependent Modulation of Chromatin Structure and Transcription by Nucleosome Binding Properties of PARP-1. *Cell* **119**, 803–814 (2004).

46.

Kouyama, K. *et al.* Single-particle analysis of full-length human poly(ADP-ribose) polymerase 1. *BIOPHYSICS* **16**, 59–67 (2019).

47.

Kraus, W. L. Transcriptional control by PARP-1: chromatin modulation, enhancer-binding, coregulation, and insulation. *Current Opinion in Cell Biology* **20**, 294–302 (2008).

48.

Kraus, W. L. & Lis, J. T. PARP Goes Transcription. *Cell* **113**, 677–683 (2003).

49.

Kudo, Y. *et al.* Measurement of Poly(ADP-ribose) Level with Enhanced Slot Blot Assay with Crosslinking. *Challenges* **9**, 27 (2018).

50.

Langelier, M.-F., Planck, J. L., Roy, S. & Pascal, J. M. Structural Basis for DNA Damage–Dependent Poly(ADP-ribosyl)ation by Human PARP-1. *Science* **336**, 728–732 (2012).

51.

Laplace, F. G. N. Agrios, Plant Pathology (3rd Edition). XVI + 803 S., 265 Abb. San Diego–New York–Berkeley–Boston–London–Sydney–Tokyo–Toronto 1988. Academic Press Inc. $ 45.00. ISBN: 0-12-044563-8. *J Basic Microbiol* **29**, 500–500 (1989).

52.

Leung, A. K. L. Poly(ADP-ribose): An organizer of cellular architecture. *Journal of Cell Biology* **205**, 613–619 (2014).

53.

Liu, Y. *et al.* Coordination of Steps in Single-nucleotide Base Excision Repair Mediated by Apurinic/Apyrimidinic Endonuclease 1 and DNA Polymerase β. *Journal of Biological Chemistry* **282**, 13532–13541 (2007).

54.

Ma, L.-J. *et al.* Comparative genomics reveals mobile pathogenicity chromosomes in Fusarium. *Nature* **464**, 367–373 (2010).

55.

Mansoory, D., Roozbahany, N. A., Mazinany, H. & Samimagam, A. Chronic Fusarium Infection in an Adult Patient with Undiagnosed Chronic Granulomatous Diseas. *Clinical Infectious Diseases* **37**, e107–e108 (2003).

56.

Marsischky, G. T., Wilson, B. A. & Collier, R. J. Role of Glutamic Acid 988 of Human Poly-ADP-ribose Polymerase in Polymer Formation. *Journal of Biological Chemistry* **270**, 3247–3254 (1995).

57.

Márton, J. *et al.* PARP10 (ARTD10) modulates mitochondrial function. *PLoS ONE* **13**, e0187789 (2018).

58.

Masson, M. *et al.* XRCC1 is specifically associated with poly(ADP-ribose) polymerase and negatively regulates its activity following DNA damage. *Mol Cell Biol* **18**, 3563–3571 (1998).

59.

Matveeva, E. A., Al-Tinawi, Q. M. H., Rouchka, E. C. & Fondufe-Mittendorf, Y. N. Coupling of PARP1-mediated chromatin structural changes to transcriptional RNA polymerase II elongation and cotranscriptional splicing. *Epigenetics & Chromatin* **12**, 15 (2019).

60.

Matveeva, E. A., Mathbout, L. F. & Fondufe-Mittendorf, Y. N. PARP1 is a versatile factor in the regulation of mRNA stability and decay. *Sci Rep* **9**, 3722 (2019).

61.

Matveeva, E. *et al.* Involvement of PARP1 in the regulation of alternative splicing. *Cell Discov* **2**, 15046 (2016).

62.

McLennan, A. G. The Nudix hydrolase superfamily. *Cell. Mol. Life Sci.* **63**, 123–143 (2006).

63.

Meder, V. S., Boeglin, M., de Murcia, G. & Schreiber, V. PARP-1 and PARP-2 interact with nucleophosmin/B23 and accumulate in transcriptionally active nucleoli. *Journal of Cell Science* **118**, 211–222 (2005).

64.

Messner, S. *et al.* PARP1 ADP-ribosylates lysine residues of the core histone tails. *Nucleic Acids Research* **38**, 6350–6362 (2010).

65.

Mikolčević, P., Hloušek-Kasun, A., Ahel, I. & Mikoč, A. ADP-ribosylation systems in bacteria and viruses. *Computational and Structural Biotechnology Journal* **19**, 2366–2383 (2021).

66.

Milo, S., Misgav, R. H., Hazkani-Covo, E. & Covo, S. Limited DNA repair gene repertoire in Ascomycete yeast revealed by comparative genomics. *Genome Biology and Evolution* evz242 (2019) doi:10.1093/gbe/evz242.

67.

Milo-Cochavi, S. *et al.* The response to the DNA damaging agent methyl methanesulfonate in a fungal plant pathogen. *Fungal Biology* **123**, 408–422 (2019).

68.

Morales, J. *et al.* Review of Poly (ADP-ribose) Polymerase (PARP) Mechanisms of Action and Rationale for Targeting in Cancer and Other Diseases. *Crit Rev Eukaryot Gene Expr* **24**, 15–28 (2014).

69.

Oliver, F. J. Resistance to endotoxic shock as a consequence of defective NF-kappa B activation in poly (ADP-ribose) polymerase-1 deficient mice. *The EMBO Journal* **18**, 4446–4454 (1999).

70.

Pearson, W. R. An Introduction to Sequence Similarity ("Homology") Searching. *Current Protocols in Bioinformatics* **42**, (2013).

71.

Perina, D. *et al.* Distribution of protein poly(ADP-ribosyl)ation systems across all domains of life. *DNA Repair (Amst)* **23**, 4–16 (2014).

72.

Poltronieri, P., Celetti, A. & Palazzo, L. Mono(ADP-ribosyl)ation Enzymes and NAD+ Metabolism: A Focus on Diseases and Therapeutic Perspectives. *Cells* **10**, 128 (2021).

73.

Prawira, A. *et al.* Assessment of PARP4 as a candidate breast cancer susceptibility gene. *Breast Cancer Res Treat* **177**, 145–153 (2019).

74.

Ray Chaudhuri, A. & Nussenzweig, A. The multifaceted roles of PARP1 in DNA repair and chromatin remodelling. *Nat Rev Mol Cell Biol* **18**, 610–621 (2017).

75.

Robu, M. *et al.* Role of poly(ADP-ribose) polymerase-1 in the removal of UV-induced DNA lesions by nucleotide excision repair. *Proc. Natl. Acad. Sci. U.S.A.* **110**, 1658–1663 (2013).

76.

Rongvaux, A., Andris, F., Van Gool, F. & Leo, O. Reconstructing eukaryotic NAD metabolism. *Bioessays* **25**, 683–690 (2003).

77.

Ruf, A., Rolli, V., de Murcia, G. & Schulz, G. E. The mechanism of the elongation and branching reaction of poly(ADP-ribose) polymerase as derived from crystal structures and mutagenesis. *J Mol Biol* **278**, 57–65 (1998).

78.

Sakurai, J., Nagahama, M., Oda, M., Tsuge, H. & Kobayashi, K. Clostridium perfringens Iota-Toxin: Structure and Function. *Toxins* **1**, 208–228 (2009).

79.

Salech, F., Ponce, D. P., Paula-Lima, A. C., SanMartin, C. D. & Behrens, M. I. Nicotinamide, a Poly [ADP-Ribose] Polymerase 1 (PARP-1) Inhibitor, as an Adjunctive Therapy for the Treatment of Alzheimer's Disease. *Front. Aging Neurosci.* **12**, 255 (2020).

80.

Schiewer, M. J. & Knudsen, K. E. Transcriptional Roles of PARP1 in Cancer. *Molecular Cancer Research* **12**, 1069–1080 (2014).

81.

Schreiber, V., Dantzer, F., Ame, J.-C. & de Murcia, G. Poly(ADP-ribose): novel functions for an old molecule. *Nat Rev Mol Cell Biol* **7**, 517–528 (2006).

82.

Semighini, C. P., Savoldi, M., Goldman, G. H. & Harris, S. D. Functional characterization of the putative Aspergillus nidulans poly(ADP-ribose) polymerase homolog PrpA. *Genetics* **173**, 87–98 (2006).

83.

Slade, D. PARP and PARG inhibitors in cancer treatment. *Genes Dev.* **34**, 360–394 (2020).

84.

Sousa, F. G. *et al.* PARPs and the DNA damage response. *Carcinogenesis* **33**, 1433–1440 (2012).

85.

Suskiewicz, M. J., Palazzo, L., Hughes, R. & Ahel, I. Progress and outlook in studying the substrate specificities of PARPs and related enzymes. *FEBS J* **288**, 2131–2142 (2021).

86.

Teloni, F. & Altmeyer, M. Readers of poly(ADP-ribose): designed to be fit for purpose. *Nucleic Acids Res* **44**, 993–1006 (2016).

87.

Thomas, C. *et al.* Hit and run versus long-term activation of PARP-1 by its different domains fine-tunes nuclear processes. *Proc Natl Acad Sci USA* **116**, 9941 (2019).

88.

Tulin, A., Stewart, D. & Spradling, A. C. The *Drosophila* heterochromatic gene encoding poly(ADP-ribose) polymerase (PARP) is required to modulate chromatin structure during development. *Genes Dev.* **16**, 2108–2119 (2002).

89.

Ummarino, S., Hausman, C. & Di Ruscio, A. The PARP Way to Epigenetic Changes. *Genes* **12**, 446 (2021).

90.

van Zon, A., Mossink, M. H., Scheper, R. J., Sonneveld, P. & Wiemer, E. A. C. The vault complex. *Cellular and Molecular Life Sciences (CMLS)* **60**, 1828–1837 (2003).

91.

Vermehren-Schmaedick, A. *et al.* Characterization of PARP6 Function in Knockout Mice and Patients with Developmental Delay. *Cells* **10**, 1289 (2021).

92.

Vítor, A. C., Huertas, P., Legube, G. & de Almeida, S. F. Studying DNA Double-Strand Break Repair: An Ever-Growing Toolbox. *Front. Mol. Biosci.* **7**, 24 (2020).

93.

Vyas, S., Chesarone-Cataldo, M., Todorova, T., Huang, Y.-H. & Chang, P. A systematic analysis of the PARP protein family identifies new functions critical for cell physiology. *Nat Commun* **4**, 2240 (2013).

94.

Vyas, S. *et al.* Family-wide analysis of poly(ADP-ribose) polymerase activity. *Nat Commun* **5**, 4426 (2014).

95.

Wang, Q. *et al.* Characterization of the Two-Speed Subgenomes of Fusarium graminearum Reveals the Fast-Speed Subgenome Specialized for Adaption and Infection. *Front. Plant Sci.* **8**, (2017).

96.

Wright, R. H. G. *et al.* ADP-ribose–derived nuclear ATP synthesis by NUDIX5 is required for chromatin remodeling. *Science* **352**, 1221–1225 (2016).

97.

Xing, J. *et al.* Identification of poly(ADP-ribose) polymerase 9 (PARP9) as a noncanonical sensor for RNA virus in dendritic cells. *Nat Commun* **12**, 2681 (2021).

98.

Yang, H., Yu, H. & Ma, L.-J. Accessory Chromosomes in *Fusarium oxysporum*. *Phytopathology*® **110**, 1488–1496 (2020).

99.

Yu, D., Liu, R., Yang, G. & Zhou, Q. The PARP1-Siah1 Axis Controls HIV-1 Transcription and Expression of Siah1 Substrates. *Cell Reports* **23**, 3741–3749 (2018).

100.

Yu, Z. L. & Zhu, Z. M. Construction of an N6-methyladenosine lncRNA- and immune cell infiltration-related prognostic model in colorectal cancer. *Protoplasma* **259**, 1029–1045 (2022).

101.

Zhao, Y. *et al.* A Literature Review of Gene Function Prediction by Modeling Gene Ontology. *Front. Genet.* **11**, 400 (2020).

102.

RStudio Team (2020). RStudio: Integrated Development for R. RStudio, PBC, Boston, MA URL http://www.rstudio.com/.